Modulating Cell Behavior with Engineered HER-Receptor Ligands

by

Luis M. Alvarez

B.S. Chemistry
United States Military Academy, 1997

S.M. Chemical Engineering
Massachusetts Institute of Technology, 1999

Submitted to the Department of Biological Engineering in Partial Fulfillment of the Requirements for the Degree of

Doctor of Philosophy in Biological Engineering

at the

Massachusetts Institute of Technology

August 2009
[September 2009]

Signature of Author:_____
Department of Biological Engineering
24 August 2009

Certified by:_____
Linda G. Griffith
School of Engineering Teaching Innovation Professor of Biological & Mechanical Engineering
Director, Biotech/Pharma Engineering Center

Certified by:_____
Richard T. Lee
Professor of Medicine
Harvard Medical School

Accepted by :_____
Peter Dedon
Professor of Toxicology and Biological Engineering
Chair, Graduate Program Committee
Associate Head, Department of Biological Engineering

Modulating Cell Behavior with Engineered HER-Receptor Ligands

by

Luis M. Alvarez

Submitted to the Department of Biological Engineering on August 24, 2009 in Partial Fulfillment of the Requirements for the Degree of Doctor of Philosophy in Biological Engineering

Abstract: The primary motivation for this work is the manipulation of EGFR family signaling to influence regenerative responses of mesenchymal stem cells (MSC). Underlying the potential of regenerative medicine is the need to understand and control cell behavior. A 'cue, signal, response' paradigm has emerged as a framework for building predictive models for manipulation of cells to achieve desired responses. The HER receptor tyrosine kinase (RTK) family is an attractive target for manipulation of cues and signals, as its four members – epidermal growth factor receptor (EGFR or HER1), HER2, HER3 and HER4 – influence processes as diverse as development, wound healing, migration, and tissue homeostasis and family members are expressed by almost every cell type. All HER receptors require either homodimerization or heterodimerization with other family members for activation of signaling pathways, and the various dimer pairs are not equivalent in their ability to activate all the downstream pathways. Hence, signaling (and phenotypic) outcomes may be dictated not only by the number (or fraction) of each type of receptor ligated, but by the quantitative distribution of these receptors into various possible dimer pairs. The canonical physiological ligands for the HER family receptors are monomeric, allowing occupied receptors to freely homodimerize or heterodimerize.

The premise of this work is that engineered bivalent ligands can drive specific dimerization events to enhance or inhibit signaling by various HER family receptors in a quantitative fashion that might be predicted on the basis of receptor expression. This work focuses on the design and implementation of engineered protein systems that are targeted to control homo and heterodimerization of HER1 and HER3. One broad consequence of using homodimer ligands is to quantitatively force ligand-occupied HER1 or HER3 to homodimerize and thus inhibit heterodimerization. Homodimerization may reinforce preferred signaling pathways (e.g, HER1-HER1 vs HER1-HER2) – with implications for tissue regeneration and inhibit undesirable pathways (e.g. HER2-HER3) – with implications in cancer. Preliminary results suggest that whereas the monomeric HER3 ligand activates canonical signaling pathways expected from HER3-HER2 interactions, dimeric ligands inhibit signaling, presumably by forcing homodimerization of the kinase-inactive HER3 receptors. This thesis focuses on developing the design principles to use bivalent ligand dimers to control signaling, experimental testing of the hypothesis that signaling pathways can be controlled by such ligands and are quantitatively different than those for monovalent ligands, and demonstration of how such ligands influence proliferation of human marrow stromal cells, a cell type important for bone regeneration. In addition, the issue of practical implementation in a tissue engineering setting is addressed by implementing approaches to tether bivalent ligands to scaffolds in a manner that preserves signaling function.

Thesis Supervisor: Linda G. Griffith
Title: School of Engineering Teaching Innovation Professor of Biological & Mechanical Engineering and Director, Biotech/Pharma Engineering Center

Thesis Supervisor: Richard T. Lee
Title: Professor of Medicine, Harvard Medical School

Thesis Committee Members

Linda G. Griffith
Department of Biological Engineering
Department of Mechanical Engineering,
Massachusetts Institute of Technology

Richard T. Lee
Department of Medicine
Brigham and Women's Hospital &
Harvard Medical School

Dane K. Wittrup (chair)
Department of Biological Engineering
Department of Chemical Engineering
Massachusetts Institute of Technology

Matthew J. Lazzara
Chemical and Biomolecular Engineering Department
University of Pennsylvania

Acknowledgements

This thesis is dedicated to Lucy and Sophia. Lucy's extraordinary work of motherhood casts my own work in a humbling light and allows me to indulge in the simple pleasures of fatherhood without worry. They have opened my eyes to true love and joy. I thank my uncle Manuel Delamata for his support during my formative years and my parents for their encouragement.

I owe an especially deep debt of gratitude to Linda Griffith and Richard Lee who shaped my scientific thinking and gave me opportunities that I could not have found elsewhere. Together they provided extraordinary guidance and support and patiently gave of their time without hesitation. Their spirit of scientific curiosity and rigorous pursuit of knowledge have shaped my views and will leave an indelible mark on my future work. As a close friend and mentor I am deeply grateful to Matthew Lazzara for his support, advice, and friendship. I admire his approach to science and have sought to emulate this wherever possible. K. Dane Wittrup provided me sage advice and guidance as the chairman of my thesis committee and countless hours of work as course professor for 20.420. I am grateful for the opportunity to have learned so much from him. Douglas Lauffenburger was instrumental in my success. He always offered his support and encouragement. The willingness of the Department of Biological Engineering to accommodate students with less-orthodox trajectories leading up to MIT is a testament to the visionary thinking that embodies the Department under Doug's leadership.

To the members of the Griffith, Lee, and Lauffenburger labs over the years I am indebted for more than I can ever repay: Linda Stockdale, Manu Platt, Robin Prince, Shannon Alford, Stacey Pawson, Shelly Peyton, Edgar Sanchez, Nathan Tedford, Hyundo-Kim, Justin Pritchard, Shan Wu, Caroline Chopko, Ta-Chun Hang, Shan Wu, Megan Palmer, Brian Joughin, Nicholas Marcantonio, Ada Au and many others too numerous to list here. I want to recognize the special contributions of Seymour de Picciotto who carried out several of the experiments described in the thesis. If his work ethic and determination are any indication he will be very successful at any endeavor he pursues.

The undergraduate students I have worked with all made contributions characteristic of seasoned investigators and are all well beyond their years in terms of scientific understanding and creativity. I want to recognize Yadir Guerrero for his exemplary contributions to this work. His handiwork is seen in every chapter. Arian Roman took an early leadership role in developing the most important findings in Chapter 4. Adan Romero and Jose Gutierrez together made very important contributions in a very short summer term and exceeded everyone's expectations. I am grateful for their efforts. Robert Warden joined the effort early on and made important initial findings that set the course for later work. Alex Fick, Christina Tamayo, and Jaymie Brower also made important contributions and I am grateful for their work.

LTC John Burpo, COL Russell Lachance, and LTC Douglas Matty provided sage career advice that has served me well. BG R. Mark Brown likewise guided my Army career development and was instrumental in my being able to develop as a technical leader. His advocacy of science in support of the Soldier is an example I will emulate in my own career. BG Stephen R. Lanza deserves special mention. His work to influence my career fate at the highest levels set the course for my return to graduate school and my future success as a leader and scientist within the Army. I should also recognize the Uniformed Army Scientist and Engineer Program (UAS&E). It would not have been possible to pursue a Ph.D. while on active duty without the flexibility this program provided. Although at the time of this writing the fate of this program is in question I hope that future leaders will recognize the need for scientists and engineers within our ranks.

I gratefully acknowledge the generous support of the Fannie and John Hertz Foundation (Livermore, CA). The Foundation's support extended far beyond the financial impact of the fellowship and gave me complete freedom to pursue new ideas.

Table of Contents

1 Background and Scope

1.1 The importance of mesenchymal stem cells in tissue engineering

Mesenchymal tissues include bone, cartilage, muscle, tendon, and fat. The differentiation of mesenchymal stem cells (MSCs) into these terminal tissue types is governed in part by a variety of growth factors and cytokines and follows a path that is similar to hematopoiesis in diversity and intermediate cellular states.[3] Injury and disease in any one of the terminally differentiated mesenchymal tissues requires the recruitment of MSCs and connective tissue progenitors (CTPs) to bring about regeneration and wound healing. Thus the study of MSC biology figures prominently in realizing regenerative therapies in a variety of tissues. This is of particular importance in orthopedics which constitutes the largest clinical segment of mesenchymally-related tissue treatments. The scarcity of MSCs currently limits the scope of what is possible. At typical frequencies of 1 in 30,000 cells the primary engineering challenge is to overcome a shortage of cells. Successful implementation of any tissue engineering approach requires careful consideration of the many biological and physical parameters which exert multifactorial effects on cells. Many of the most important questions in this field are aimed at discovering what happens at the interfaces between cells and their immediate environment. In the context of tissue engineering the environment typically includes an artificial material.

1.2 Scaffold materials for MSCs tissue engineering

Exogenous materials are widely used clinically for bone regeneration. Surgical techniques incorporating materials in mandibular bone were pioneered by Bränemark in the 1950s. Today, auto- and allo-grafts as well as synthetic β-tricalcium phosphate (BTCP) and hydroxylapatite (HA) are common materials in bone regeneration procedures, particularly for non-load bearing small or medium bone defects. These approaches all rely on the recipient's own MSC population to bring about tissue regeneration and often involve impregnation of the matrix with extracted bone marrow to seed an appropriate number of MSCs and CTPs. In current clinical practice autologous bone marrow aspirate containing MSCs and CTPs has been used as a source of progenitors in both ceramic and demineralized bone grafts.[4-6] Further, the success of bone grafts in canine models of spinal fusion and segmental defect can be increased by using methods which selectively retain MSCs , i.e., that enrich them compared non-progenitor cells.[7-9] These methods have shown significant improvement in outcomes over less invasive interventions, presumably due to the role of MSC delivery to the site of injury.[10] The treatment of implants with bioactive components such as growth factors represents a growing area of study and is likely to extend the benefits achieved thus far with MSC enrichment.

Bone morphogenetic proteins (BMPs) and some other growth factors have gained clinical acceptance in orthopedic medicine and are in various stages of pre-clinical development.[10, 11] BMPs, like most growth factors, are typically delivered soluble or adsorbed to a matrix, which creates great variability in local retention and release. Further, BMPs act on bone-forming cells to foster differentiation toward the osteogenic

phenotype, hence are arguably less effective in large defects that have a clinical deficiency of MSCs, where driving differentiation may deplete the progenitor compartment before it has multiplied sufficiently to fill the wound. Members of the EGFR family act on stem cells and early progenitor cells, hence interventions targeted to this family may increase survival and proliferation of cells at a stage that feeds into the steps influenced by BMPs. This thesis will demonstrate precisely this effect.

1.3. Mesenchymal stromal cell biology: cues, signals, and responses in MSCs

Debate continues over how closely regeneration recapitulates development yet analysis of developmental biology of bone and cartilage has yielded insights into factors important in regeneration of functional bone and cartilage. In the endochondral mode of bone formation during early stages of development bone begins to nucleate at ossification centers within a cartilage "model". For skeletal bone the origin of these early osteogenic cells is the embryonic mesenchyme. Ossification extends outward from primary nodes guided by gradients in differentiation stimuli which include numerous cytokines, growth factors, small molecules, and juxtacrine interactions.[12, 13] During early development of cranial bones and during fracture repair later in life intramembranous ossification is the primary mode of bone formation. This process differs from endochondral ossification in that MSCs and CTPs play a larger role and initiate tissue formation in the absence of a chondral supporting environment.[14]

Many aspects of later developmental processes leading to mature bone and cartilage remain uncharacterized. Details such as the vacularization of trabecular bone have yet to be elucidated.[15] However, early bone development from cartilaginous tissue is

reasonably well characterized and can be used to inform approaches to the early regeneration of these tissues in a wound healing context. Presentation of the correct cues early in the wound healing process is essential for proper tissue regeneration. The cues arising from EGFR family receptor stimulation are particularly important in this regard.[16]

Epidermal growth factor (EGF)

EGF is the canonical ligand for EGFR and can bring about proliferation,[17-23] migration,[24-27] homeostasis,[19] and synergistic effects leading to differentiation in concert with other ligands.[28-30] The broad effects of this ligand are due to the large number of tissues in which EGFR is expressed and the diversity of the downstream signaling network, thus making EGF an important stimulus in wound healing contexts.

In MSCs, EGF has been shown to affect a number of cell behaviors in a context specific manner. EGF can promote proliferation,[19] osteogenic differentiation,[31] and survival.[32] In one case EGF exerted different effects on human telomerase immortalized MSCs (hTMSCs) and primary rat MSCs.[19] In another study survival enhancement was dependent on the surface tethering of EGF.[32] In a wound healing context EGF can serve as an important cue leading to bone development and homeostasis following surgery.[33-36] EGF has also been shown to play a role as a regulator of CTP behavior[31, 37-41] and can also give rise to expansion of MSCs without inducing differentiation.[19] In addition to its potential in wound healing applications EGF has a high degree of receptor specificity for EGFR and thus offers an advantage in tissue engineering approaches to control EGFR receptor dimerization, as is explained in later sections.

Neuregulin-1β (NRG1)

The effects of neuregulin1-β1 (NRG1), the canonical ligand for HER3 and HER4, are well characterized in neurogenesis and neurological development.[42-44] Most notably NRG1 induces neural differentiation of rat pheochromocytoma (PC12) cells.[45, 46] Its role in neuromuscular junction (NMJ) formation is also well characterized where it serves to stimulate acetylcholine receptor (AChR) expression at the NMJ synapse.[47] NRG1 has also been shown to enhance the ability of MSCs to repair damaged muscle tissues, thus implicating NRG1 as a potential myogenic stimulus.[48]

Recent work by Gui *et al.* indicates that NRG1 has a protective effect on MSCs exposed to hypoxic or serum deprived conditions.[49] Protection of MSCs in hypoxic environments is of particular importance following surgical intervention where seeding of MSCs into large defects will necessarily lead to hypoxic conditions in a large segment of the wound before vascularization occurs.[50] In addition to its potential as a differentiation and hypoxia protective ligand NRG1 has a high degree of receptor specificity for HER3 and HER4 and, like EGF, is an attractive means to control dimerization of its cognate receptors, HER3 and HER4, in a specific manner.

Integrins

Although the focus of this work is on modulating HER signaling, the cell adhesion background impacts almost every aspect of cell behavior. The density of integrin ligand on connective or supporting substrates provides a basis for cell adhesion and migration which is particularly important in a wound healing context.[51] The most common adhesion proteins found in bone healing environments are fibronectin,

vitronectin, and collagen.[52-54] In some facets of this study, the integrin ligand GRGDSP which is present in fibronectin will be used to control the adhesion of cells to substrates given that it has been shown to bind to both αvβ3 and α5β1 *in vitro*.[55] The GRGDSP motif can be included as a fusion or bivalent partner protein with other ligands and can be used modulate cell adhesion and migration in a systematic manner.

1.4 HER receptors and cell signaling

Since the discovery of EGF in the 1960s, the EGFR family (EGFR, HER2, HER3, HER4) has been intensely studied and is arguably the most well-characterized peptide growth factor signaling network.[2, 19, 22, 23, 32] The HER signaling network is among the most diverse and tightly coupled to distinct phenotypic outcomes of any network characterized to date.[1, 17, 56-61] A simplified schematic depicting the HER signaling network is shown in figure 1.1.[2] EGFR family members are receptor tyrosine kinases, with the general structure of an extracellular ligand-binding domain, a transmembrane domain, a cytoplasmic tyrosine kinase domain, and a cytoplasmic regulatory domain. EGFR and HER4 possess all of these domains, while HER2 lacks a ligand-binding domain and HER3 lacks an active tyrosine kinase.[2, 18, 57] There are 12 known ligands that can bind one or more of three family members (EGFR, HER3, and HER4) to give rise to 10 possible different HER homo- and hetero-dimer combinations. Ligand binding causes conformational changes which lead to receptor dimerization and subsequent phosphorylation of intracellular receptor tyrosines that then propagate signals into the downstream network, which includes Erk, Akt, PI3Kand PLCγ pathways.

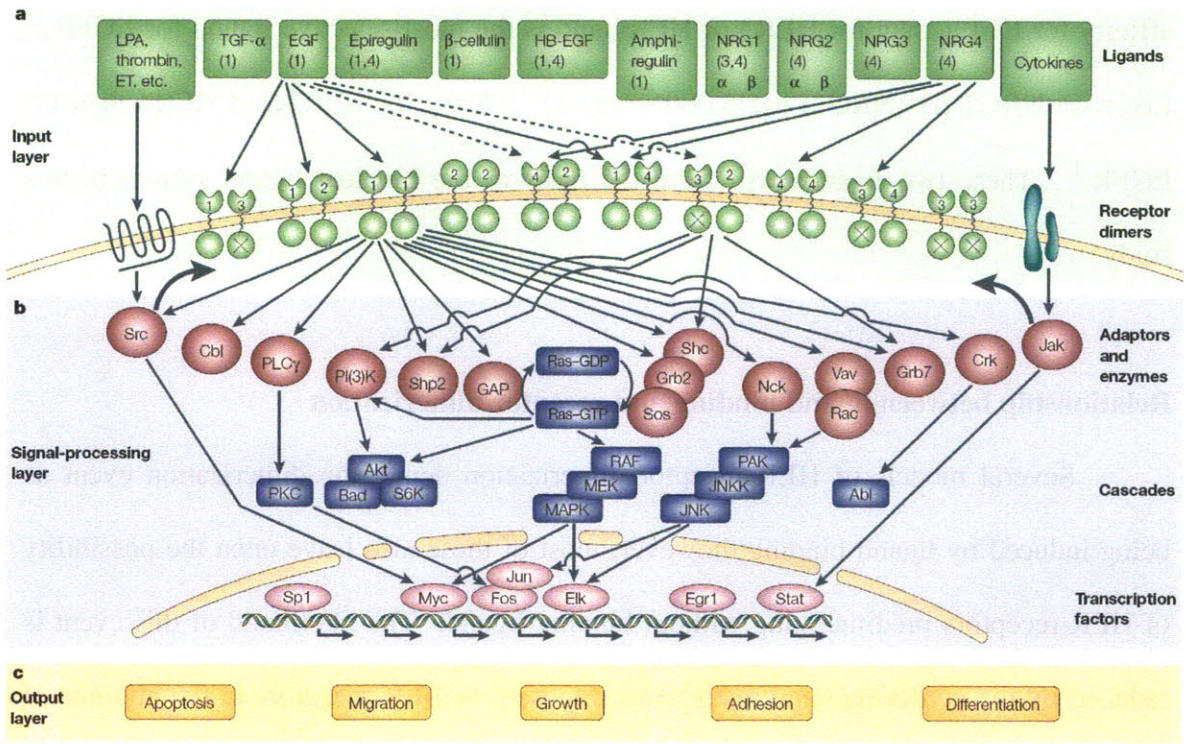

Figure 1.1 - The HER receptor signaling network [2]

Although many facets of ligand binding and receptor dimerization among EGFR family members remain controversial, in part due to differences in cell types, receptor expression levels, and experimental methods used to probe events, some generalized features important for this thesis work can be delineated. These include:

Ligand specificity

We seek a highly selective ligand that can bind EGFR at the exclusion of other HER receptors, thus offering control over receptor monomer binding. Likewise we seek a ligand that can bind HER3 and HER4 selectively. Orthogonal selectivity will confer a high level of control over receptor binding and permit construction of bivalent ligands which can control receptor recruitment into dimer complexes. EGF has 1000X greater

affinity for EGFR than for HER3 or HER4 and is the most selective ligand for EGFR.[18] Likewise NRG1-β1 (NRG1) has 5,000X greater affinity for HER3 and HER4 than for EGFR.[17] These two ligands will form the basis of the bivalent ligand system in this study.

Relationship between ligand binding and receptor dimerization

Several models of HER receptor dimerization depict the dimerization event as being induced by ligand binding; however, most of these also leave open the possibility of HER receptors predimerizing without binding ligand. The likelihood of this event is reduced by the conformational restrictions imposed on HER receptors in the absence of ligand. Ligand binding stabilizes a conformational change which exposes a dimerization loop. Dimerization in turn stabilizes the receptor dimer pair in this final conformation. Extensive biophysical characterization of EGFR by Kuriyan and others supports this model of HER receptor dimerization.[2, 62] Further evidence of this is found in the mechanism of dimerization exhibited by HER2 which has a constitutively exposed dimerization loop due to unique structural differences which stabilize this conformation. Hence HER2 can dimerize with EGFR,3,4 without binding ligand.[57, 63] Conversely EGFR, HER3, & HER4 generally require at least one ligand binding event to initiate dimerization with another EGFR, HER3, & HER4.[2] Thus ligand stimulation can influence HER receptor dimerization. Some studies provide evidence that is suggestive of pre-homodimerization of HER receptors before ligand binding.[64] However, there is extensive evidence of heterodimerization between HER receptors, particularly with HER2 which does not require a ligand.[2, 65] Thus the question of how HER receptors

select dimer partners remains open and also suggests the possibility of influencing receptor dimer pairings the approach described here.

Specificity of signaling pathways induced by various HER family members

High signaling diversity in the HER network is an attractive feature that can give rise diverse phenotypic outcomes. Work by MacBeath and Jones offers a glimpse into this complex signaling network by mapping the downstream interactome for a subset of each HER receptor tyrosine/p-tyrosine as shown in figure 1.2.[1] At first glance one can observe well known interactions at mid nM affinities between each HER receptor and downstream effectors. These include: EGFR(pY1172):SHC1, HER2(pY1139):GRB2, and HER3(pY1260):PI3K. One can generalize these findings to predict signaling network activation and phenotypic outcomes that might result from specific receptor pairings. This is illustrated in figures 1.1 and 3.1 which taken together capture the central premise of this work.

The diversity and associated complexity of the HER network originate in the receptor dimerization event. The type of ligand that initiates dimerization has some influence on the type of receptor dimer that eventually forms and this in turn determines the specific tyrosine residues which are phosphorylated on each receptor. In addition to this the relative levels of each HER receptor also influences dimerization outcomes.[63] Having a specific mechanism based on ligand specificity to control how HER receptors dimerize might enable an additional level of control over many aspects of this signaling network.

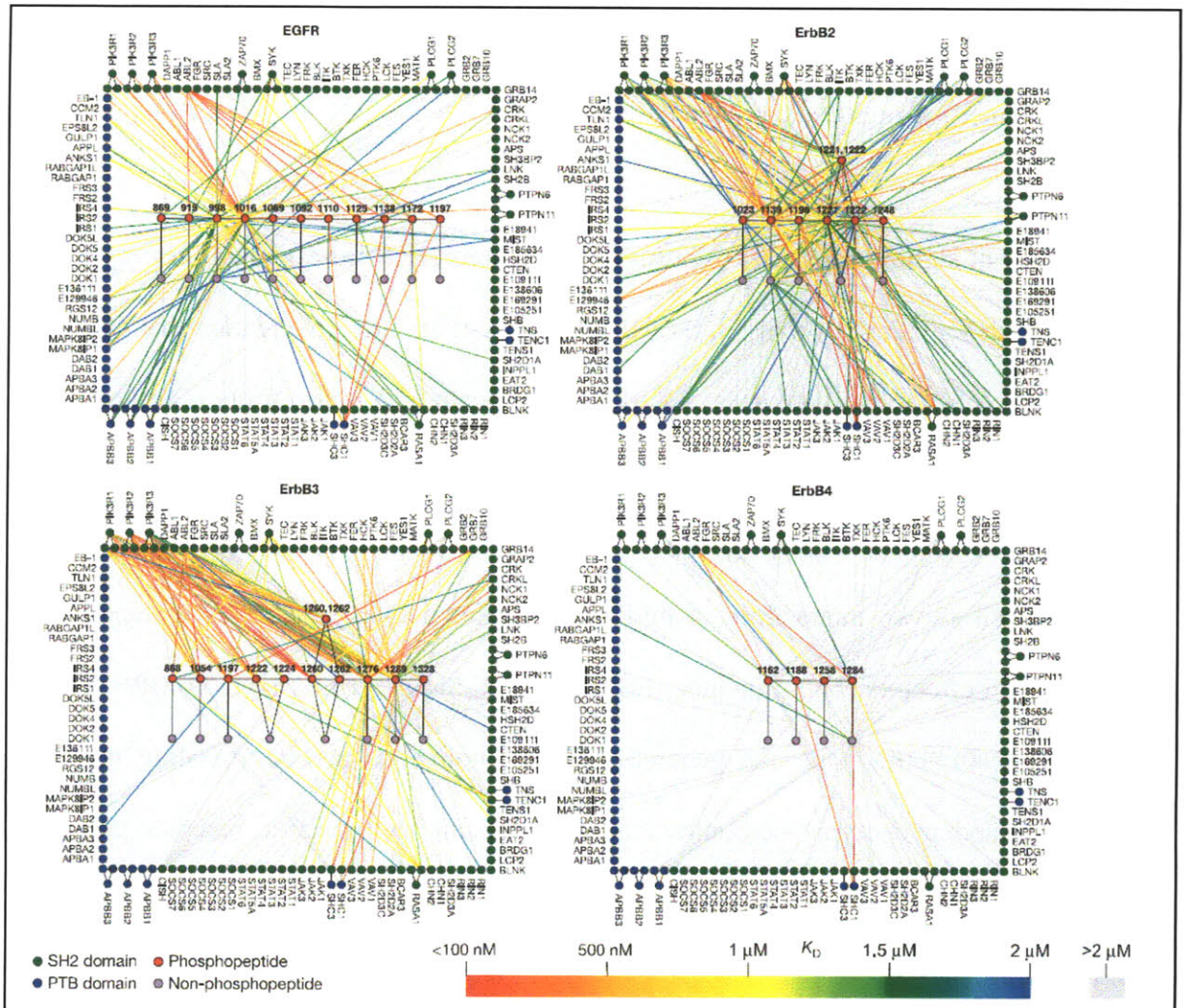

Figure 1.2 - The HER Y/pY interactome.[1]

Stimulating cells with soluble ligands from among the 12 known HER ligands will give rise to signaling predominantly through receptors that exhibit the highest affinities for that ligand. Dimer parings are also influenced by the relative surface density of the various receptor types. Some ligands exhibit varying degrees of promiscuity for several receptors. For example, betacellulin, heparin-binding EGF, and epiregulin all can bind to EGFR and HER4 with comparable affinity.[66] Other ligands exhibit high specificity for a single receptor. EGF and NRG1β are two such ligands and

each exhibits high affinity for EGFR and HER3/4, respectively. This specificity provides a basis for controlled receptor dimerization.

1.5 Controlled HER receptor dimerization and phenotype

Seminal work by Brugge *et al.*[67] employed genetically engineered cells to demonstrate how cell phenotype could be driven by forcing specific homo-dimerization and hetero-dimerization events between EGFR and HER2. This group developed a method of controlling HER receptor dimization by engineering an intracellular fusion on EGFR and HER2 that permits a forced homo- or heterodimerization by way of a bridging small molecule, either rapamycin or AP1510. This study identified a number of differences in both signaling and phenotype resulting from forced homo- and heterodimerization between EGFR and HER2 in fibroblasts. The first important finding was that activation of HER homodimers results in induction of cell cycle progression, receptor tyrosine phosphorylation, and recruitment of Src homology 2 domain-containing proteins (Shc and Grb2) which lead to pErk2 and pAkt signaling. Interestingly they confirmed that only EGFR homodimers were internalized and only EGFR homodimers were able to associate with and induce phosphorylation of c-Cbl. Cells with forced EGFR homodimers were able to form foci; however, cells with forced HER2 homodimers displayed a five- to sevenfold higher focus-forming ability. Lastly they found that EGFR and HER2 homodimers differ in their abilities to transform fibroblasts.

The results of this study demonstrate the utility of forced HER receptor dimerization to control phenotypic outcomes. This approach however is not amenable to exogenous control as it requires expression of chimeric variants of the HER receptors.

Any clinically useful strategies in this area will require completely exogenous control over HER receptor dimerization as genetic intervention is not feasible or approved.

1.6 Biomaterials and Scaffolds

The clinical utility of any results from HER ligand engineering would be enhanced if those results could be replicated on biomaterials and scaffolds that are currently used in surgical procedures. One such substrate is β-tricalcium phosphate (BTCP) which is used in orthopedic procedures as bone void filler.[68] Often this material is flushed with bone marrow aspirate to seed MSCs and promote bone formation.[69] BTCP is an osteoconductive material that supports bone mineralization by easily dissolving at low pH and serves as a rigid substrate for cell attachment.[21, 69]

One drawback of BTCP is the lack of available surface treatments to functionalize this material. No reliable methods to treat the surface of BTCP with proteins or similar coatings are described in the literature or in clinical case studies. Flushing BTCP with bone marrow aspirate is the current state of the art in BTCP surface treatment; however, this produces a highly heterogeneous distribution and uncontrolled adhesion of serum proteins. Attempts to make polymer composites with BTCP have shown some promise but these new materials require extensive characterization and regulatory approvals. The utility of BTCP as a substrate for orthopedic procedures would be enhanced if surface treatments were available to permit direct attachment of bioactive components. The ability to tether ligands and other bioactive components to the surface of BTCP implants would bring improvements in patient outcomes and would open the field to spatially

guided tissue regeneration. This is of particular importance in the vascularization of regenerated bone tissue.

One approach to this problem is to attempt discovery of peptide sequences that exhibit tight binding to BTCP by using phage display. Preliminary results from a 12-mer unconstrained phage panning experiment on BTCP have produced promising results. The details of this work are given in Chapter 4. One objective is to discover optimized configurations of multiple n-mer binding peptides that can be used as fusion partners to confer tight binding of ligands to BTCP substrates. The engineered proteins described in this study incorporate features which permit fusion to optimized BTCP binding peptides.

1.7 Outline of Thesis

The overall objective of this work is to develop new molecular approaches to control cellular outcomes that will have clinical significance in regenerative medical applications, and is addressed in three major aims. The first focuses on the design and biochemical characterization of ligands to control HER receptor dimerization; covered in chapter 2. The second aim consists of detailed characterization of the bivalent ligands to determine impact on HER dimerization in both model cells lines (ie., lines with defined HER expression profiles) and in the practical target cell of of application, MSCs; covered in chapter 3. The last aim focuses on the characterization of engineered HER ligands in tethered form and will explore the effect on MSCs of tethered ligand presentation on clinically important materials; covered in chapter 4. The last chapter will summarize the conclusions of this work. Various appendices include detailed protocols, information on protein expression constructs, and discussion of future directions.

1.8 References:

1. Jones, R.B., Gordus, A., Krall, J.A. & Macbeath, G. A quantitative protein interaction network for the ErbB receptors using protein microarrays. *Nature* (2005).
2. Yarden, Y. & Sliwkowski, M.X. Untangling the ErbB Signaling Network. *Nature Reviews - Molecular Cell Biology* **4**, 5 (2001).
3. Caplan, A.I. Review: Mesenchymal Stem Cells: Cell-Based Reconstructive Therapy in Orthopedics. *Tissue Engineering* **11**, 1198-1211 (2005).
4. Connolly, G.R., Tiedeman J, et al. Autologous marrow injection as a substitute for operative grafting of tibial nonunions. *Clin Orthop Relat Res*, 259-270 (1991).
5. Garg, N.K. & Gaur, S. Percutaneous autogenous bone-marrow grafting in congenital tibial pseudarthrosis. *Journal of Bone & Joint Surgery, British Volume* **77**, 830-831 (1995).
6. Healey, Z.P., McDonnell JM, et al Percutaneous bone marrow grafting of delayed union and nonunion in cancer patients. . *Clin Orthop Relat Res*, 280-285 (1990).
7. Brodke, D. et al. Bone grafts prepared with selective cell retention technology heal canine segmental defects as effectively as autograft. *J Orthop Res* **24**, 857–866 (2006).
8. Muschler, M.Y., Nitto H, et al. Selective retention of bone marrow-derived cells to enhance spinal fusion. *Clin Orthop Relat Res*, 242-251 (2005).
9. Muschler, N.H., Matsukura Y, et al Spine fusion using cell matrix composites enriched in bone marrow-derived cells. *Clin Orthop Relat Res*, 102-118 (2003).

10. Patterson, T.E., Kumagai, K., Griffith, L. & Muschler, G.F. Cellular Strategies for Enhancement of Fracture Repair. *The Journal of Bone and Joint Surgery* **90**, 111 (2008).

11. Jones, A.L. et al. Recombinant Human BMP-2 and Allograft Compared with Autogenous Bone Graft for Reconstruction of Diaphyseal Tibial Fractures with Cortical Defects. A Randomized, Controlled Trial. *The Journal of Bone and Joint Surgery* **88**, 1431 (2006).

12. Masi, L. et al. In Vitro Structural and Functional Relationships Between Preosteoclastic and Bone Endothelial Cells: A Juxtacrine Model for Migration and Adhesion of Osteoclast Precursors. *JOURNAL OF CELLULAR PHYSIOLOGY* **162**, 199-212 (1995).

13. Bruder, S.P., Fink, D.J. & Caplan, A.I. Mesenchymal stem cells in bone development, bone repair, and skeletal regeneration therapy. *J Cell Biochem* **56**, 283-294 (1994).

14. Netter, F.H. The Ciba collection of medical illustrations. Vol. 8, Muscoskeletal system. Anatomy, physiology, and metabolic disorders. (Ciba-Geigy, 1987).

15. Barou, O. et al. Relationships between trabecular bone remodeling and bone vascularization: a quantitative study. *Bone* **30**, 604-612 (2002).

16. Kolf, C.M., Cho, E. & Tuan, R.S. Mesenchymal stromal cells. Biology of adult mesenchymal stem cells: regulation of niche, self-renewal and differentiation. *Arthritis Res Ther* **9**, 204 (2007).

17. Pinkas-Kramarski, R. et al. Diversification of Neu differentiation factor and epidermal growth factor signaling by combinatorial receptor interactions. *EMBO J* **15**, 2452-2467 (1996).

18. Tzahar, E. et al. A hierarchical network of interreceptor interactions determines signal transduction by Neu differentiation factor/neuregulin and epidermal growth factor. *Molecular and Cellular Biology* **16**, 5276-5287 (1996).

19. Tamama, K., Fan, V.H., Griffith, L.G., Blair, H.C. & Wells, A. Epidermal Growth Factor as a Candidate for Ex Vivo Expansion of Bone Marrow-Derived Mesenchymal Stem Cells. *Stem Cells* **24**, 686 (2006).

20. Griffith, L.G. Emerging Design Principles in Biomaterials and Scaffolds for Tissue Engineering. *Annals of the New York Academy of Sciences* **961**, 83-95 (2002).

21. Muschler, G.F., Nakamoto, C. & Griffith, L.G. Engineering Principles of Clinical Cell-Based Tissue Engineering. *The Journal of Bone and Joint Surgery* **86**, 1541-1558 (2004).

22. Bublil, E.M. & Yarden, Y. The EGF receptor family: spearheading a merger of signaling and therapeutics. *Current Opinion in Cell Biology* **19**, 124-134 (2007).

23. Citri, A. & Yarden, Y. EGF-ERBB signalling: towards the systems level. *Nat Rev Mol Cell Biol* **7**, 505-516 (2006).

24. Miettinen, P.J. et al. Epidermal growth factor receptor function is necessary for normal craniofacial development and palate closure. *Nature Genetics* **22**, 69-73 (1999).

25. Gibbs, S. et al. Epidermal growth factor and keratinocyte growth factor differentially regulate epidermal migration, growth, and differentiation. *Wound Repair and Regeneration* **8**, 192-203 (2000).

26. Tokumaru, S. et al. Ectodomain Shedding of Epidermal Growth Factor Receptor Ligands Is Required for Keratinocyte Migration in Cutaneous Wound Healing. *The Journal of Cell Biology* **151**, 209-220 (2000).

27. Maheshwari, G., Wells, A., Griffith, L.G. & Lauffenburger, D.A. Biophysical Integration of Effects of Epidermal Growth Factor and Fibronectin on Fibroblast Migration. *Biophysical Journal* **76**, 2814-2823 (1999).

28. Traverse, S. et al. Research Paper EGF triggers neuronal differentiation of PC12 cells that overexpress the EGF receptor. *Current Biology* **4**, 694-701 (1994).

29. Freeman, M. Reiterative use of the EGF receptor triggers differentiation of all cell types in the Drosophila eye. *Cell* **87**, 651-660 (1996).

30. Miettinen, P.J., Vol. 127 2617-26272000).

31. Kratchmarova, I., Blagoev, B., Haack-Sorensen, M., Kassem, M. & Mann, M., Vol. 308 1472-1477 (American Association for the Advancement of Science, 2005).

32. Fan, V.H. et al. Tethered Epidermal Growth Factor Provides a Survival Advantage to Mesenchymal Stem Cells. *Stem Cells* **25**, 1241 (2007).

33. Wang, K., Yamamoto, H., Chin, J.R., Werb, Z. & Vu, T.H. Epidermal Growth Factor Receptor-deficient Mice Have Delayed Primary Endochondral Ossification Because of Defective Osteoclast Recruitment. *Journal of Biological Chemistry* **279**, 53848 (2004).

34. Sibilia, M. et al. Mice humanised for the EGF receptor display hypomorphic phenotypes in skin, bone and heart. *Development* **130**, 4515-4525 (2003).

35. Qin, L. et al. Amphiregulin Is a Novel Growth Factor Involved in Normal Bone Development and in the Cellular Response to Parathyroid Hormone Stimulation. *Journal of Biological Chemistry* **280**, 3974 (2005).

36. Chan, S.Y. & Wong, R.W.C. Expression of Epidermal Growth Factor in Transgenic Mice Causes Growth Retardation. *Journal of Biological Chemistry* **275**, 38693-38698 (2000).

37. Kuznetsov, S.A., Friedenstein, A.J. & Gehron Robey, P. Factors required for bone marrow stromal fibroblast colony formation in vitro. *British Journal of Haematology* **97**, 561-570 (1997).

38. Kimura, A., Katoh, O. & Kuramoto, A. Effects of platelet derived growth factor, epidermal growth factor and transforming growth factor-ß on the growth of human marrow fibroblasts. *British Journal of Haematology* **69**, 9-12 (1988).

39. Gronthos, S. & Simmons, P.J. The growth factor requirements of STRO-1-positive human bone marrow stromal precursors under serum-deprived conditions in vitro. *Blood* **85**, 929-940 (1995).

40. Owen, M.E., Vol. 87 731-7381987).

41. Satomura, K. et al. Receptor tyrosine kinase expression in human bone marrow stromal cells. *Journal of Cellular Physiology* **177**, 426-438 (1998).

42. Gamett, D.C. et al. Heregulin-stimulated signaling in rat pheochromocytoma cells. Evidence for ErbB3 interactions with Neu/ErbB2 and p85. *J Biol Chem* **270**, 19022-19027 (1995).

43. Gamett, D.C. & Cerione, R.A. Oncogenically activated or ligand-stimulated neu kinase stimulates neurite outgrowth in PC12 cells. *FEBS Lett* **351**, 335-339 (1994).

44. Morrissey, T.K., Levi, A.D., Nuijens, A., Sliwkowski, M.X. & Bunge, R.P. Axon-induced mitogenesis of human Schwann cells involves heregulin and p185erbB2. *Proceedings of the National Academy of Sciences of the United States of America* **92**, 1431 (1995).

45. Oshima, M., Weiss, L., Dougall, W.C., Greene, M.I. & Guroff, G. Down-Regulation of c-neu Receptors by Nerve Growth Factor in PC12 Cells. *J. Neurochem.* **65**, 427-433 (1995).

46. Kim, D. et al. Neuregulin Stimulates Myogenic Differentiation in an Autocrine Manner. *Journal of Biological Chemistry* **274**, 15395-15400 (1999).

47. Fu, A.K.Y. et al. Cdk5 is involved in neuregulin-induced AChR expression at the neuromuscular junction. *Nature Neuroscience* **4**, 374-381 (2001).

48. Dezawa, M. et al., Vol. 309 314-317 (American Association for the Advancement of Science, 2005).

49. Gui, C. et al. Heregulin protects mesenchymal stem cells from serum deprivation and hypoxia-induced apoptosis. *Molecular and Cellular Biochemistry* **305**, 171-178 (2007).

50. Stadelmann, W.K., Digenis, A.G. & Tobin, G.R. Impediments to wound healing. *Am J Surg* **176**, 39S-47S (1998).

51. Herard, A.L. et al. Fibronectin and its alpha 5 beta 1-integrin receptor are involved in the wound-repair process of airway epithelium. *American Journal of Physiology- Lung Cellular and Molecular Physiology* **271**, 726-733 (1996).

52. Deans, R.J. & Moseley, A.B. Mesenchymal stem cells Biology and potential clinical uses. *Experimental Hematology* **28**, 875-884 (2000).

53. Irvine, D.J., Hue, K.A., Mayes, A.M. & Griffith, L.G. Simulations of Cell-Surface Integrin Binding to Nanoscale-Clustered Adhesion Ligands. *Biophysical Journal* **82**, 120-132 (2002).

54. Koo, L.Y., Irvine, D.J., Mayes, A.M., Lauffenburger, D.A. & Griffith, L.G. Co-regulation of cell adhesion by nanoscale RGD organization and mechanical stimulus. *Journal of Cell Science* **115**, 1423-1433 (2002).

55. Hersel, U., Dahmen, C. & Kessler, H. RGD modified polymers: biomaterials for stimulated cell adhesion and beyond. *Biomaterials* **24**, 4385-4415 (2003).

56. Wiley, H.S. Trafficking of the ErbB receptors and its influence on signaling. *Experimental Cell Research* **284**, 78-88 (2003).

57. Sliwkowski, M.X. et al. Coexpression of erbB2 and erbB3 proteins reconstitutes a high affinity receptor for heregulin. *Journal of Biological Chemistry* **269**, 14661-14665 (1994).

58. Tzahar, E. et al. Bivalence of EGF-like ligands drives the ErbB signaling network. *The EMBO Journal* **16**, 4938-4950 (1997).

59. Zhan, L., Xiang, B. & Muthuswamy, S.K., Vol. 66 5201-5208 (AACR, 2006).

60. Linggi, B. & Carpenter, G. ErbB receptors: new insights on mechanisms and biology. *Trends in Cell Biology* **16**, 649-656 (2006).

61. Jorissen, R.N. et al. Epidermal growth factor receptor: mechanisms of activation and signalling. *Experimental Cell Research* **284**, 31-53 (2003).

62. Zhang, X., Gureasko, J., Shen, K., Cole, P.A. & Kuriyan, J. An Allosteric Mechanism for Activation of the Kinase Domain of Epidermal Growth Factor Receptor. *Cell* **125**, 1137-1149 (2006).

63. Witton, C.J., Reeves, J.R., Going, J.J., Cooke, T.G. & Bartlett, J.M.S. Expression of the HER 1-4 family of receptor tyrosine kinases in breast cancer. *The Journal of Pathology* **200**, 290-297 (2003).

64. Tao, R.H. & Maruyama, I.N. All EGF (ErbB) receptors have preformed homo- and heterodimeric structures in living cells. *Journal of Cell Science* **121**, 3207 (2008).

65. Lemmon, M.A. Ligand-induced ErbB receptor dimerization. *Experimental Cell Research* **315**, 638-648 (2009).

66. Ii, D.J.R. & Stern, D.F. Specificity within the EGF family/ErbB receptor family signaling network. *Bioessays* **20**, 41 - 48 (1998).

67. Muthuswamy, S.K., Gilman, M. & Brugge, J.S. Controlled Dimerization of ErbB Receptors Provides Evidence for Differential Signaling by Homo-and Heterodimers. *Molecular and Cellular Biology* **19**, 6845 (1999).

68. Erbe, E.M., Marx, J.G., Clineff, T.D. & Bellincampi, L.D. Potential of an ultraporous beta-tricalcium phosphate synthetic cancellous bone void filler and bone marrow aspirate composite graft. *Eur Spine J* **10**, S141-146 (2001).

69. Fleming Jr, J.E., George, F., Muschler, C.B. & Isador, H. Intraoperative Harvest and Concentration of Human Bone Marrow Osteoprogenitors for Enhancement of

Spinal Fusion. *Orthopedic Tissue Engineering: Basic Science and Practice* (2004).

2 Design and Synthesis of Bivalent Ligands

2.1 Introduction

The approach taken in this work to exert control over HER receptor dimerization is to design a panel of ligands that can recruit specific receptors into dimer complexes based on the affinity and specificity of natural ligand-receptor interactions within the HER receptor family. Such bivalent dimer ligands should bias dimerization. This chapter addresses the design and synthesis of this panel of ligands and details the protein-based characterizations required to validate the design features of the final products.

2.2 Protein design and characterization

The design of ligands is first guided by the dimerization geometry of HER receptors when bound to ligand. This geometry is most precisely described by the 2 Å crystal structure of the EGF-bound homodimerized extracellular domain of EGFR (figure 2.1).[1] This figure shows that wild-type ligands assume an anti-parallel orientation with respect to their termini when bound to dimerized receptor and that the distance between ligands is approximately 10 nm.

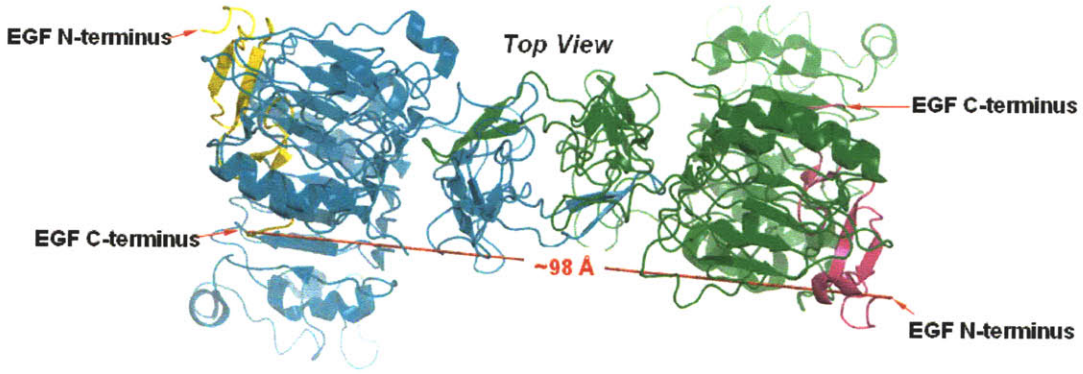

Figure 2.1 – Crystal structure of EGFR extracellular domain liganded with two EGFs

These features inform the initial design of the bivalent ligand system by imposing constraints on the minimum length between ligand domains and on the relative orientation of ligands once bound to dimerized receptor. Further, the five terminal amino acid residues on both termini of EGF are not captured in the crystal structure, indicating that these residues are unstructured and do not participate in receptor binding. Taken together these features describe the geometric parameters required for bivalent ligand binding. The overall design must accommodate these features if it is to achieve its stated purpose.

2.2.1 Modular Bivalent Ligand Design

A modular protein design can facilitate the investigation of homo- as well as heterodimers in both EGFR and HER3 without requiring repetitive cloning, expression, and purification. The bivalent design with modularity can be realized by using a tight binding region that brings ligands together with the correct orientation and spacing to permit simultaneous receptor dimer binding. One implementation of this design is shown in figure 2.2. As illustrated a coiled-coil domain allows for cognate coil containing ligands to form a bivalent structure. The coil sequences were selected from previously published work and have been reported by several investigators to exhibit a K_d as low as 10^{-15} M.[2-4]

The coils are separated from the ligand by a protease resistant spacer designed by Sauer *et al.* that confers flexibility, solubility, and together with the coils a sufficient extension to bridge a gap 20 nm long.[5] This is twice the distance between the most extreme termini in EGFs bound to dimeric EGFR. A schematic of the bivalent ligand is

shown in figure 2.2, which also depicts additional functional moieties, including antibody detection epitopes, and a biotin acceptor peptide (BAP) sequence to permit biotinylation and subsequent immobilization on neutravidin coated matrices.

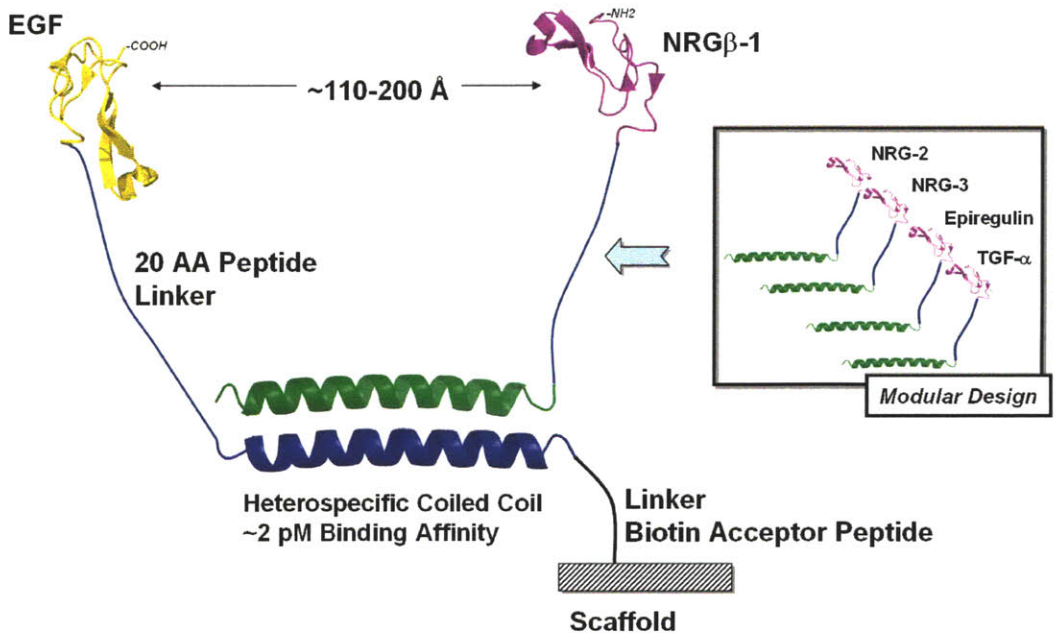

Figure 2.2 – **Bivalent ligand design**
The formation of a bivalent structure is mediated by a tight binding coiled coil interaction. This permits the formation of various bivalent ligand compositions.

The components of this system are shown in table 2.1. A modular design allows the formation of bivalent EGF "EE", bivalent EGF-NRG "EN" (a mixed ligand), or bivalent NRG "NN". The monomeric ligands that serve as the components of this system are denoted C1 and C2 (the EGF containing ligands), and C3 and C4 (the NRG containing ligands). Based on the coiled heterospecificities the following bivalent ligands can be formed: C12 ("EE"), C13 ("EN), C24 ("EN"), C34 ("NN"). The panel exhibits a degeneracy of one in the mixed ligand combination "EN". The C13 combination was used for all studies of the EN bivalent ligand, unless otherwise noted.

Name	Ligand Type	Can Pair	Biotin Acceptor
C1	EGF	C2 or C3	Yes
C2	EGF	C1 or C4	No
C3	NRG	C1 or C4	No
C4	NRG	C3 or C2	Yes

Table 2.1 – List of ligand components by type, bivalent binding partner, and presence of a biotin acceptor peptide sequence

2.2.2 Cloning and Protein Expression

Coding DNA for fusion proteins consisting of the human sequences of EGF or NRG-1b domains fused to protease resistant hydrophilic spacer arms fused to coiled coil domains followed by biotinylation sequences and epitopte tags (as per Table 2.1) were designed in silico (using VectorNTI) then ordered as a whole gene product with an E.coli codon bias from GeneArt (Regensburg, Germany). Coding sequences were amplified by PCR mutagensis with flanking restriction sites to permit cloning into expression vectors.

Intially two T7 promoter based expression systems were used to produce the ligand components: a pET28(a) His-tagged system (Novagen) for C1 and C4; and a maltose binding protein (MBP) tagged system: pMAL-c2X (New England Biolabs) for C2 and C3. The pET28a vector tended to produce inclusion bodies which require solubilitzation in 6 M urea + 100 mM dithiothretol followed by dialysis against a refolding buffer of reduced and oxidized glutathione.

Evaluation of both expression systems revealed that the pMAL system was far superior in that it could produce large quantities of properly folded soluble protein and did not require the difficult isolation of inclusion bodies, denaturnation, extensive

refolding, and subsequent separation of mis-folded isomers by reverse phase chromatography. This advantage represented a ten fold improvement in performance over the pET expression system in terms of time and materials required. As a result, C1 and C4 were removed from the pET backbone and cloned into pMALc2x expression vectors (NEB) and used as such for all experiments.

All expression constructs were sequenced prior to transformation into the expression strain BL21(DE3)pLysS (Stratagene). Transformed strains were grown to OD~0.6 with agitation at 37°C. Cultures were then brought to 25°C and protein expression was induced with a single pulse of 100 nM IPTG for 4 hours. Protein was harvested following cell lysis with Bug Buster Master Mix reagent (Novagen) supplemented with PMSF and protease inhibitor cocktail (Sigma).

Lysates were clarified by centrifugation at 3500g for 1 hour at 4°C. Clear lysate was subjected to purification on amylose resin in accordance with the pMAL System protocol (New England Biolabs). Eluted protein was concentrated using an ultracentrifugation cassette (10 kDa MWCO, Pierce). Purification tags were cleaved by factor Xa digestion overnight at 30°C in 20 mM tris, pH 7.4.

2.3 Validating Protein Identity

Purified proteins were analyzed by coomassie staining of sodiumdodecylsulphate polyacrylamide gels (SDS-PAGE), immunoblot, mass spectrometry, absorbance at 280 nm (A280), and in vitro cell response vs wild type ligands EGF and NRG-1β (Peprotech). A representative set of Coomassie and immunoblot analyses is shown in figure 2.3. Coomassie staining gives estimated molecular weight and relative purity. Typical

purities ranged from 80-95%. Immunoblots confirm the presence of full length protein when probed for terminal epitopes as shown in figure 2.X.

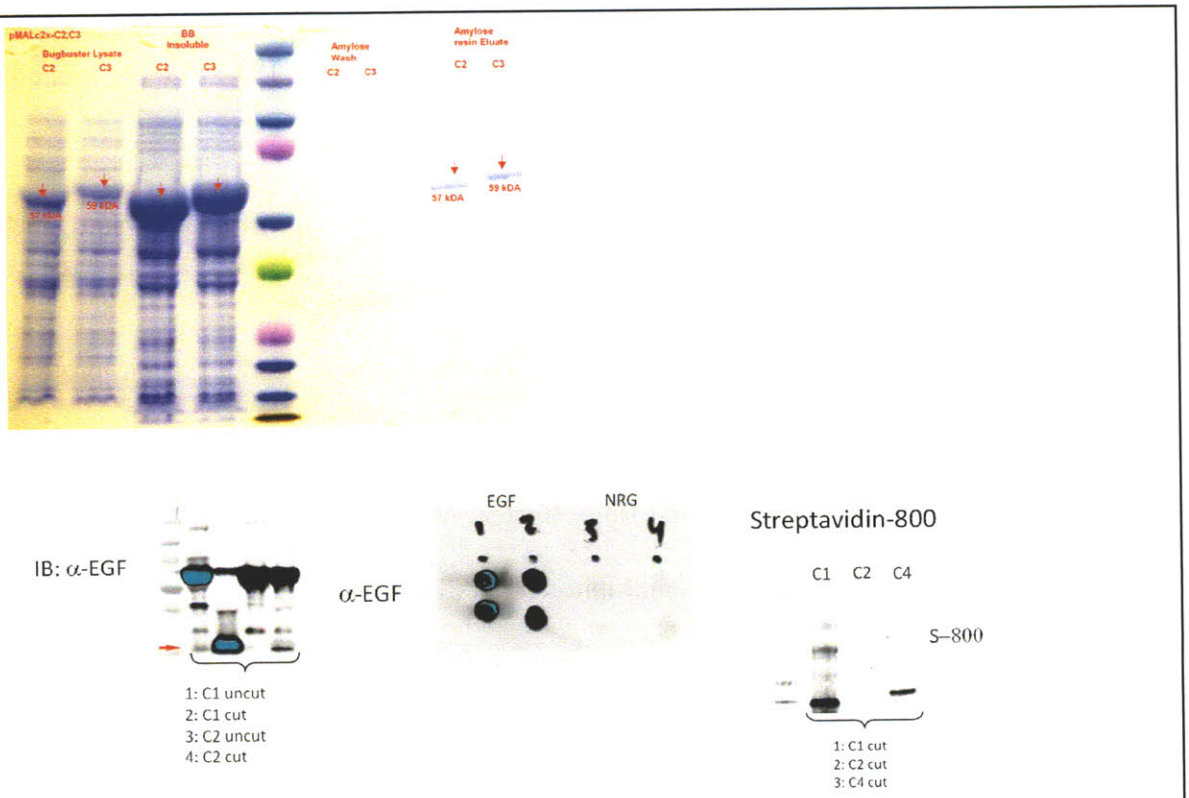

Figure 2.3 – Characterization of expressed proteins
(Top) Coomassie stained SDS-PAGE gel of purified C2 and C3. The purity and estimated molecular weights of the purified proteins are evident from the rightmost two lanes. (Bottom) Immunoblots of ligands (cut indicates cleaved with factor Xa); spot blots confirm absence of EGF from NRG containing C3 and C4. Probing blots with streptavidin-800IRDye confirms the presence of biotin on C1 and C4 (the BAP is a C-terminal sequence on each protein).

2.3.1 Confirming ligand bioactivity

Bioactivity of purified fractions was confirmed by in vitro cell response vs wild type ligands EGF and NRG-1β (Peprotech). Specificity for HER receptor activation was further assessed by including inhibitor controls using the pan-Her kinase inhibitor N-(4-

((3-Chloro-4-fluorophenyl)amino)pyrido[3,4-d]pyrimidin-6-yl)2-butynamide (Calbiochem #324840). Bioactivity and HER specificity were validated in HeLa and MCF-7 cells (for EGF and NRG containing ligands, respectively). HeLa cells express EGFR and HER2 and are responsive to EGF while MCF-7 cells express HER3 and HER4 and are responsive to NRG. Figure 2.4 is an immunoblot of pERK(1/2) stimulation following ligand dosing.

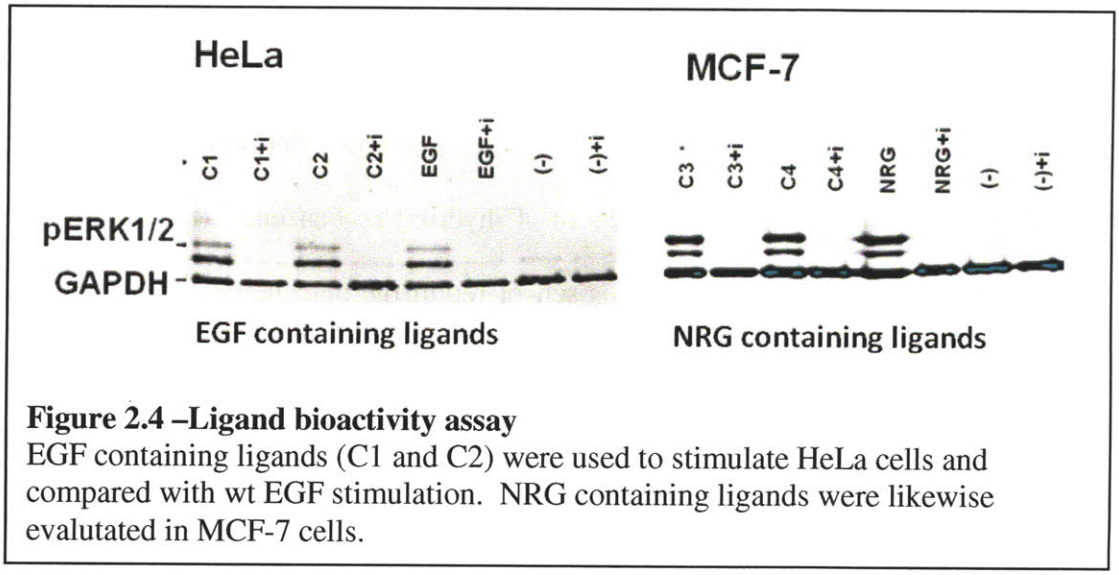

Figure 2.4 –Ligand bioactivity assay
EGF containing ligands (C1 and C2) were used to stimulate HeLa cells and compared with wt EGF stimulation. NRG containing ligands were likewise evalutated in MCF-7 cells.

The singly-dosed ligands produce pERK activation which is indistinguishable from their native analogues, and which is capable of being specifically inhibited by a pan-HER kinase inhibitor. This assay illustrates the effectiveness of the purification methods and validates the use of these ligands for use in bivalent experiments.

2.3.2 Biotinylation of Ligands

Incorporation of a tethering motif into the ligand design allows for greater flexibility in surface immobilization on tissue engineering scaffolds and for purposes of

detection. The biotin-streptavidin interaction is one of the tightest non-covalent interactions known ($k_D \sim 10^{-15}$ M) and is essentially irreversible over a broad range of conditions. The incorporation of a biotin acceptor peptide (BAP) sequence as a terminal fusion to C1 and C4 permits the biotinylation of these ligands and subsequent immobilization via interaction with immobilized streptavidin. The BAP is a 15 amino acid sequence that acts as a substrate for biotin ligase (BirA).

During expression in E. coli some fraction of the ligand is biotinylated by endogenous BirA. To achieve a higher level of biotinylation (>80%) exogenous BirA can be used following ligand purification. The degree of biotinylation can be measured by the degree of change in absorbance of 4'-hydroxyazobenzene-2-carboxylic acid (HABA) at 500 nm. Assays based on this sensor report the percentage of ligand that is biotinylated. In addition to quantitative assays the biotinylation of ligand can be detected by spotting on a nitrocellulose membrane and probing with IR-fluorescently labeled streptavidin and by SPR analysis with a streptavidin coated gold chip. Biotinylated ligands can be used in a variety of experimental schemes which incorporate a streptavidin (neutravidin or captavidin) tethering surface. Details to accomplish this are described in later sections.

2.4 Characterizing the Coiled Coil Interaction

The first generation of coils selected was from work published by Arndt and produced an interaction which exhibited mico-molar affinity as shown in figure 2.5. [6, 7] This set of coils was replaced with a modified set of coils by site directed mutagenesis of the original construct. When assayed by an enhanced immuno-fluorescence binding

method the new coils yielded a Kd of ~ 30 pM. This figure is approximately two orders of magnitude below the lowest relevant dose of EGF or NRG used in vitro and would ensure complete binding of the bivalent components.

2.4.1 Immunofluorescent Binding Assay

Characterization of the coiled coil interaction shown in figure 2.2 was performed by an immuno-fluorescent binding assay on streptavidin coated wells. Biotinylated C1 was incubated on the well surface and a titration of cognate coil concentrations was used to generate a binding curve. Controls include non-biotinylated ligand to measure non-specific adsorption and staining of biotinylated ligand with 2^{o} antibody to control for variations in bound ligand. Fitting these data to a one-parameter binding isotherm gives a K_d of 30 pM.

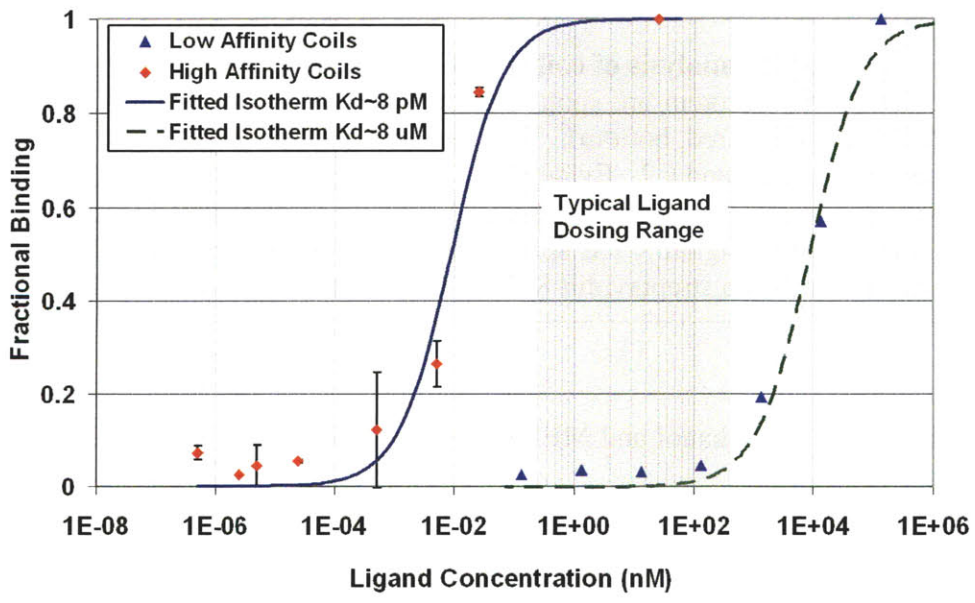

Figure 2.5 – Immunofluorescent binding assay
An ELISA based method using streptavidin coated EIA plates as used to achieve very sensitive detection of bound ligand. n=3, +/- s.d.

2.4.2 Far Western Blotting

Coiled coil binding was also investigated using far-western blotting. This was carried out by spotting 0.5 ul of sample ligand binding partner and controls in duplicate at 1 μM concentration onto a nitrocellulose membrane that was pre-wetted with 1 X transfer

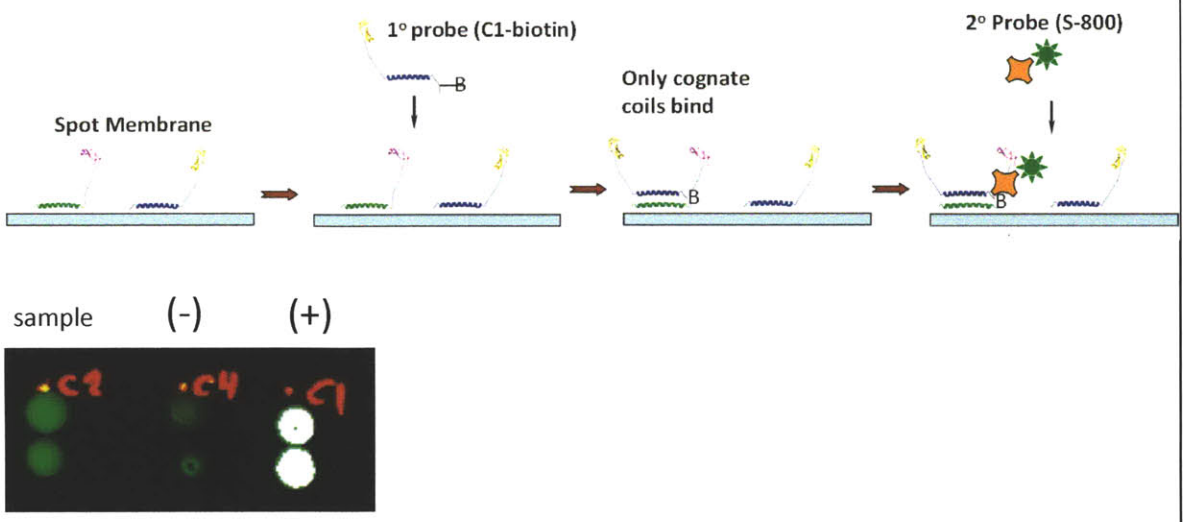

Figure 2.6 – Far western analysis of coiled coil interaction
C2, C4 and C1(control) protein are spotted in duplicate onto a nitrocellulose membrane (labeled C2, C4, and C1 in red, bottom). The membrane is then probed with soluble C1 to allow binding between C1 and C2. Evidence of binding is seen in the positive signal seen over the two C2 spots. The negative control C4 should not bind C1 and is shown to produce only background signal. C1 is spotted directly (positive control, rightmost spots). Membrane was probed with streptavidin-800 IR dye to detect biotinylated C1.

buffer (4:1 MQ water:methanol and MES buffer). Membranes were washed three times with 20 mM tris-buffered saline + tween-20 (TBST), pH 7.4 (TBST) then blocked for 1 hour with Licor Odyssey blocking buffer (OBB) then biotinylated cognate binding proteins were added to the blocking buffer at 100 nM and incubated overnight at 4°C. The membranes were then washed three times with TBST and probed for 1 hour with IR

dye conjugated streptavidin (Rockland #) diluted 1:10,000 in OBB. The membranes were then washed three times in TBST and scanned on a Licor Odyssey IR scanner. Figure 2.6 illustrates the experimental concept and the resulting data. Binding due to the coiled coil interaction is evident from the significant signal in the cognate binding pair C1+C2.

2.4.3 Surface Plasmon Resonance

Surface plasmon resonance was performed on a Biacor2000 instrument using a streptavidin coated gold analysis chip. Biotinylated C1 was immobilized on the chip surface and brought to equilibrium with running buffer. The conjugation of C1 to the chip surface exhibited a stable baseline within a 90 seconds of flowing C1 and remained stable over long buffer wash times, indicating a stable surface binding of C1. Attempts to conjugate additional C1 showed no change in the based line, indicating saturation of the chip surface.

Cognate binding partner C2 was then flowed over the surface and binding signal collected. Figure 2.7 shows data from the biotin – streptavidin chip conjugation and the C2 binding analysis. Data analysis is performed on the separate binding and unbinding portions of the response curve. During binding the partner in the mobile phase (C2) undergoes both binding an unbinding and so the data produced contain a combination of both effects. This is captured in the lumped variable called k_{obs} as shown in equation 2.1. The unbinding portion of the data reflects purely unbinding since the mobile phase does not contain appreciable amounts of C2 during this step. The pure unbinding is captured by k_{off} as shown in equation 2.2. In order to obtain the on rate during the binding step the

k_{obs} is transformed by subtracting k_{off} and normalizing by the ligand concentration in the mobile phase during the binding step. In this way both k_{off} and k_{on} are obtained, allowing the dissociation constant to be calculated as shown in equation 2.4.

$$S(t) = S_o + S_m(1 - e^{-k_{obs}t}) \quad (2.1)$$

$$S(t) = S_o + S_m e^{-k_{off}t} \quad (2.2)$$

$$k_{on} = \frac{k_{obs} - k_{off}}{[C2]} \quad (2.3)$$

$$K_d = \frac{k_{off}}{k_{on}} \quad (2.4)$$

The data produced by SPR are generally acceptable for binding affinities weaker than low nanomolar. Very tight binding interactions that are high picomolar and below generally produce data which cannot be fit reliably with the approach outlined above. This happens to be the case for the binding interaction between C1 and C2. As seen in figure 2.7 the k_{on} fitting gives a non-physical value. This can be interpreted as an effect of the extremely tight binding of this coil pair. The binding affinity obtained from the immunofluorescent binding assay (30 pM) confirms this effect.

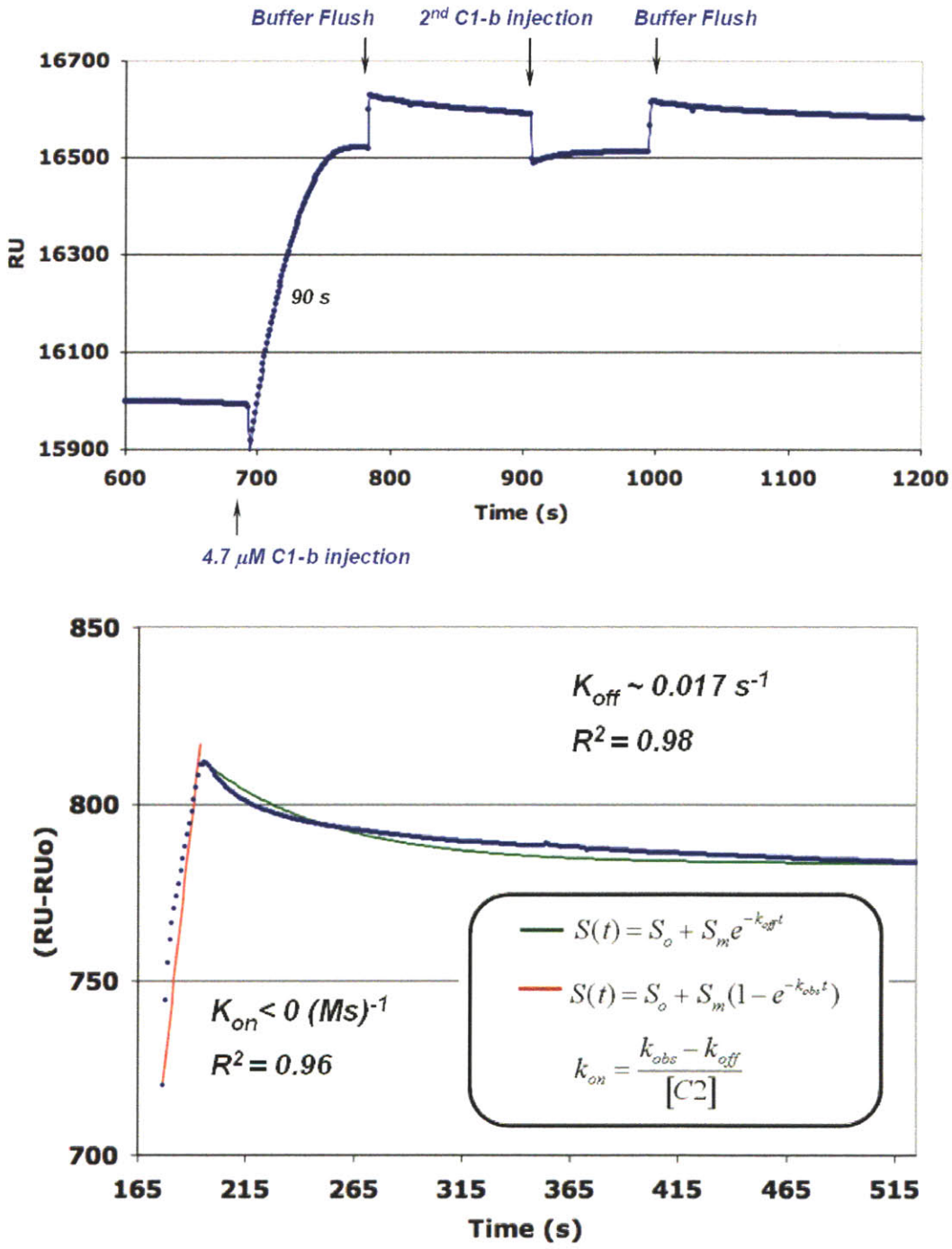

Figure 2.7 – Surface plasmon resonance analysis of coiled coil interaction

2.4.4 Isothermal titration calorimetry

Isothermal titration calorimetry can be used to study interactions between proteins with dissociation constants that are between 100 nM – 100 uM. The ability of this method to detect very tight interactions is limited by the ability to track changes in differential heat transfer that occur over a small range of titration volumes. This effect is illustrated in figure 2.8 by the sharp transition observed at 90 minutes. Although these data cannot be fit to obtain a binding constant they are suggestive of previous results of an extremely tight binding interaction. *(additional analysis of binding will be included in the manuscript and will include analytical ultracentrifugation data.)*

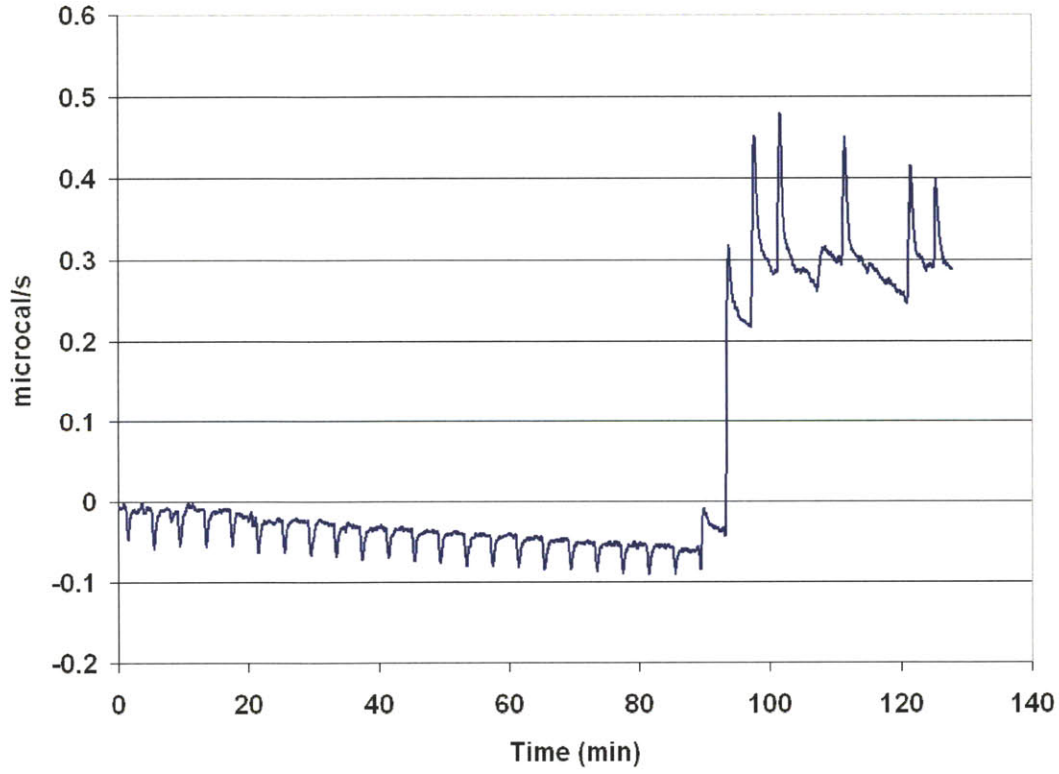

Figure 2.8 – Isothermal titration calorimetry of C1 and C2
The tight binding interaction between the cognate coils produces a very sharp transition consistent with very tight binding.

2.5 Conclusions

This chapter has outlined the methods used to design and characterize a panel of genetically encoded ligands with motifs to permit biotinylation, dimerization, and specific biological activity. The design was successfully implemented and the panel of ligands was shown to exhibit the expected binding characteristics and bioactivity necessary for subsequent experiments. The groundwork laid here is a necessary prerequisite for biological studies using this panel of ligands. Subsequent chapters will investigate the effects of bivalent ligands on various cell types.

2.6 References

1. Ogiso, H. et al. Crystal Structure of the Complex of Human Epidermal Growth Factor and Receptor Extracellular Domains. *Cell* **110**, 775-787 (2002).
2. Moll, J.R., Ruvinov, S.B., Pastan, I. & Vinson, C. Designed heterodimerizing leucine zippers with a ranger of pIs and stabilities up to 10-15 M. *Protein Science* **10**, 649 (2001).
3. Zhang, K., Diehl, M.R. & Tirrell, D.A. Artificial polypeptide scaffold for protein immobilization. *J. Am. Chem. Soc* **127**, 10136-10137 (2005).
4. Shen, W., Zhang, K., Kornfield, J.A. & Tirrell, D.A. Tuning the erosion rate of artificial protein hydrogels through control of network topology. *Nat. Mater* **5**, 153-158 (2006).
5. Martin, A., Baker, T.A. & Sauer, R.T. Rebuilt AAA+ motors reveal operating principles for ATP-fuelled machines. *Nature* **437**, 1115-1120 (2005).
6. Arndt, K.M., Müller, K.M. & Plückthun, A. Helix-stabilized Fv (hsFv) antibody fragments: substituting the constant domains of a Fab fragment for a heterodimeric coiled-coil domain. *J. Mol. Biol* **312**, 221-228 (2001).
7. Arndt, K.M., Pelletier, J.N., Müller, K.M., Plückthun, A. & Alber, T. Comparison of In Vivo Selection and Rational Design of Heterodimeric Coiled Coils. *Structure* **10**, 1235-1248 (2002).

3 Influence of Soluble Bivalent Ligands on Cell Signaling & Phenotype

3.1 Introduction

Overwhelming evidence supports the concept that EGFR family members must homo- or hetero-dimerize in order to initiate intracellular signaling events, and that ligand binding to at least one dimer member is required under most normal physiological circumstances.[1, 2] However, the sequence of events leading to an active ligand-occupied receptor dimer pair is still debated and may ultimately depend on the cellular context. In the canonical model, applicable to the ligand-binding receptors EGFR, HER3 and HER4, receptors exist on the surface in a closed configuration stabilized by interactions between extracellular subdomains II and IV.[3] When ligand binds, the receptor opens and adopts a new stable configuration, exposing a "dimerization arm" on the extracellular domain, leading to creation of dimers stabilized by both extracellular and intracellular domains of the receptor.[3-6] An alternate model, supported by experimental data from several labs, holds that receptors exist in pre-formed dimers or higher-level aggregates,[7-10] but that activation requires conformational changes induced by ligand binding.[4, 11] HER2 does not precisely fit either model, as it has no known ligands and is constitutively present in a conformation with the dimerization loop exposed to allow heterodimerization with EGFR, HER3, and HER4, even in the absence of ligand.[1, 2, 12] Notably, cells that overexpress HER2 – i.e., that express HER2 at levels associated with some pathology - have constitutively active HER2 due to homodimerization.[13] Thus, bivalent ligands may serve to drive particular dimerization events between lone receptors; to stabilize pre-existing dimers; or to disrupt pre-existing unoccupied receptor interactions (such as

HER3 clusters) and drive new ones. Although certain outcomes might be predicted from consideration of "equilibrium binding" at the cell surface, the observed outcomes will result from the integrated kinetics of ligand binding, receptor diffusion in the membrane, and receptor internalization and are thus not intuitive to predict.

For all members of the EGFR family, signal attenuation is achieved by at least two known mechanisms: tyrosine phosphatase deactivation; and receptor internalization and intracellular trafficking to lysomal degradation.[14, 15] Upon ligand binding, EGFR is internalized within minutes and later degraded in lyzosomes.[16] The internalization depends on the dimerization status, as HER2 heterodimerization with EGFR decreases the internalization rate constant for EGFR and increases the fraction of EGFR recycled to the cell surface following internalization.[17] Dimer composition can also affect the relative rate of dephosphorylation by altering the trafficking and localization of a liganded receptor dimer as well as by differentially recruiting phosphatases to adaptor sites.

Much of our understanding of the HER receptor signaling pathway comes from studies with either natural or deliberate genetic mutations of ligands and receptors in cell lines, and use of inibitors of binding and signaling. The development of the bivalent ligand system described in Chapter 2 allows a new approach to manipulating the HER system by using a purely exogeous method, in the form of bivalent ligands, to form selective HER dimers as shown in figure 3.1. The central hypothesis of this work is that stimulation with bivalent ligands can bias receptor dimerization outcomes in a predictable way.

3.1.1 Biasing EGFR Family Receptor Dimerization

Figure 3.1 depicts possible outcomes of HER receptor dimerization when a cell expressing all four types of HER receptors is stimulated with either wild type (monovalent) ligands (EGF or NRG) or with dimer ligands (EE, EN, or NN). Although few cells express appreciable amounts of all four receptors, the figure illustrates the key conceptual innovation in this work: stimulation with dimer ligands can potentially bias the degree of homo- or hetero-dimerization, with the practical outcome of either fostering formation of desirable dimerizations, or excluding potentially deleterious dimerizations (e.g., sequestering HER3 in inactive pairs; preventing EGFR-HER2 dimers). In addition to the dimeric outcomes illustrated in Fig 3.1, it is also conceivable that a bivalent ligand could lead to formation of oligomers, by serving as a bridge between two different adjacent receptor dimers.

The quantitative outcome of stimulation by either monovalent or bivalent ligand is expected to depend on both the absolute number of reach EGFR family member expressed as well as the relative numbers. For example, in cells that express high levels of any single receptor (>200,000 per cell), pre-formed receptor dimers may dominate effects of ligand dimers. Although in theory, the EGF-EGF ligand dimer should drive EGFR homodimerization and thereby inhibit EGFR-HER2 heterodimerization, it may be difficult to prevent EGFR-HER2 dimers from forming when stimulating tumor cells that overexpress one or both receptors. Thus, a particular dimer ligand may exert very different phenotypic and signaling responses in epithelial cells expressing high levels of multiple EGFR receptor family members compared to mesenchymal stem cells, which

express EGFR, HER2 and HER3 at levels below 10,000 receptors/cell, and do not express HER4.

Despite the complexity of how the context of an individual cell may influence outcomes, it is possible to make some general predictions about how particular types of receptor biasing might influence downstream signaling based on what is known about the signaling pathways initiated by each HER receptor dimer. For example, activation of the HER1 homodimer could be expected to produce increases in pERK leading to proliferative signaling that are weaker than those produced by HER1-HER2 heterodimers.[18] EGFR homodimers are trafficked via endocytosis at a higher rate than its heterodimers[17] and so preferential recruitment of EGFR homodimers might result in increased receptor internalization and degradation.[18]

Bivalent dimers of EGF-NRG would bring together HER1-HER3 or HER1-HER4 heterodimers and would likely give rise to canonical HER1 signaling through STAT3 as well as HER3 mediated PI3K signaling.[19] The phenotypic outcomes resulting from this type of stimulation will likely depend on the relative expression levels of the various HER receptors with respect to each other.

The EGF-NRG bivalent ligand may reduce the mitogenic signaling that arises from the free association between HER2 and HER3 that normally occurs in cells expressing high amounts of these receptors.[20] The HER2-3 heterodimer is the most potent mitogenic pair in certain tumor cell types,[21] hence inhibiting heterodimerization with N-N bivalent ligands may have therapeutic potential.

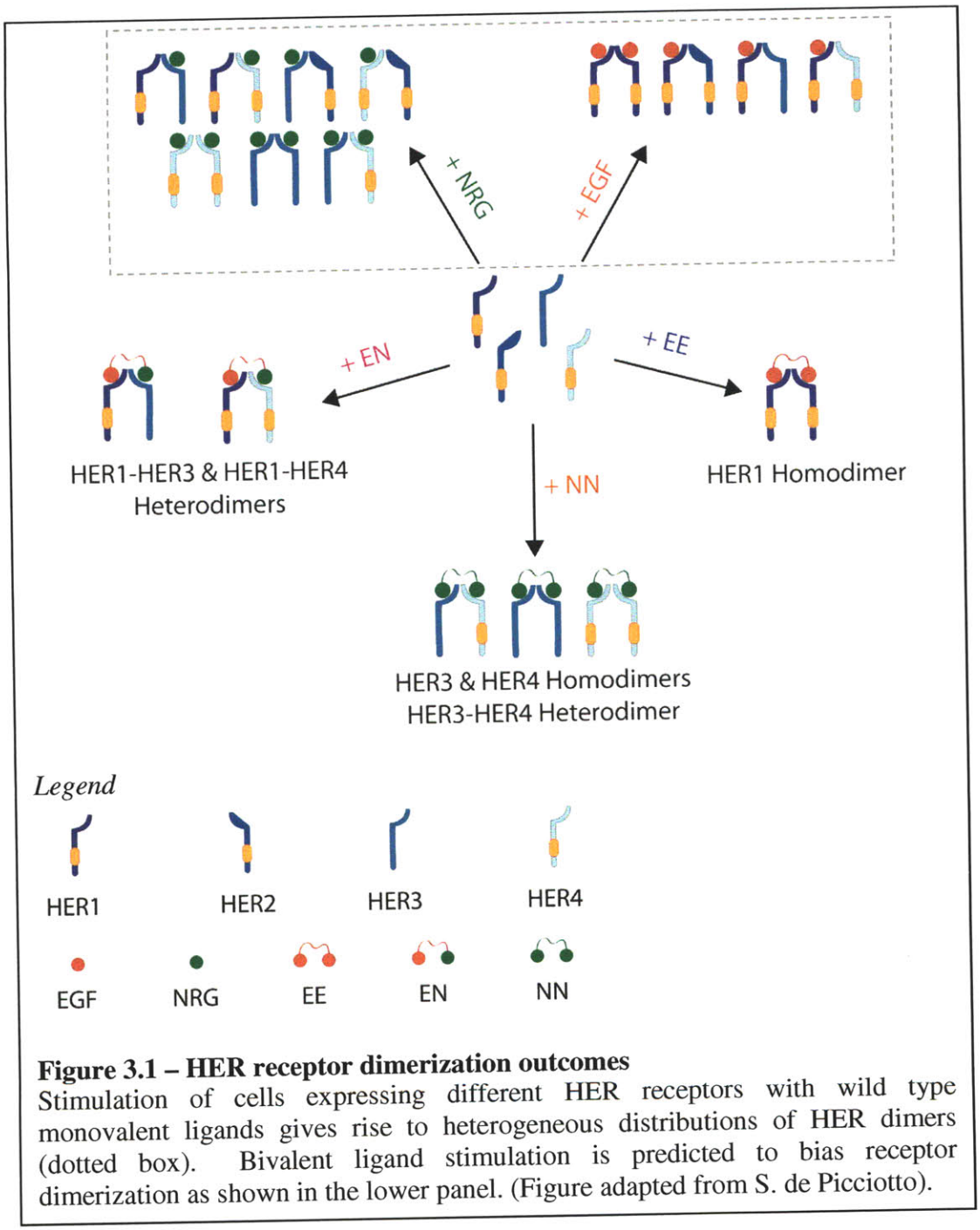

Figure 3.1 – HER receptor dimerization outcomes
Stimulation of cells expressing different HER receptors with wild type monovalent ligands gives rise to heterogeneous distributions of HER dimers (dotted box). Bivalent ligand stimulation is predicted to bias receptor dimerization as shown in the lower panel. (Figure adapted from S. de Picciotto).

Stimulation of cells expressing HER3 along with EGFR or HER2 and lacking HER4 using the N-N homodimer is expected to silence HER3-mediated signaling because HER3 receptors are kinase deficient and must heterodimerize to signal. As NRG also binds with high affinity to HER4, stimulation of cells expressing both HER3 and HER4

(a relatively uncommon situation) will have a complex response that might be parsed using inhibitors that block binding to HER4.

Finally, the effects of dimer ligands are likely to depend on dose in a complex manner. Although we expect the ligands to bind in bivalent fashion at low ligand concentrations, at concentrations an order or magnitude or more above K_D and where ligand is in great excess over receptor they may bind in monovalent fashion. Under such circumstances, the ultimate cell response may still be different than that observed for binding of true monovalent ligand, as the bivalent ligands may influence interactions with other receptors, internalization, or other events.

3.1.2 Rationale for Choice of Cell Lines used in Signaling and Phenotypic Studies

The primary motivation for work conducted in this thesis is manipulation of EGFR family signaling to influence regenerative responses of mesenchymal stem cells (MSC). Signaling by members of the EGFR family has been implicated in numerous facets of bone development, homeostasis, and regeneration.[22] Human MSC, even very early after isolation from marrow, express EGFR, HER2, and HER3 but no detectable levels of HER4.[23] The expression levels of EGFR family members in both an hTERT-immortalized human MSC line and in primary bone marrow-derived MSC are relatively low and regulated by culture conditions: EGFR is expressed at 5,000- 10,000 copies per cell, HER2 at about half the level of EGFR, and HER3 at low but detectable levels.[19, 23] It is expected that all monovalent and bivalent NRG stimulation acts through HER3, as MSC do not express detectable levels of HER4. Hence, in MSC, we expect that all three bivalent ligands – EE, EN, and NN – will exert different effects than their monovalent

counterparts through biasing EGFR homodimers at the expense of EGFR-HER2 heterodimers (EE), inhibiting HER3 signaling by preventing heterodimerization with HER2 or EGFR (NN), and driving EGFR-HER3 heterodimers at the expense of the more highly favored HER3-HER2 heterodimers (EN). Phenotypic responses of MSC to EGFR family ligands include colony formation, survival, growth, migration and differentiation. Although the MSC system is attractive for regeneration medicine, it has limitations for exploring the effects of bivalent EGFR family ligands on cell signaling and phenotypic responses. Many phenotypic responses have been studied; however, relatively few investigations have focused on EGFR family-mediated signaling in MSCs. Because these cells have relatively few receptors, some signaling responses may be at the limit of detection with available reagents, even though phenotypic responses are robust. The relative paucity of receptors is also representative of only one end of the spectrum of parameter space of interest – cells with one or more EGFR family members highly expressed may represent a different regime of balance between binding and signaling phenomena by virtue of having a different dynamic equilibrium among dimer states.

Therefore, in addition to analyzing responses in human MSC, we investigated responses in two epithelial tumor lines that express select EGFR family members at relatively high levels and have well-characterized EGFR family-mediated behaviors. HeLa cells, a cervical cancer-derived line that is often used as a model of EGFR-mediated signaling, have relatively high EGFR and HER2 expression (~50,000 surface receptors for both EGFR and HER2) with robust response to EGF treatment and low HER3 and HER4 expression with weak response to NRG treatment.[24] Because HeLa cells express roughly comparable levels of EGFR and HER2, and EGFR-HER2

heterodimers signal more robustly for growth than do EGFR-EGFR homodimers, HeLa cells would likely respond to EE ligand dimers by exhibiting both a HER2 phosphorylation level and a level of proliferation that is between monomeric EGF-stimulated and completely unstimulated HeLa cells. Thus HeLa cells are well suited to characterize bivalent ligands which contain EGF.

As a model cell system for analyzing cell responses to bivalent ligands containing NRG, without confounding effects of high EGFR expression, we use the mammary tumor line MCF-7, which express HER3 at relatively high levels, and EGFR at relatively low levels (<5000 EGFR/cell). MCF7 cells also express low levels of HER2 and HER4, exhibit a robust response to NRG stimulation, and have well characterized HER3 signaling pathways. Because MCF7 express HER4, and antibodies that block NRG binding to HER4 are available, these cells represent an especially useful model to screen primary phenomena occurring during stimulation with NRG-containing bivalent ligands. It is expected that MCF-7 and other HER3-dependent cancer cell lines may respond to N-N ligand dimers by forming HER3 homodimers thus becoming quiescent or apoptotic due to the kinase deficiency of HER3 and sequestration of HER3 receptors into silent complexes; this effect would likely be mitigated in cells (such as MCF7) that also express HER4.

3.2 Materials and Methods

3.2.1 Cell Culture

Human telomerase reverse transcriptase (hTERT)-immortalized human Mesenchymal Stem Cells (hTMSC) were a gift from Dr. Junya Toguchida (Kyoto University, Kyoto, Japan). HeLa cells were obtained from (ATCC). HeLa and htMSCs were maintained in Dulbecco's modified Eagle's medium (DMEM) containing: 10% fetal bovine serum (FBS), 1% L-glutamine, and 1% penicillin/streptomycin at 37°C, 95% humidity, and 5% CO2. MCF7 cells were maintained in phenol red free medium of the same composition and under the same incubation conditions. For single-cell migration studies, hTMSCs were maintained in a DMEM medium containing: 0.5% dialyzed fetal bovine serum (FBS), 1% L-glutamine, and 1% penicillin/streptomycin at 37°C, 95% humidity, and 5% CO2.

Cells were washed with PBS at 37°C and trypsinized. Once the cells had detached, trypsin action was blocked by adding growth medium. Cell solution was then centrifuged for 3 minutes at 500rpm at 4°C. The solution was then aspirated and the pellet was resuspended in quiescent medium – Dulbecco's modified Eagle's medium (DMEM), 0.5% dialyzed FBS (dFBS), 1mM pyruvate, 1mM L-glutamine, 1 μM nonessential amino acids, and 100 units/ml penicillin-streptomycin (Invitrogen) – to obtain a concentration of 300'000 cells per ml. In a twelve-well plate, 1 ml of cell solution was added per well (area is 3.8 cm^2). After 16-20 hours, medium was aspirated and replaced with stimulation medium (quiescent medium containing ligand at known concentration). The ligand solutions were prepared just before stimulation and

maintained at 37°C. After stimulation the lysates were collected according to phophoprotein assay protocols (described in the next section).

3.2.2 Phosphoprotein Assays

Cell signaling data of common nodes (pERK1/2, pEGFR, pHER3, pHER3, pHER4, etc.) were collected using standard immunobloting, in-cell western, or Luminex assay (Biorad). Immunoblotting was performed by normalizing cell lysates to total protein content as determined by BCA assay (Pierce) and running on SDS-PAGE 4-12% tris-acetate gels (Invitrogen). These were transferred to nitrocellulose then probed with corresponding primary antibodies (9106 pERK, 2236 pEGFR, 4791 pHER3, 4757 pHER4, Cell Signaling) and secondary IR-Dye conjugate antibodies (IR-Dye700/800, Rockland). Membranes were scanned using a Licor Odyssey IR scanner (Licor Systems, Inc.). In cell western analyses were similarly performed in black-walled 96 well plates and using correspondingly higher dilutions of antibodies.

Novagen bead kits were used for phosphorylated HER2 (pTyr) and total EGFR and HER2 determination (EMD Sciences), and Bioplex bead kits were used for phosphorylated ERK½ (Thr_{202}/Tyr_{204}, Thr_{185}/Tyr_{187}). Phosphorylated EGFR (pTyr) determination was performed with Bioplex bead kits for dose responses and with Novagen bead kits for time courses. The fluorescent beads are coated with antibodies that bind target proteins in cells lysates and the assays are designed to work with a Bioplex 200 System (BioRad, Luminex technology). Linearity of the pTyrEGFR and pERK½ Bio-Rad assays was checked using varying ratios of stimulated lysates from hTMSC and results were used to determine the optimal loading per well. For phosphoprotein detection

10 μg of protein lysates and 5 μg for total protein detection from each sample were incubated overnight in filter plates (Millipore) with the appropriate antibody-bead conjugates. Unbound proteins were washed away by vacuum filtration of the plate, trapping the beads in the well. Beads were rinsed with vendor-supplied buffers and incubated with a biotinylated antibody specific for a second epitope on the target. Beads were rinsed again and incubated with streptavidin phycoerythin (Strep-PE), fluorescently tagging the antibody bound to the second epitope. The beads are intrinsically fluorescent at a wavelength matched to the target protein in the Bioplex software, hence, intensity of PE fluorescence relative to the fiduciary fluorescence of the bead allows quantification of the target protein. Total EGFR and HER2 fluorescence was normalized to a standard curve generated with increasing concentrations of the extracellular domain of EGFR provided by the manufacturer (Novagen). Phosphorylated protein signals were normalized to the signal of an unstimulated lysate for the time course experiments.

3.2.3 In vitro inhibition experiments.

Low passage MCF7 cells (ATCC) were plated into 12 well plates at 250,000 cells per well in serum containing medium and incubated for 48 hours. Cells were then serum starved for 5 hours prior to ligand treatment. Inhibition experiments which blocked HER4 with anti-HER4 antibody clone H4.72.8 (Millipore # 05-478) were pretreated with 10 uM antibody 30 minutes prior to subsequent treatments. IC50 measurements were made by dosing cells with concentrations of bivalent NRG ligand (C34) in the range of 1 uM to 1 fM for 10 minutes followed by a pulse of 3 nM NRG for an additional 10 minutes (this dose of NRG and endpoint time were validated by generating a NRG dose response curve for MCF-7s in the concentration range 1 uM to 1 fM for 20 minutes. 3nM

NRG was the lowest dose that produced near maximal pERK signal at 20 minutes, data not shown). Following all stimulation experiments cells were placed on ice, medium aspirated, washed with ice cold PBS, and lysed with lysis buffer Calbiochem # FNN0011; 10 mM Tris, pH 7.4, 100 mM NaCl, 1 mM EDTA, 1 mM EGTA, 1 mM NaF, 20 mM Na4P207, 2 mM Na3VO4, 1% Triton X-100, 10% glycerol, 0.1% SDS, 0.5% deoxycholate, 1 mM PMSF, protease inhibitor cocktail (Sigma Cat. # P-2714) and two phosphatase inhibitor cocktails (Sigma Cat. #P28504 and P5726).

3.2.3 Cell Survival and Apoptosis Assays

MCF7 cells were treated as described above an evaluated for viability at various timepoints post treatment. Cells were subjected to either a flow cytometric assay to measure the PI positive population or terminal deoxynucleotidyl transferase dUTP nick end labeling (TUNEL) staining. PI staining was performed by diluting PI in growth medium following resuspension of trypsinized cells from each condition. Cells were then directly read on an Acuri Flow cytometer. Unstained MCF7 cells were used as a negative control to set the analysis gate and calculate percent PI positive. TUNEL staining was performed on cells according to the manufacturer's instructions (Trevingen).

3.2.4 Migration Assays

Transwell Assays

HTS Fluoroblock transwell well chambers (Beckton Dickinson) for a 24 well plate format were seeded with hTMSCs in expansion medium supplemented with mitomycin-c. After seeding and attachment for 2 hours the chambers were transferred to

their respective conditions and cells were allowed to migrate for 12 hours. At the end of the experiment the upper chambers were transferred to 4% formaldehyde, washed twice in PBS then incubated in Sytox-16 nuclear stain (Invitrogen) for 15 minutes. These were again washed with PBS then placed in a clean 24 well plate and read using a SpectraMax M2e multi-well fluorescent plate reader (Molecular Devices Corp.CA, USA). A standard curve correlating fluorescence with cell number was obtained by plating known numbers of cells in a 12 well plate in culture medium containing mitomycin-C (Calbiochem). Standard cell numbers were confirmed by a ViCell hemacytometer (Beckman-Coulter) (data not shown).

3.2.5 Time Lapse VidoMicroscopy Assays

Surface Preparation

A solution of 3 ug/mL of human fibronectin (FN, Sigma) in PBS was used to coat the bottom of a glass-bottom 24-well plate (MatTek) for 2 hours at room temperature, followed by two PBS washes. A 1% (w/v) of BSA solution was then added to each well to block any uncoated regions on the glass for 1 hr at room temperature. Each well was then washed three times with PBS, and the plate was then UV-sterilized for 30 min.

CMFDA-Cell Tagging

A 1 μM solution of CellTracker Green (5-Chloromethylfluorescein diacetate) from Molecular Probes (Invitrogen) was made by adding 10 uL of stock CMFDA (1 mM) to 10 mL of a serum-free DMEM media containing: 1% L-glutamine, and 1% penicillin/streptomycin. A 70-80% confluent htMSC petri dish washed with 10 mL of

sterile PBS followed by the addition of 10 mL of the CMFDA-containing serum-free DMEM media. Cells were then incubated at 37°C, 95% humidity, and 5% CO2 for 20 minutes. CMFDA-containing medium was then aspirated and replaced with 10 mL serum-free DMEM media and incubated (37°C, 95% humidity, 5% CO2) for 30 minutes. Cells were then washed with sterile PBS followed by treatment with 5 mL of trypsin (1X) solution. Upon cell detachment, adding 10 mL of growth medium blocked trypsin action, and cell solution was spun down at 1000 rpm for 5 minutes. Growth media was then aspirated and cell pellet was resuspended in 5 mL of quiescent media. Cell solution was counted and diluted in quiescent media to give a concentration of 4000 cells per mL. In a 24-well plate, 1.5 mL of cell solution was added per well to seed about 6000 cells per well or about 5000 cells per cm^2. Cells were allowed to seed for 16-24 hours at 37°C, 95% humidity, 5% CO2 conditions. After initial seeding time, medium was aspirated and replaced with stimulation medium (quiescent medium containing ligand at known concentration). The ligand solutions were prepared just before stimulation and maintained at 37°C. Stimulation was carried out for 6 hours before beginning imaging.

Time-lapse Microscopy and Data Analysis

To generate time-lapse movies of cells migrating on the 2D FN coated surfaces, GFP-widefield images were taken every 10 min for 12 h using a BD CARVII spinning disk confocal with an Axio Observer Zeiss microscope equipped with environmental control (37°C, 95% humidity, 5% CO2). Cells were imaged using a field of view of 1306 x 13006 um with 2.551 x 2.551-um pixels. All movies with the slightest drifts in x or y-direction were assessed and were not included for further analysis. Imaris (Bitplane,

Zurich, Switzerland) was used to visualize the 2D time-lapse images. The spots function was used to calculate centroids of fluorescent CMFDA-htMSCs and migratory tracks of individual cells were generated by using the Brownian motion tracking algorithm previously described (H.-D. Kim et al, 2008). All generated tracks were then manually verified for accuracy and modified when the automated logarithm presented errors. Cells undergoing division, death as identified as the release of fluorescence, or blebbing were not tracked. Additionally, cells were seeded on a surface at a low density to minimize any cell-to-cell contact. Wind-Rose plots were generated from the tracks produced from randomly choosing 50 tracks from the motile population and overlaying the starting coordinates at the origin of the plots to graphically represent average cell dispersion during migration. Only tracks longer than 2 hrs that had migrated independently without physical contact with other cells were used for the calculation of directional persistence. To calculate cell speed cell tracks were used as long as their migration was independent of any physical contact with other cells and no cell death or division occurred during their tracks. Average individual speeds (S) were calculated from individual cell tracks by averaging the distances over the time interval. Mean squared displacements(MSD), $\langle d^2 \rangle$, at various time intervals (t) were calculated using the method of nonoverlapping intervals (Dickinson and Tranquillo, 1993) and directional persistence time (P) was obtained by fitting data to the persistent random walk model (PRW):

$$\left\langle d^2 \right\rangle = 2S^2 P\left[t - P\left(1 - e^{-\frac{t}{P}} \right) \right] \qquad (3.1)$$

3.3 Results

3.3.1 Activation of EGFR and Erk1/2 Signaling by Bivalent EGF-containing Ligands

We first examined the dose response for activation of EGFR in hT-MSC by the bivalent ligands EE and EN, using a pan-phospho antibody. Stimulation by EGFR by canonical ligands such as EGF typically leads to a dramatic increase in pEGFR within a minute, peaking in the first few minutes, and a slow decay over 1-2 hr, as we have previously illustrated for stimulation of hTMSC. Hence, to assess dose-response, we measured pY-EGFR after 1 min and 15 min of stimulation by EE or EN (Fig 3.2). The data are best fit with a two parameter model including a Hill coefficient as shown in equation 3.2, where L is the ligand concentration and EC50 is a parameter representing the dose of ligand which produces a half maximal response.

$$\Theta = \frac{L^2}{L^2 + EC50} \qquad (3.2)$$

yielding an EC_{50} of 10 nM for stimulation by EE at both the 1 min and 15 min time points (Fig 3.2). This value is slightly higher than the EC50 for wild type EGF. At equimolar concentrations of bivalent ligand (which results in half the concentration of E ligand for the case of EN compared to EE), EN stimulates only a fraction (at most, half) of the signal of EE for pY-EGFR at both 1 min and 15 minutes post-stimulation, up to ligand concentrations of 100 nM. To interpret these results, we consider the different ways that EE and EN ligands can activate EGFR in the context of hTMSC, which are

known to express about 10,000 EGFR, 2,000 HER2, moderate levels of HER3 and no HER4 . Options for bivalent EE ligand include: (i) bivalent EE binds to individual EGFR and acts essentially through only one EGF moiety, allowing both EGFR homodimers and EGFR-HER2 heterodimers to form (ii) bivalent EE binds to EGFR and either stabilizes pre-formed homodimers or drives homodimerization to the exclusion of heterodimerization with HER2 (iii) bivalent EE ligand binds to individual EGFR through a single EGF as described in *(i),* and two such individual, bivalent ligand-occupied receptors homodimerize, allowing recruitment of additional free EGFR into oligomers which may also include HER2.

In all of these scenarios, it is theoretically possible for essentially all cell surface EGFR to bind ligand and become phosphorylated, through interactions with other ligand-bound EGFR or with HER2. It is possible that dimer ligands may alter the kinetics of phosphorylation/dephosphorylation compared to wtEGF, by imposing steric constraints on the receptors, fostering different ratios of homo and heterodimers, or altering the ability of the EGFR to interact with other cell surface receptors that are implicated in transactivation. The theorectical limit of EGFR-HER2 heterodimers in these cells is about one third of total possible EGFR in heterodimers when all EGFR are occupied and dimerized (i.e., 2000 heterodimers and 4000 homodimers). Further, differences in the relative phosphorylation of particular phosphosites may be affected by the receptor dimer composition.[25]

Using a similar analysis for the binding of bivalent EN, the possibilities are that (i) bivalent EN binds to individual EGFR and acts essentially through only one EGF moiety, allowing both EGFR homodimers and EGFR-HER2 heterodimers to form (ii)

bivalent EN binds to EGFR and drives heterodimerization with HER3 to the exclusion of heterodimerization with HER2 (iii) bivalent EN ligand binds to individual EGFR through a single EGF as described in (i), and two such individual, bivalent ligand-occupied receptors homodimerize, allowing recruitment of HER3 into oligomers which may also include HER2; (iv) bivalent EN binds to HER3 via a single NRG moiety, allowin HER2-Her3 heterodimerization and possibly oligomerization, as well as HER3-Her3 homodimerization (v) bivalent EN binds to individual EGFR or HER3 but heterodimers are sterically inhibited from forming.

If scenario (i) were predominant, we would expect similar responses from EE and EN, presuming similar receptor-ligand affinities. The degree to which HER3 acts as a "sink" as described in scenario EN (iv) or (v) is difficult to estimate precisely, because the total number of HER3 relative to EGFR is unknown in these cells (presumed to be <10,000), but is a plausible explanation for the effects observed. A more tenuous explanation is that EGFR-HER3 heterodimers are relatively ineffective in these cells at phosphorylating EGFR. Finally, we used a pan-pY antibody to assess phosphorylation. It is also possible that the antibody reacts with different affinity to different pY sites on the EGFR, or that more than one antibody can bind to a single pYEGFR if it is phosphorylated on different sites, so that different patterns of pY on EGFR might result in different signal strength even if the total number of pYEGFR is the same.

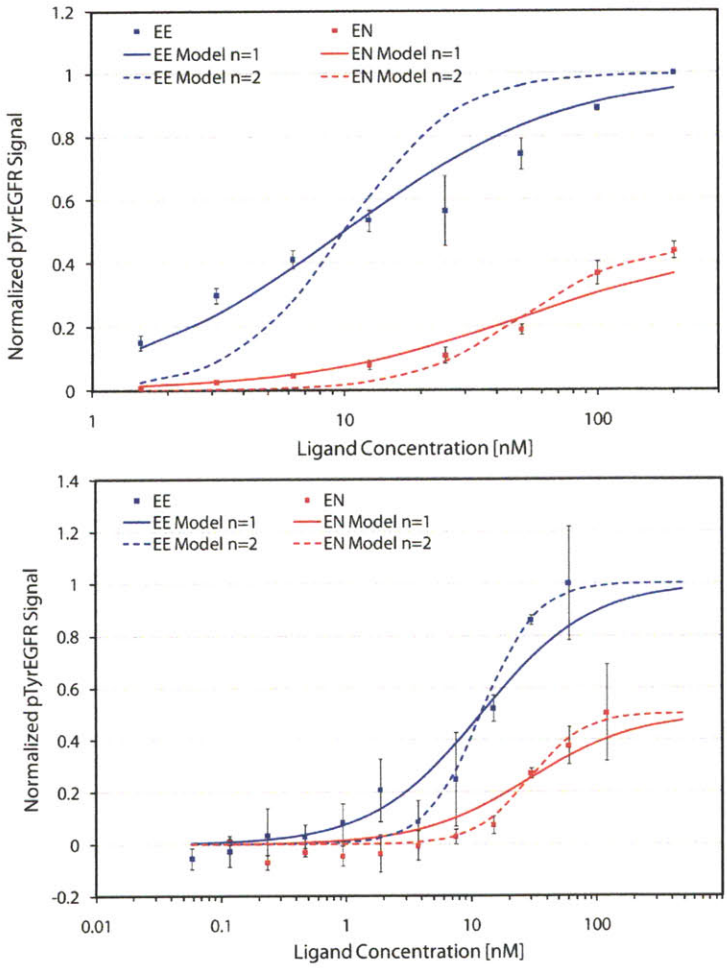

Figure 3.2 – pTyrEGFR dose-response for EE and EN at 1 and 15 minutes
hTMSC were stimulated for 1 (A) or 15 minutes (B) with serial dilutions of EE (blue) or EN (pink). Lysates were collected according to BioRad protocol and pTyrEGFR fluorescence levels were measured by luminex technology as described in the materials and methods section. Data were normalized by the average signal of the maximum EE concentration. The experimental data were fitted to a Hill-function of first (solid line) and second-order (dashed line). For EN, the model was weighted by the signal ratio at maximum concentration. At 15 minutes the models plotted here have an EC50 of 10 nM for EE and 50 nM for EN. Data are shown from n=3 biological replicates. (figure courtesy of S. De Picciotto)

With the pY-EGFR dose-response in hand, we next examined the time course of EGFR and HER2 activation using WT EGF and bivalent EE, under conditions of comparable

EC_{50} and under conditions that should saturate the EGFR (i.e., concentrations 3-10 fold above EC_{50}).

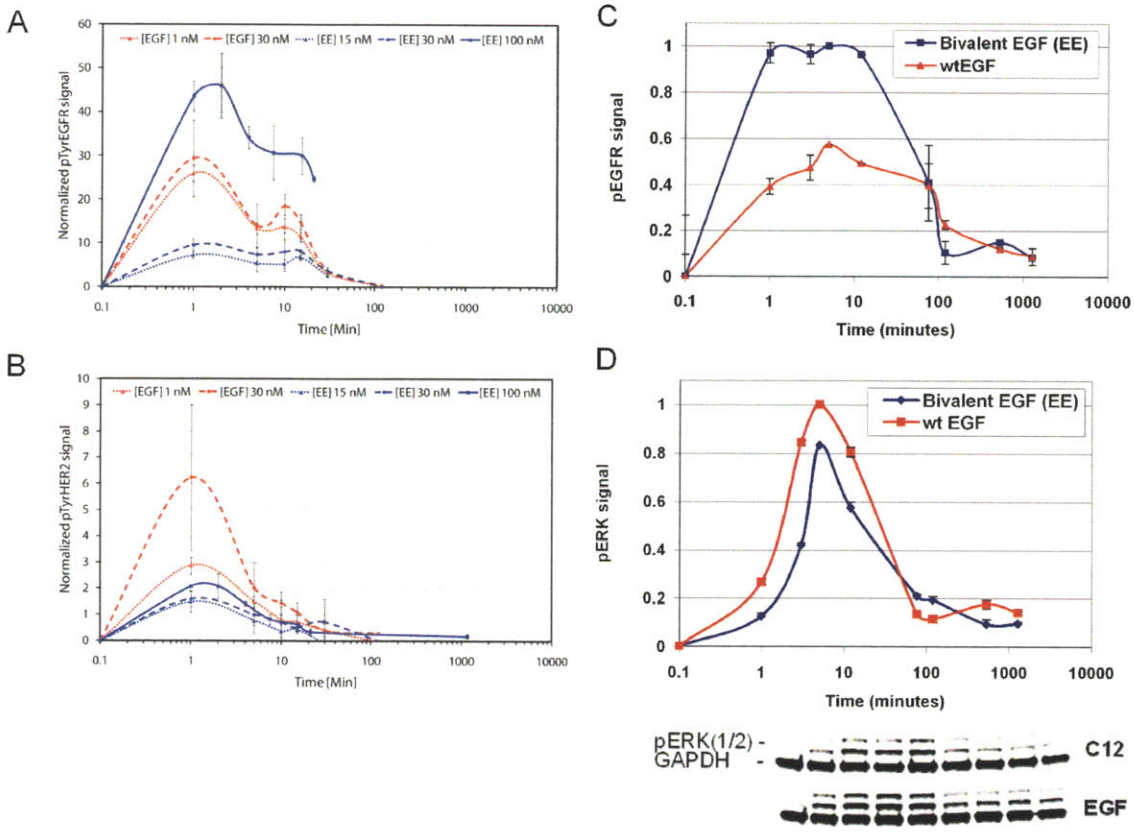

Figure 3.3 – Time course of EE and EGF stimulation
Data plotted in red are EGF-stimulated and in blue are EE-stimulated. A&B) Time course of bivalent EGF ('EE') and wtEGF stimulation in hTMSC cells. Lysates were collected according to Novagen protocol and pTyrEGFR (A) and pTyrHER2 (B) fluorescence levels were measured by luminex technology as described in section 3.4. The figure represents normalized levels of pTyrEGFR and pTyrHER2 with respect to an unstimulated control. Data are shown with n=3 biological replicates. C&D). Time course of bivalent EGF ('EE') and wtEGF stimulation in HeLa cells at 100 nM. Errors are (+/-) standard error of the mean for n = 2 independent experimental replicates. (figures A and B courtesy of S. De Picciotto)

For the EE saturating concentration we chose 100 nM because it is 3 times higher than the EC_{50} of EE. For EGF we used 30 nM which is 30 times above its EC_{50}, therefore signal maximum should be achieved, also this concentration is the same as the EC_{50} of

EE, thus we also have a means in each case of comparing EE and EGF at equimolar concentrations. Finally, we stimulated the cells with 15 nM of EE because in this case the number of EGF molecules (2 EGF molecules in EE) would be identical to 30 nM of EGF, and with 1 nM EGF (EC50 of wtEGF).

From the data shown on figure 3.3 (A) and 3.3 (B), comparing each condition at equimolar concentration, EGF-stimulated cells show both a stronger EGFR and HER2 phosphorylation than EE stimulated cells. However, for 100 nM EE stimulation (solid blue curve), the phosphorylated EGFR levels are considerably higher over the whole course of the experiment. Yet, this strong increase of phosphorylated EGFR for EE compared to EGF is not correlated with an increase in pTyrHER2 signal. Indeed, even at 100 nM EE, the phosphorylated HER2 signal is lower than that of 1 nM EGF.

Weaker HER2 activation with bivalent EGF, EE, indicates that HER2 might be prevented from dimerizing with EGFR by the bivalent EE ligand. At the saturating concentrations (i.e., concentrations of ligand several-fold excess above EC_{50}) we would expect all EGFR to be ligand-bound and phosphorylated, and thus expect comparable levels of receptor activation for WT EGF and for the bivalent EE at saturating conditions. The more robust phosphorylation signal for bivalent EE may indicate that EE alters phosphorylation patterns and/or renders pY-EGFR less susceptible to phosphatase activity.

It is notable that the pY-HER2 levels are significantly reduced for the bivalent ligand EE case. Taken together, the results in Fig 3.3A and 3.3B suggest that EE is capable of inhibiting EGFR-HER2 heterodimerzation, or at least, of allowing HER2 to become activated if such dimers form.

We further explored the kinetics of EGFR activation and downstream signaling using HeLa cells, as they express abundant EGFR and HER2. Using 100 nM EGF and EE a marked increase (almost two-fold) of EGFR phosphorylation is observed in the EE-stimulated case vs wtEGF over much of the early stimulation time course (<100 minutes). This observation suggests a differential effect exerted by EE vs wtEGF. Further characterization of trafficking and dephosphorylation of the various Her-receptor dimers would be required to definitively provide an explanation for these differences and.

Stimulation of EGFR prominently activates the downstream kinase pathway leading to Erk1/2, a key signaling node integrating multiple signaling networks.[17, 25] Interestingly, despite the more robust EGFR signal elicited by EE bivalent ligands compared to WT EGF (Fig 3.3C), activation of Erk1/2 is substantially lower for stimulation by EE compared to WT EGF (Fig 3C). This observation is consistent with previous findings by other groups which have shown reduced signaling potency of EGFR homodimers compared to EGFR-Her2 heterodimers . Taken together these data suggest that EE is able to bias EGFR dimerization toward homodimers compared to heterodimers.

3.3.2 Manipulation of EFGR Family Signaling Pathways with Bivalent NRG-Containing Ligands.

A major prediction of this work is that the bivalent neuregulin (NN) ligand should shut off NRG-mediated signaling in cells where HER3 is expressed and where HER4 is either not expressed or is able to be specifically excluded from binding NRG (e.g., through the use of blocking antibodies. Because HER3 is kinase-deficient, recruitment of

HER3 homodimers would produce a null signaling outcome. To assay this effect we used two cell types that have known HER3 and HER4 expression profiles; MCF7s known to express both HER3 and HER4; and htMSCs known to express only HER3. Signaling mediated by wtNRG is typically robust and can be readily detected by measuring pERK(1/2).

When hTMSC, which express HER3 but not HER4, are stimulated with monovalent engineered NRG1, a robust dose-dependent pERK response is observed that is similar for either configuration of the engineered ligand and similar to WT NRG1 (Fig 3.4). In stark contrast, stimulation with bivalent NN ligand appears to activate Erk1/2 modestly at low doses, but this mild effect is erased at higher ligand doses, suggesting that the bivalent NN ligand captures HER3 in homodimers - which are inherently incapable of downstream signal propagation.

Dose responses with bivalent EGF (EE) and mixed ligand EGF-NRG (EN) show a rightward shifted EC50 (mid nM) and a steeper response region consistent with bivalent avidity. A closer examination of the dose response curve and apparent avidity effects produced with bivalent ligands which do signal is given in later sections. One possible explanation for the rightward shifted EC50 is the exclusion of HER2 from receptor dimer complexes. Jones demonstrated that HER2 plays a role in increasing ligand binding affinity of both EGF to EGFR and NRG to HER3 (or HER4) and in the case of NRG lowered the EC50 by one order of magnitude, thus suggesting a stabilizing role for HER2, the exclusion of which could contribute to a reduction in apparent affinity as evidence by the rightward shifted EC50.

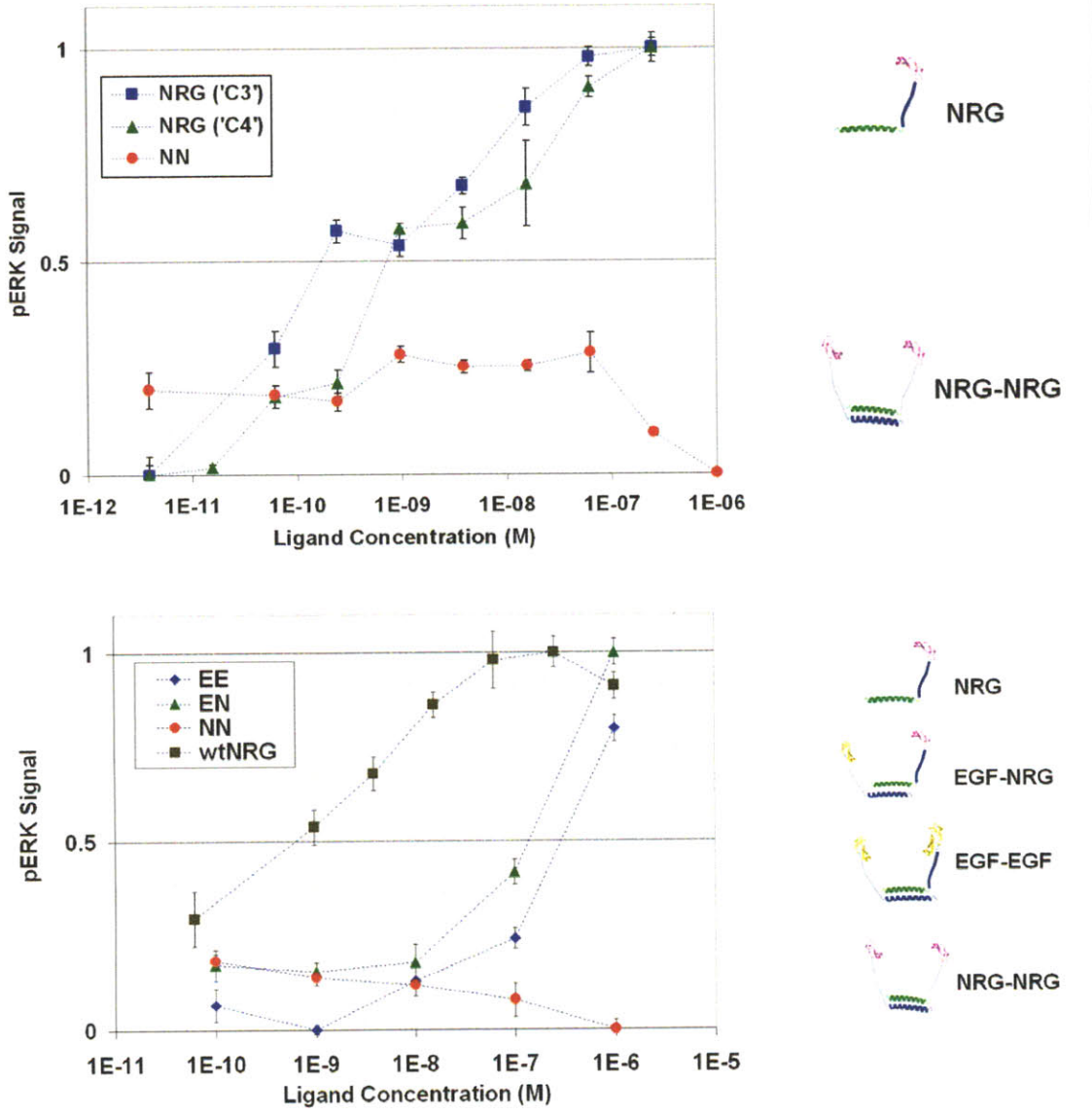

Figure – 3.4 Signal silencing in MSC cells with bivalent NRG (NN)
The effect of stimulating MSCs with a range of doses of various bivalent ligand combinations, including comparisons of NN signaling. Signal is measured as pERK(1/2) levels relative to unstimulated minima. Errors are (+/-) standard error of the mean for n = 3 independent experimental replicates

The ability of the bivalent NN ligand to silence signaling through HER3 suggested a possible therapeutic use in cancer cell signaling. We therefore investigated responses in a cancer cell line, MSCF, which expresses HER3 at a much more robust

level than hTMSC. Because MCF7 also express HER4, which also binds NRG1, they are a reasonable model for analyzing the effects of co-expression of Her 4. Figure 3.5 depicts data from an inhibition experiment where bivalent neuregulin (NN) is used to inhibit signaling in a dose dependent manner versus a 3 nM wtNRG challenge. Signal silencing is mediated by the putative recruitment of HER3 homodimers to produce a silent phenotype.

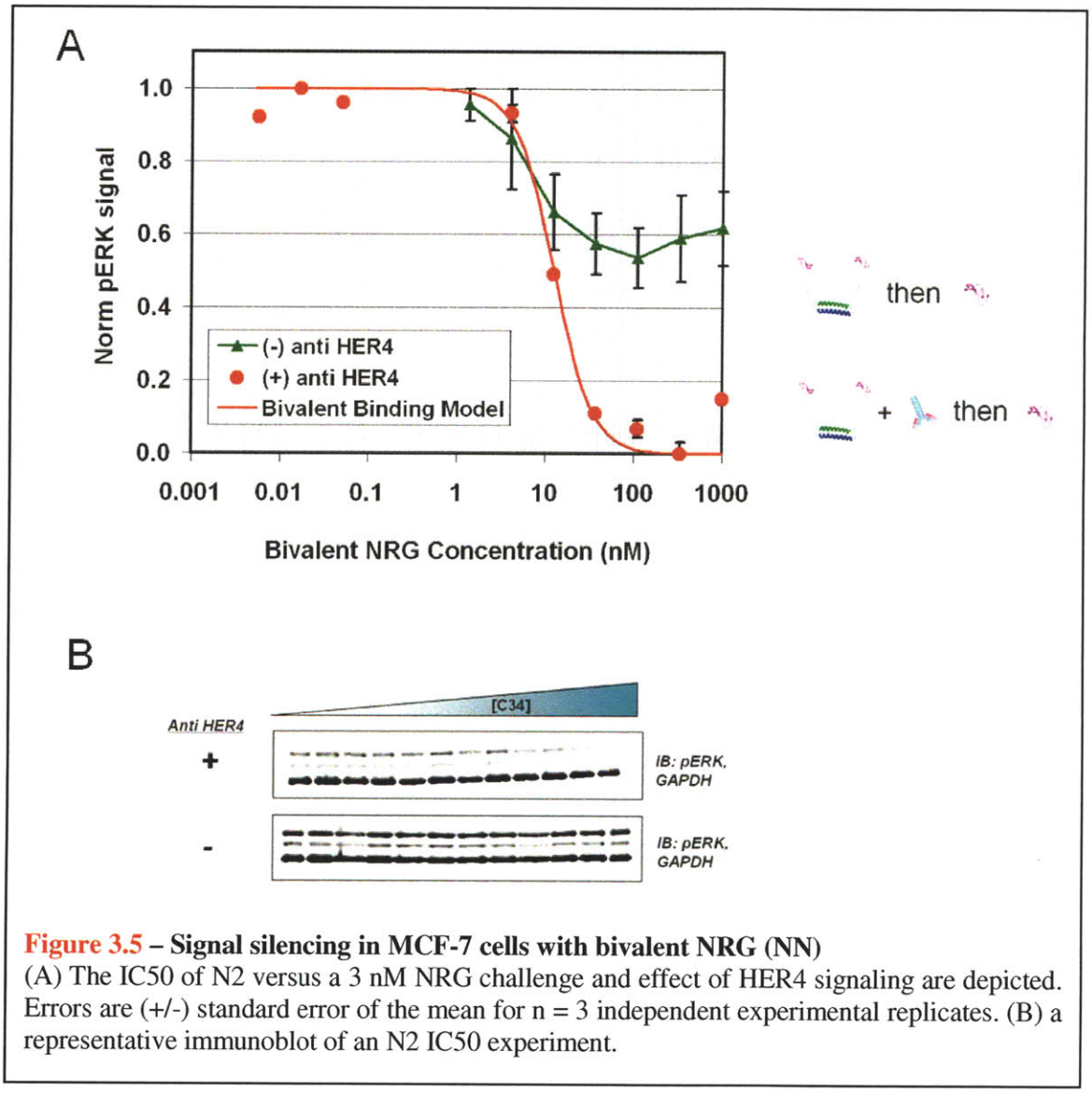

Figure 3.5 – Signal silencing in MCF-7 cells with bivalent NRG (NN)
(A) The IC50 of N2 versus a 3 nM NRG challenge and effect of HER4 signaling are depicted. Errors are (+/-) standard error of the mean for n = 3 independent experimental replicates. (B) a representative immunoblot of an N2 IC50 experiment.

Pretreatment of MCF7s with an anti-HER4(ECD) antibody specifically excludes HER4 from ligand binding and thus excludes HER4 from participating in signaling following wtNRG stimulation. Absence of anti-HER4 antibody pretreatment reconstitutes wtNRG-stimulated signaling. The NN inhibition curve (circles) was fit with a second order model to yield an IC50 of 12 nM and a Hill coefficient of n=2, which is indicative of bivalent avidity.

Taken together, results from time course experiments in HeLas and inhibition in MCF7s indicate that bivalent ligands may recruit respective HER receptors into dimeric complexes of known composition and more importantly produce expected signaling outcomes consistent with known mechanisms of ligand binding and receptor dimerization.

3.3.2 Stimulation of MSC With Bivalent Ligands Influences Cell Migration

The effects of EGF family ligands on cell migration are well documented.[26] The stimulation of EGFR with EGF can give rise to increases in both speed and persistence. To screen bivalent ligands for possible effects on cell migration phenotypes, we used transwell migration assays. Transwell assays measure chemotactic migration and can give a rapid readout of ligand effects that arise from modulated speed or persistence. Although in a transwell experiment one cannot determine speed and persistence, modulation of these parameters would manifest itself as a difference in transwell migration. As seen in figure 3.6 monovalent ligands stimulate increased transwell migration by approximately 40% and 25% for EGF and NRG, respectively. In contrast all bivalent ligands produce reductions in transwell migration relative to an unstimulated

control. This is consistent with previous findings by Zhan et al. in which reduced migration is observed for cells in which the predominant signaling mode is through HER1 homodimers.[27, 28]

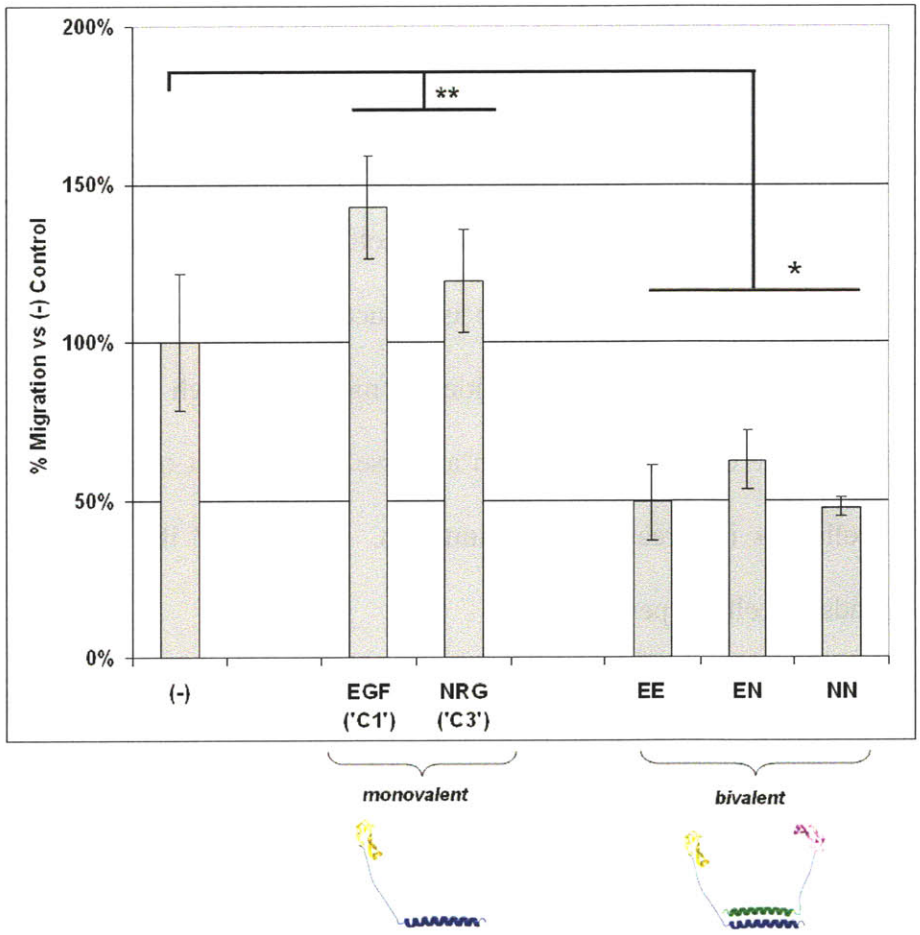

Figure 3.6 – Inhibition of cell migration with bivalent ligands versus natural ligand stimulation
Inhibition of cell migration with bivalent ligands forces HER1-1, HER1-3, and HER3-3 recpetor dimers versus natural ligand stimulation. Errors are (+/-) standard error of the mean for n = 3 independent experimental replicates *p=0.01, **p=0.05 vs (-) control; n=3; Error bars: 99% C.I. All ligands were dosed at 100 nM.

Although limited data are available on the effect of forced HER1-HER3 heterodimers on migration it appears that exclusion of HER2 from signaling complexes may contribute to this effect for all the bivalent ligand combinations studied here.

Reduced transwell migration of cells stimulated with bivalent ligands may result from the exclusion of HER2 from signaling complexes, as HER2 increases cell persistence.[29, 30] If this is the case then the physical parameters which underlie cellular motility should reflect this change. In the context of transwell migration the parameter of directional persistence can be expected to play an important role in the fate of a cell. It is reasonable to expect that a cell with reduced directional persistence would encounter a transwell pore with a different frequency than a cell with high directional persistence. If the frequency of encounters with a pore is reduced in cells with reduced directional persistence then the number of opportunities to migrate through a pore would also be reduced. In the case of a membrane with a sparse arrangement of pores relative to the number of cells this is a reasonable assumption. Figure 3.7 illustrates the effect of bivalent ligands on cellular persistence.

As expected, the bivalent ligands EN and NN appear to reduce the directional persistence of cells. In particular this effect appears to be dose dependent in the case of EN (figure 3.7, top), where the effect becomes statistically different than the control at the EC50 of EN. In the case of EN and NN the effect is equivalent in magnitude and appears to reflect the transwell migration results at the same dose (100 nM). The reduction in directional persistence at this dose is approximately 55% versus the unstimulated control. In terms of cell motility this means that a cell spends half as long moving in one direction and will explore a smaller area over long times than cells with higher persistence. By comparison the reduction in transwell migration was 50% for bivalent ligand stimulation at this dose.

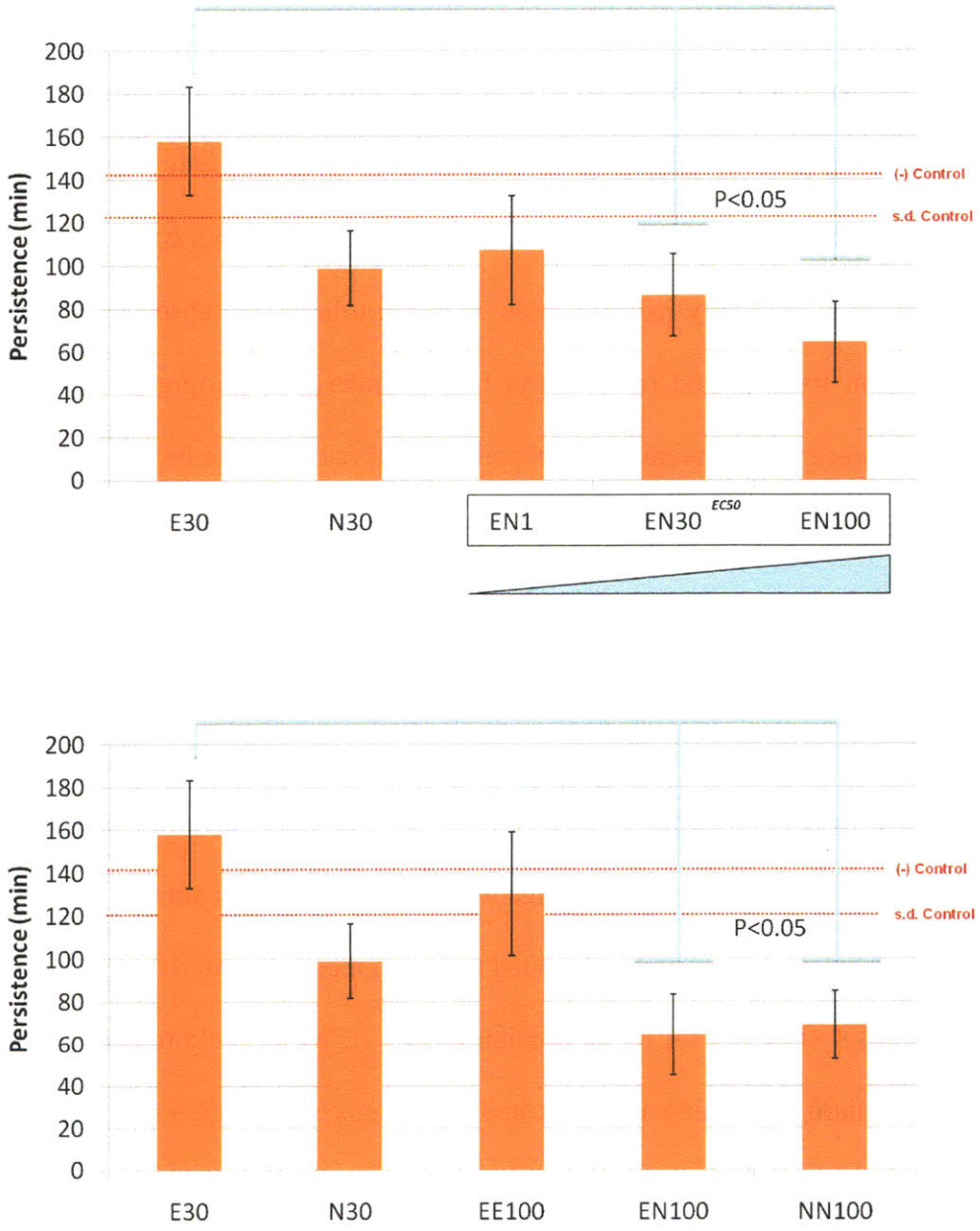

Figure 3.7 – Persistence analysis: time-lapse micrcoscopy of 2D cell migration
Bivalent ligand stimulation with EN results in reduced directional persistence that is dose dependent (top graph). Both EN and NN resulted in reduced directional persistence of approximately 55% vs the EGF stimulated condition (bottom plot).

3.3.2 Stimulation of Cells With Bivalent Ligands Influences Cell Survival and Proliferation

The human telomerase reverse transcriptase immortalized human mesenchymal stem cells used in the migration studies described above have been shown to survive serum free conditions for several days if cultured at sufficiently high confluence (>50%). While cell division is greatly reduced these cells can tolerate the absence of serum and remain quiescent for a period of 3-7 days before undergoing programmed cell death. This behavior presents a convenient breakpoint in cell fate that can be influenced by the addition of survival stimuli such as EGF or NRG. Previous work has shown that MSCs can be rescued from stressful or pro-death conditions by addition of EGF or NRG. The ability of wild type ligands to rescue MSCs from apoptosis during stressful conditions is mediated by signaling through the HER receptors which stimulates a number of pro-survival down stream effectors. Variation in cell survival outcomes resulting from stimulation with any of the bivalent ligands as compared to natural ligands would indicate modulated signaling, perhaps related to biased receptor dimerization.

Figure 3.8 shows a set of photomicrographs of MSCs cultured for 30 days in serum free medium containing the indicated conditions. Medium was changed every three days during the 30 day period. After a period of 10 days the wells containing EGF and EE showed early signs of apoptosis and reduced rates of medium acidification as evidenced by phenol red indicator color.

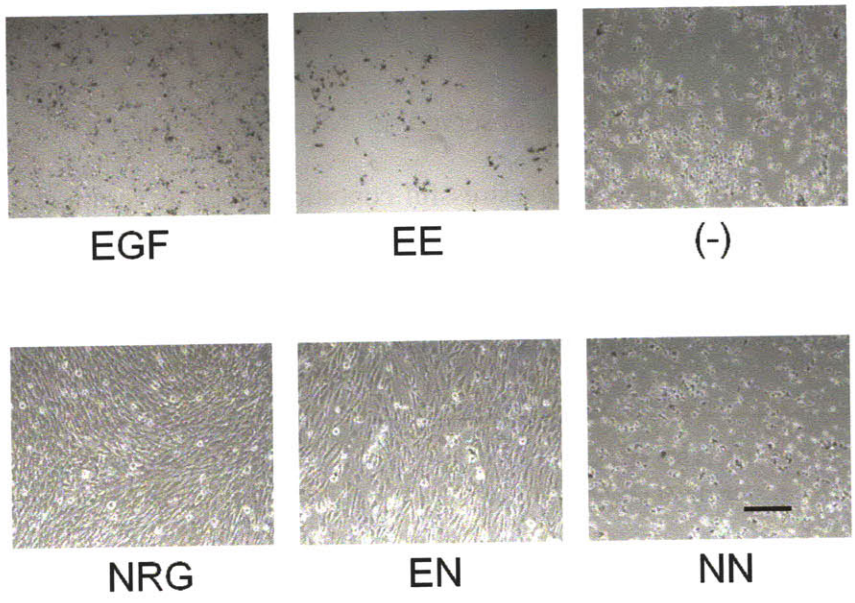

Figure 3.8 – Micrographs of cell cultures of htMSCs at 30 days
Stimulation with NRG and EN may promote viability in long term serum free cultures. EGF, EE, and NN consistently result in reduced viability under these conditions. The absence of viability in NN cultures corresponds with the expected outcome given the silencing of signaling. Comparison of (-) with NN illustrates the very similar outcomes. Scale bar is 100 μm.

After 14 days the wells containing NN and (-) showed similar characteristics. At 21 days the wells containing EGF, EE, NN, and (-) appeared to be completely dead and no longer caused changes in phenol red indicator. Wells containing NRG and EN showed a normal morphology and exhibited signs of metabolism by rapid acidification of medium. The addition of NRG appears to confer a survival advantage under these conditions which is consistent with previous findings. The addition of EN appears to recapitulate this effect even though the presence of an EGF moiety in the bivalent construct might be expected to counteract this effect based on the results from wild type EGF stimulation. More strikingly, the NN condition did not perform better than the (-)

control, a result which is entirely consistent with signaling the data showing no stimulation of pERK in MSCs with NN.

The inhibition of signaling observed in MCF7 cells should also produce a phenotypic survival differences under stressful conditions such as serum starvation. The same conditions described in figure 3.4 were used to replicate the signaling effect but were maintained for several days (48 to 96 hours, depending on the experiment).

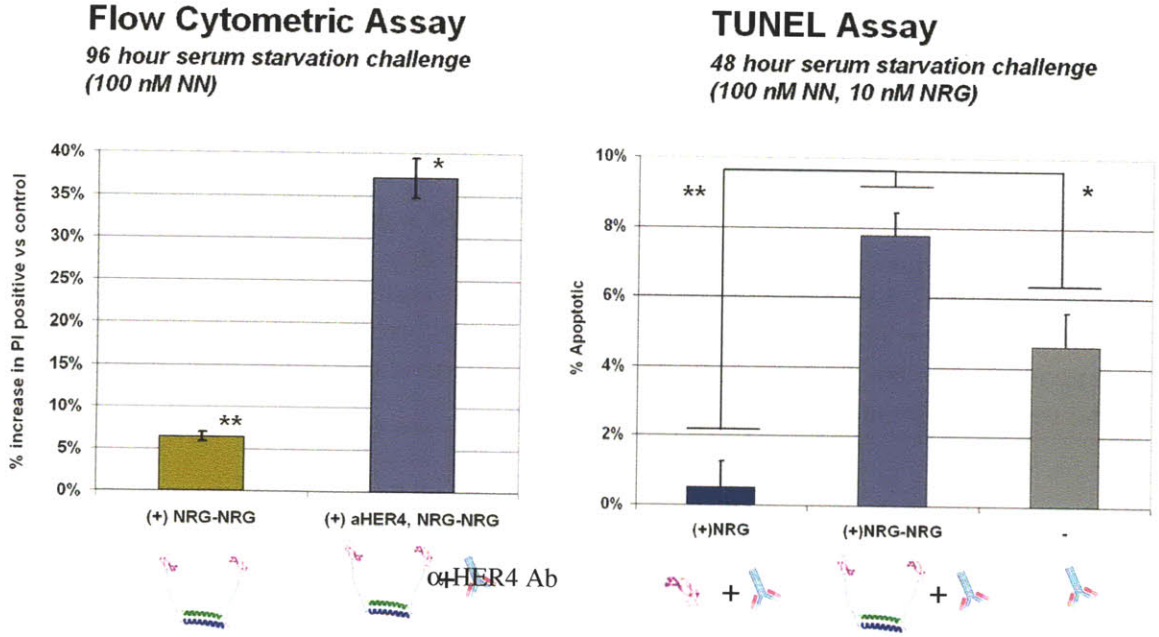

Figure 3.9 – Bivalent NRG effect on the survival of serum starved MCF7s
A significant increase in the %PI positive population of MCF7s results from treatment with bivalent NRG under conditions which lead to signal attenuation through the HER3 and HER4 mediated pathway. Likewise a significant increase in apoptotic (TUNEL positive) cells is seen by 48 hours under the same conditions. These results are suggestive of the proposed signaling attenuation mechanism. Left plot: *p=0.01 vs control (10 nM NRG), **p=0.02 vs control (10 nM NRG), n=3, (+/-) SEM; Right plot *p=0.009 NN vs (-) control, **p=0.001 NN vs 10 nM NRG; p=0.01 10 nM NRG vs (-), n=3, (+/-) s.d.

The extended time period under these conditions permits sufficient differences in survival to be detected. Two types of assays were performed to study this effect in MCF7 cells: a

cell permabilization assay which is a late marker of apoptosis and a terminal deoxynucleotidyl transferase dUTP nick end labeling (TUNEL) assay which measures breaks in double stranded DNA, a mid to late maker of apoptosis. In the cell permeabilization assay a total propidium iodide (PI) positive population is measured using flow cytometry and gives a relative measure of cell death. TUNEL labeling is more specific to apoptosis and gives a quantitative indication of cells undergoing programmed cell death. Figure 3.9 shows the results of these two assays for MCF7 cells cultured under the indicated conditions.

Imposing conditions which result in signal attenuation also result in increased cell death under serum starvation. An increase of 35% in PI% cells is seen over the control condition (figure 3.9, left). The exclusion of anti-HER4 antibody treatment allows NRG to rescue cells from death (7% PI+) and reflects the signaling data shown earlier. The TUNEL analysis shows the same effect. In this case the treatment that results in signal attenuation produces 8% apoptotic cells vs <1% in the positive control. Phenotypic results such as these agree well with the signaling data and support the proposed mechanism of signal attenuation. These data are highly suggestive of the exclusion of HER3 receptors from productive signaling complexes through the action of bivalent NRG.

3.4 Conclusions

In this chapter it has been shown that bivalent HER ligands produce different signaling patterns compared to their monovalent analogs. Current understanding of the activation mechanism of HER receptors is still incomplete yet the system described here may serve as a tool to elucidate some of these details. The results illustrated here demonstrated that differential bivalent ligand signaling data are reflected in phenotypic outcomes such as migration and survival. This could be of interest in applied contexts such as tissue engineering or cancer. Further work in developing bivalent ligands for the HER receptor system will likely yield valuable insights into this important regulator of cell behavior.

3.5 References

1. Yarden, Y. & Sliwkowski, M.X. Untangling the ErbB Signaling Network. *Nature Reviews - Molecular Cell Biology* **4**, 5 (2001).
2. Sliwkowski, M.X. et al. Coexpression of erbB2 and erbB3 proteins reconstitutes a high affinity receptor for heregulin. *Journal of Biological Chemistry* **269**, 14661-14665 (1994).
3. Ferguson, K.M. et al. EGF activates its receptor by removing interactions that autoinhibit ectodomain dimerization. *Molecular cell* **11**, 507-517 (2003).
4. Jura, N. et al. Mechanism for Activation of the EGF Receptor Catalytic Domain by the Juxtamembrane Segment. *Cell* **137**, 1293-1307 (2009).
5. Macdonald-Obermann, J.L. & Pike, L.J. The Intracellular Juxtamembrane Domain of the Epidermal Growth Factor (EGF) Receptor Is Responsible for the Allosteric Regulation of EGF Binding. *Journal of Biological Chemistry* **284**, 13570 (2009).
6. Red Brewer, M. et al. The Juxtamembrane Region of the EGF Receptor Functions as an Activation Domain. *Molecular Cell* **34**, 641-651 (2009).
7. Liu, P. et al. Investigation of the dimerization of proteins from the epidermal growth factor receptor family by single wavelength fluorescence cross-correlation spectroscopy. *Biophysical journal* **93**, 684-698 (2007).
8. Park, E., Baron, R. & Landgraf, R. Higher-Order Association States of Cellular ERBB3 Probed with Photo-Cross-Linkable Aptamers†. *Biochemistry* **47**, 11992-12005 (2008).

9. Szabo, A., Horváth, G., Szöll si, J. & Nagy, P. Quantitative characterization of the large-scale association of ErbB1 and ErbB2 by flow cytometric homo-FRET measurements. *Biophysical Journal* **95**, 2086-2096 (2008).

10. Tao, R.H. & Maruyama, I.N. All EGF (ErbB) receptors have preformed homo- and heterodimeric structures in living cells. *Journal of Cell Science* **121**, 3207 (2008).

11. Zhang, X., Gureasko, J., Shen, K., Cole, P.A. & Kuriyan, J. An Allosteric Mechanism for Activation of the Kinase Domain of Epidermal Growth Factor Receptor. *Cell* **125**, 1137-1149 (2006).

12. Witton, C.J., Reeves, J.R., Going, J.J., Cooke, T.G. & Bartlett, J.M.S. Expression of the HER1-4 family of receptor tyrosine kinases in breast cancer. *The Journal of Pathology* **200** (2003).

13. Penuel, E., Schaefer, G., Akita, R.W. & Sliwkowski, M.X. Structural requirements for ErbB2 transactivation. *Semin Oncol* **28**, 36-42 (2001).

14. Linggi, B. & Carpenter, G. ErbB receptors: new insights on mechanisms and biology. *Trends in Cell Biology* **16**, 649-656 (2006).

15. Sorkin, A. & Goh, L.K. Endocytosis and intracellular trafficking of ErbBs. *Experimental cell research* **314**, 3093-3106 (2008).

16. Haugh, J.M., Schooler, K., Wells, A., Wiley, H.S. & Lauffenburger, D.A. Effect of epidermal growth factor receptor internalization on regulation of the phospholipase C-gamma1 signaling pathway. *J Biol Chem* **274**, 8958-8965 (1999).

17. Hendriks, B.S., Orr, G., Wells, A., Wiley, H.S. & Lauffenburger, D.A. Parsing ERK Activation Reveals Quantitatively Equivalent Contributions from Epidermal Growth Factor Receptor and HER 2 in Human Mammary Epithelial Cells. *Journal of Biological Chemistry* **280**, 6157-6169 (2005).

18. Bublil, E.M. & Yarden, Y. The EGF receptor family: spearheading a merger of signaling and therapeutics. *Current Opinion in Cell Biology* **19**, 124-134 (2007).

19. Olayioye, M.A., Neve, R.M., Lane, H.A. & Hynes, N.E. The ErbB signaling network: receptor heterodimerization in development and cancer. *EMBO J* **19**, 3159-3167 (2000).

20. Tamama, K., Fan, V.H., Griffith, L.G., Blair, H.C. & Wells, A. Epidermal Growth Factor as a Candidate for Ex Vivo Expansion of Bone Marrow-Derived Mesenchymal Stem Cells. *Stem Cells* **24**, 686 (2006).

21. Gui, C. et al. Heregulin protects mesenchymal stem cells from serum deprivation and hypoxia-induced apoptosis. *Molecular and Cellular Biochemistry* **305**, 171-178 (2007).

22. Gavrieli, Y., Sherman, Y. & Ben-Sasson, S.A. Identification of programmed cell death in situ via specific labeling of nuclear DNA fragmentation. *Journal of cell Biology* **119**, 493-501 (1992).

23. Wiley, H.S. Trafficking of the ErbB receptors and its influence on signaling. *Experimental Cell Research* **284**, 78-88 (2003).

24. Adam, L. et al. Heregulin Regulates Cytoskeletal Reorganization and Cell Migration through the p21-activated Kinase-1 via Phosphatidylinositol-3 Kinase. *Journal of Biological Chemistry* **273**, 28238-28246 (1998).

25. Kumar, N., Wolf-Yadlin, A., White, F.M. & Lauffenburger, D.A. Modeling HER2 effects on cell behavior from mass spectrometry phosphotyrosine data. *PLoS Comput Biol* **3**, e4 (2007).

26. Harms, B.D., Bassi, G.M., Horwitz, A.R. & Lauffenburger, D.A. Directional persistence of EGF-induced cell migration is associated with stabilization of lamellipodial protrusions. *Biophysical journal* **88**, 1479-1488 (2005).

27. Muthuswamy, S.K., Gilman, M. & Brugge, J.S. Controlled Dimerization of ErbB Receptors Provides Evidence for Differential Signaling by Homo-and Heterodimers. *Molecular and Cellular Biology* **19**, 6845 (1999).

28. Zhan, L., Xiang, B. & Muthuswamy, S.K., Vol. 66 5201-5208 (AACR, 2006).

29. Xue, C. et al., Vol. 66 1418-1426 (AACR, 2006).

30. Feldner, J.C. & Brandt, B.H. Cancer cell motility—on the road from c-erbB-2 receptor steered signaling to actin reorganization. *Experimental cell research* **272**, 93-108 (2002).

4 Discovery and application of BTCP binding peptides

4.1 Introduction

Beta-tricalcium phosphate (BTCP) is a clinically important material with broad applications in bone repair. It is widely used in surgical procedures to fill bone voids and serves as an important material in a variety of orthopedic compositions such as putties and pastes that easily conform to wound geometries. Its continued evolution as a medical product is limited by its material properties which do not permit direct chemical surface modification and its physical properties which limit its handling. The ability to easily modify the surface of BTCP would permit the design of molecular surface treatments which would extend its bio-functionality and improve clinical performance. In this chapter the discovery of a BTCP binding peptide and its subsequent engineering to permit stable surface tethering of epidermal growth factor on BTCP is presented.

A key objective of this work is to demonstrate that tethered EGF results in increased proliferation without compromising the early differentiation of primary human MSCs cultured on 3D BTCP scaffolds. As important is the demonstration that tethered EGF confers a strong survival advantage to MSCs cultured under serum starved conditions for prolonged periods. This will serve to simulate the harsh conditions which can exist in a wound following surgery. The approach described here can be adapted to modify the surface of BTCP with a variety of proteins or peptides to achieve desired phenotypes.

4.2 Proliferation versus multipotency: a regenerative medical challenge

The ability to expand a progenitor population without compromising differentiation potential is one of the key objectives of regenerative medicine. Achieving this effect would have significant clinical implications. Because many procedures rely on autologous MSC transplantation, increasing patient native progenitor populations to improve bone wound healing is an important objective.

Many studies have characterized the effects of EGF on tissues *in vitro* and *in vivo*. EGF is the canonical ligand for the epidermal growth factor receptor (EGFR), and induction of this pathway can produce proliferation,[1-7] migration,[8-11] homeostasis,[3] and synergistic effects leading to differentiation when dosed with other ligands.[12-14] The broad effects of this ligand result from the diversity of the downstream signaling network, thus making EGF an important stimulus in wound healing contexts. In MSCs, EGF has been shown to affect a number of cell behaviors in a context specific manner. EGF can promote proliferation,[3] osteogenic differentiation,[15] and survival.[16] In a wound healing context EGF can serve as an important cue leading to bone development and homeostasis following surgery.[17-20] EGF has also been shown to play a role as a regulator of MSC behavior[15, 21-25] and can give rise to expansion of MSCs without inducing differentiation.[3]

The clinical utility of these effects cannot be fully exploited without a viable method to deliver EGF to sites of injury in a spatially controlled manner; particularly on clinically important substrates. One such clinically important substrate is BTCP which is routinely used in orthopedic procedures.[26] BTCP is an osteoconductive material that supports bone mineralization by easily dissolving at low pH and serves as a rigid substrate for cell attachment.[5, 27] Muschler and others have used this material in

conjunction with autologously harvested bone marrow to improve outcomes. In those kinds of procedures the BTCP is flushed with bone marrow aspirate to seed MSCs and further promote bone formation.[27]

Although the intrinsic properties of BTCP favor bone healing in many clinical applications, addition of osteogenic growth factors BMP-2 and OP-1 to BTCP scaffolds at the time of implant enhances healing in both experimental animal models and clinical applications.[28] It is reasonable to speculate that in large defects, where a source of stem and/or progenitor cells (e.g. marrow aspirate) is added to overcome a local deficiency of osteogenic cells, presentation of tethered EGF may enhance cell survival and stimulate proliferation of early progenitors to populate the site, upstream of BMP activity.[16, 29, 30] Although physisorption of PDGF to BTCP has been shown to enhance proliferation of osteogenic cells on BTCP scaffolds in vitro, the in vivo loss of growth factor is much faster than that observed in vitro.[31] The utility of BTCP as an existing substrate for orthopedic procedures would be enhanced if surface treatments were available to permit stable attachment of bioactive components such as EGF.

4.3 Discovery of BTCP binding peptides using phage display

The approach taken to address this problem and which is described in detail in this section is to discover novel peptide sequences that exhibit tight binding to BTCP by using phage display. This approach has been used in other contexts to find peptide sequences which bind inorganic substrates.[32-34] This section will describe the use of sequences discovered through phage display as fusion partners to confer tight binding of protein ligands to BTCP substrates. This concept is illustrated in figure 4.1 and includes

features from the bivalent ligand design to permit future work in bivalent ligand presentation. This chapter will focus on monovalent ligand tethering studies.

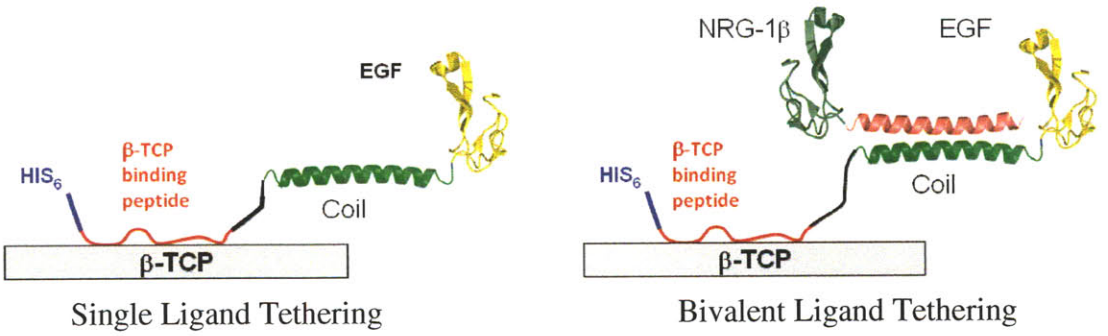

Single Ligand Tethering

Bivalent Ligand Tethering

Figure 4.1 – Ligand tethering concept using a BTXΠ binding peptide (TCPBP) Either single or bivalent ligand tethering is possible by retaining the coil region from construct C1 (described in chapter 2).

4.4 Fabrication of BTCP and BTCP-polymer composite scaffolds

Scaffolds were fabricated at Therics (Akron, OH) from either BTCP or a composite of BTCP and polylactide-co-glycolide (PLGA) using the TheriForm 3D rapid prototyping platform.[35] Briefly, to create BTCP scaffolds, granulated BTCP powder was sintered and sieved. Scaffolds were fabricated in the shape of a cross by depositing binder in a programmed sequence onto a BTCP powder bed and sucrose as a porogen. The scaffolds were then sintered for 20 h, dried for 1 day, leached for 2 days to remove porogen, and dried one day to yield crosses measuring 5 x 5 x 3mm (Figure 4.2). Each implant is approximately 60% porous with a mean pore diameter of 60 microns and a pore diameter range of 5-900 microns.

The internal structure shows an open spongy type structure (figure 4.x). Chemically, the scaffolds are >95% BTCP with the remaining portion being other resorbable forms of calcium phosphate. Composite BTPC-PLGA scaffolds were

fabricated in a similar fashion by mixing PLGA and BTCP powders with a porogen. *(more detailed manufacturing detail will be included in the manuscript).*

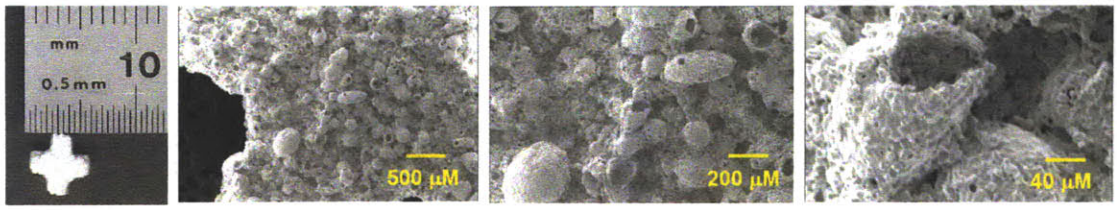

Figure 4.2 – **Photograph and scanning electron micrographs of a Therics Therilok β-TCP scaffold;** High magnification shows the detailed pore structure of these scaffolds. (Scanning electron micrographs courtesy of L. Stockdale).

4.5 Phage display against BTCP scaffolds

BTCP scaffolds were crushed into powder, autoclaved for 35 minutes at 121°C and stored under dry sterile conditions prior to all experiments. The resulting sterile BTCP powder was blocked for 24 hours at 4°C under moderate agitation with either sterile filtered salmon protein buffer (Licor) or 5 % bovine serum albumin in phosphate buffered saline (BSA, Sigma). Blocked BTCP powder was pelleted at 2000 RPM for 2 minutes, washed 3X with PBS then subjected to three rounds of phage display using the New England Biolabs linear 12-mer Ph.D. kit (Andover, MA). Orthogonally blocked BTCP (i.e. blocked with BSA vs salmon protein) provided a control against panning against components of the blocking buffers. Additional controls included a β-BTCP/PLGA composite scaffold, crushed into powder, similarly blocked with BSA or salmon protein buffer as well as a mock tube to control against panning against tube components. After three rounds of panning, ten plaques from each condition were picked, amplified, then sequenced (the mock condition and the BTCP/PLGA blocked with BSA did not produce plaques after the second and third round, respectively).

Sequences were analyzed for consensus using JalView Multiple Sequence Alignment Editor.[36, 37] Figure 4.3 shows the aligned sequences.

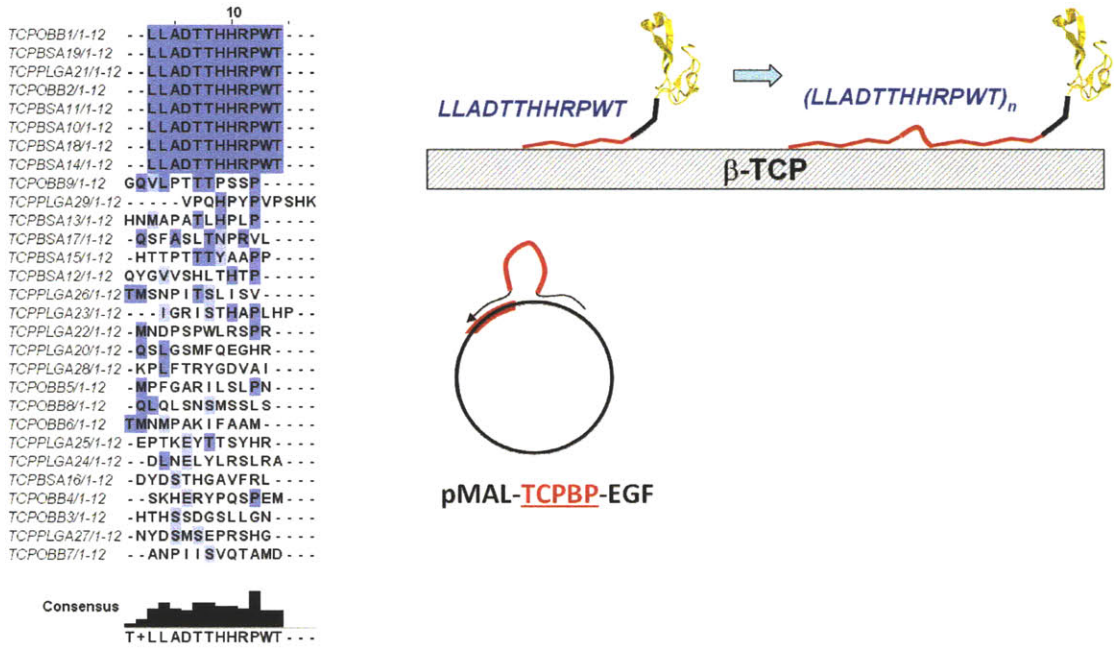

Figure 4.3– Multiple sequence alignment of phage clone sequences (left) and concatenated peptide cloning concept (right)
A strong consensus sequence is immediately evident from the alignment. Eight of 29 sequences are identical (28%). Shading is based on the BLOSUM62 score. Concatenation of multiple TCPBP regions results in increased affinity for bTCP. Generation of concatenated multimers with a primer which contains the TCPBP coding region wholly within the primer with no flanking sequences facilitates the creation of multiple insertion clones per PCR reaction.

4.6 Mutagenesis

The highest ranked sequence from third round phage display panning. (LLADTTHHRPWT) was serially cloned into a pMAL expression cassette using PCR mutagenesis and a short primer to generate a library of multimer insertions fused to epidermal growth factor (figure 4.3). PCR mutagenesis was performed with a Quickchange Ligthtning II kit from Stratagene (Eugene, OR). Previous work in our lab produced a pMAL-c2X vector (New England Biolabs) expressing human epidermal

growth factor in fusion with various epitopes. PCR primers were designed to prime wholly within the BTCP binding peptide coding region thus allowing multiple insertions during a single PCR mutagenesis round. Multimer clones were sequenced to confirm DNA identity with target sequence, transformed into BL21(DE3)pLysS E. coli and plated on ampicillin LB agar. The library evaluated included $(TCPBP)_{n= 1, 2, 3, 5, 8, \text{and } 10}$ clones.

4.7 Protein Expression

Clones of 1-, 2-, 3-, 5-, 8, and 10- mers of the TCPBP sequence (LLADTTHHRPWT) were expressed in 1L LB cultures grown at 37°C until OD 0.6, then induced with IPTG and incubated at 22°C for 4 hours. Proteins were harvested by pelleting cultures at 3700 RPM on an Allegra G3.8 rotor at 4°C for 30 minutes then freezing the pellet at -80°C overnight followed by cell lysis using Bugbuster Reagent (EMD Chemicals) supplemented with PMSF and protease inhibitor cocktail (Sigma). Lysed cells were centrifuged at 3700 RPM on an Allegra G3.8 rotor at 4°C for 1 hour. The supernatant was then diluted 1:4 in tris buffered saline and subjected to maltose binding protein affinity chromatography in accordance with the manufacturer's instructions (New England Biolabs). Pooled fractions were subjected to ultrafiltration through a 50,000 MWCO membrane U-tube concentrator (Novagen) and twice exchanged into PBS. Concentrated protein was sterile filtered through a 0.2 micron filter. Purity was confirmed by SDS-PAGE commassie staining. Protein quantification was performed on a Nanodrop A280 spectrophotometer. Concentrated proteins were stored at minus 80°C until use. Based on preliminary results with 1- and 2-mers which showed modest binding affinity, the 3-, 5-, and 10- mers were selected for further evaluation.

4.8 Tethering TCPBP-EGF on BTCP scaffolds and binding characterization

BTCP scaffolds or sieved pure BTCP powder was blocked for 1 hour with salmon serum buffer then incubated at room temperature for two hours in purified TCPBP protein diluted in salmon serum buffer. After incubation, scaffolds or powder were washed three times in three volumes of 20 mM tris buffered saline at pH 7.4 followed by a final wash and storage in PBS. Qualitative assessment of binding was performed by fluorescence microscopy using a FITC-anti-HIS tag antibody and a goat-anti-hEGF (R&D) primary and a TMR-anti-goat secondary as shown in figure 4.4. Control protein incorporating all elements of the TCPBP sequence except the TCPBP region $(LLADTTHHRPWT)_n$ was used as a negative control for non-specific binding in all experiments (figure 4.4, bottom right). *(For the manuscript time release studies will be performed to determine the long term stability of tethered peptide.)*

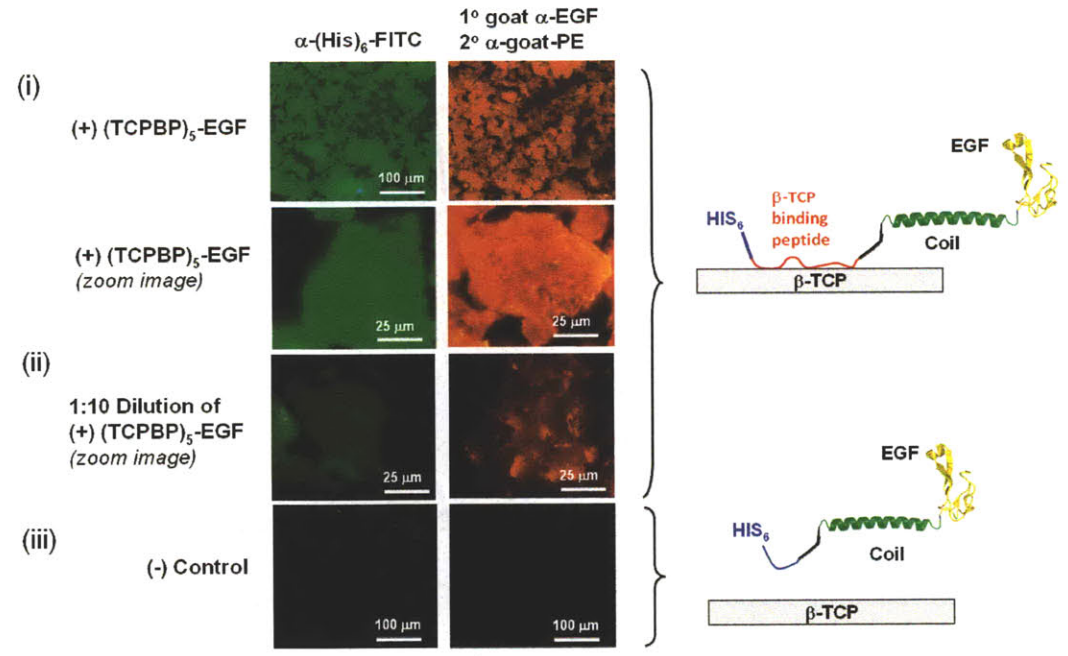

Figure 4.4 – TCPBP binding characterization
(left) Immunofluorscence micrograph of TCPBP-EGF binding to sieved TCP powder treated with $(TCPBP)_5$-EGF or a control protein lacking the TCPBP region. All images are 3 second exposures. Incubations performed at (i) 10 μM and (ii) 1 μM (TCPBP)5-EGF, and (iii) 10 μM control EGF.

Characterizing the binding of each of the concatenated multimers of TCPBP is required in order to determine if increases in multimer insertion increase binding affinity and to determine if the effect reaches a limiting value. Serial dilutions of TCPBP of 3-, 5-, and 10- multimers were incubated with BTCP as described above. Scaffolds were then washed in PBS and bound protein was eluted by incubating the scaffolds in pH 2.2 glycine buffer for one hour and quantifying the amount of TCPBP in the eluate with IR-dye immunofluorescence using a western blot format read with a Licor Odyssey IR flatbed scanner. The results of this analysis are shown in figure 4.5.

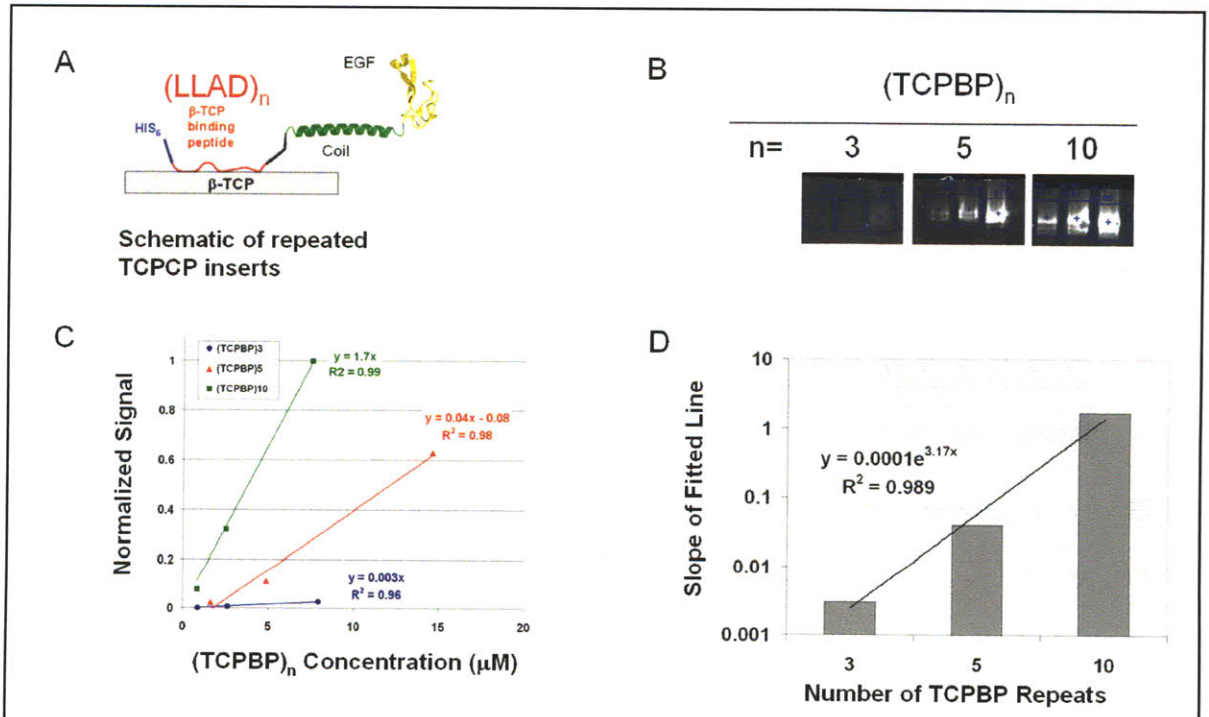

Figure 4.5 – **Affinity of TCPBP for BTCP with increasing number of TCPBP repeats** (A) Clones incorporating 3, 5, and 10 repeats of the TCPCP sequence were assayed for binding to TCP. (B) Bound protein was eluted from scaffolds and assayed by SDS-PAGE & immunoblot. (C) Desitometry of bands from immunoblots reveals increasing amounts of recovered protein for the same incubation concentration of TCPBP as the number of TCPBP repeats is increased. (D) The slope of the fitted lines plotted versus number of repeats reveals a strong dependence on TCPBP repeat number.

TCPBP binding affinity exhibits a strong dependence on multimer number, as expected. The relative change in affinity is illustrated in figure 4.5 (C) and (D). The slope of the response signal as a function of $(TCPBP)_n$ incubation concentration gives a relative indication of the retained protein which reflects the affinity at a given concentration. Figure 4.5 (D) shows the strong dependence of repeat number on relative affinity. Based on the multimer binding screen shown in figure 4.5 the 10-mer TCPBP was selected for further experiments.

Quantitative analysis of binding was performed by incubating a serial dilution of $(TCPBP)_{10}$ with 35 mg intact TCP scaffolds treated as described above and analyzed using a quantitative spot blot format read with a Licor Odyssey IR flatbed scanner. The results of this analysis are shown in figures 4.6 and 4.7.

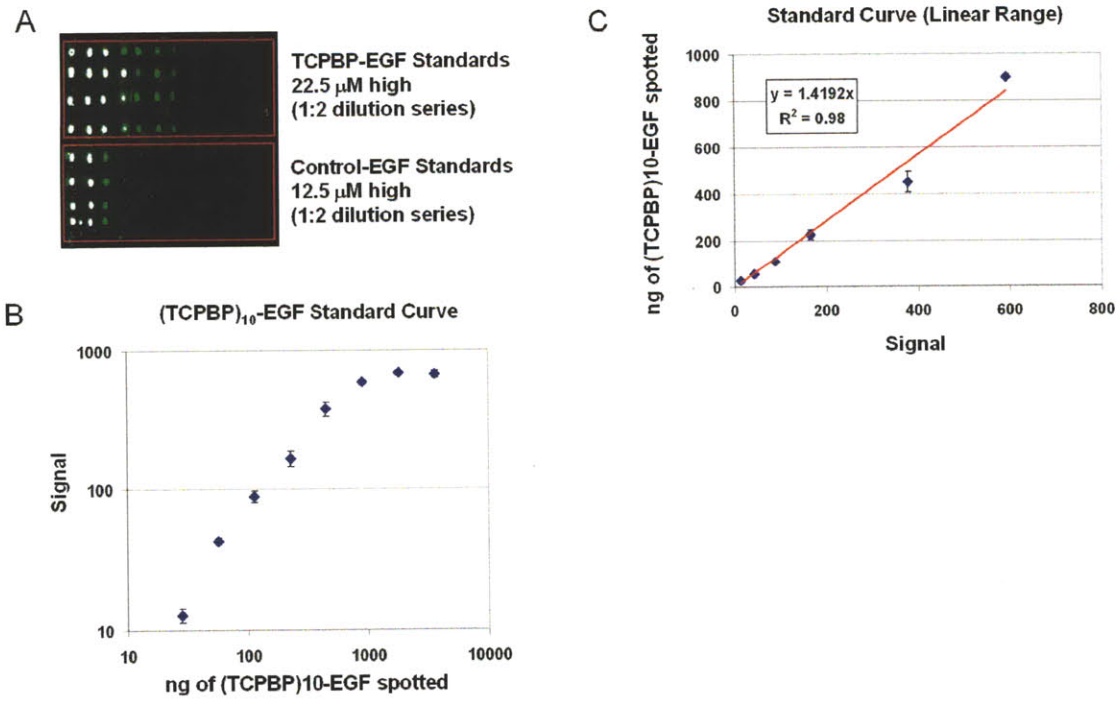

Figure 4.6 – Quantification of (TCPBP)10-EGF affinity for BTCP
(A) Two microliters of standard curve dilutions of (TCPBP)10-EGF and control EGF were spotted onto nitrocellulose membranes and probed with goat-a-EGF 1^{o} and a-goat-IRDye800 2^{o} antibodies. (B) Spot intensity was correlated with the amount of protein spotted to find (C) the linear range used for further quantification: 0 to 900 ng.

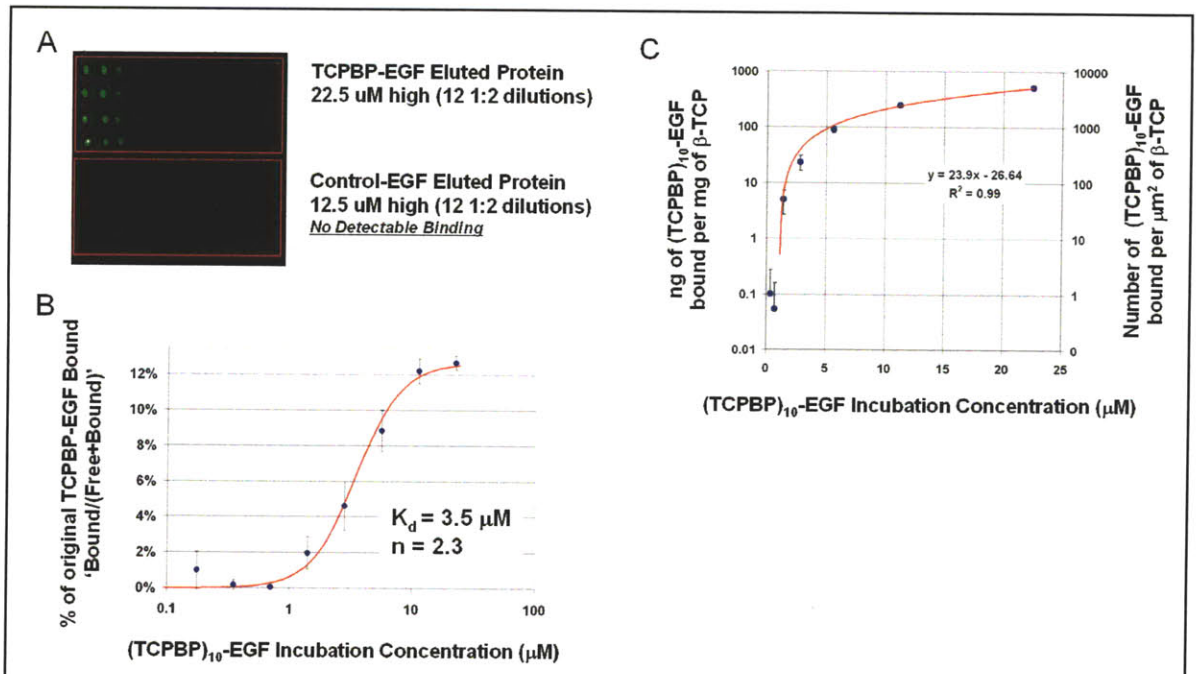

Figure 4.7 – Quantification of (TCPBP)10-EGF affinity for BTCP
(A) Two microliters of eluted (TCPBP)10-EGF or eluted control EGF were spotted onto nitrocellulose membranes and probed with goat-a-EGF 1o and a-goat-IRDye800 2o antibodies. No eluted control protein was detected. (B) Eluted protein fraction was quantified and plotted as a function of incubation concentration. A two parameter binding model was fit to the data: apparent Kd = 3.5 mM, Hill coeffcient = 2.3, indicative of avidity. (C) Binding capacity of BTCP at various concentrations of (TCPBP)10-EGF. This curve can be used to tune the surface density of (TCPBP)10-EGF on BTCP by selecting the appropriate incubation concentration.

Quantifying the amount of bound protein requires the creation of a standard curve for both the sample and control protein. Figure 4.6 illustrates the results for the standard curve. To make each curve a known amount of $(TCPBP)_{10}$ or control (C1 protein as shown in figure 4.4, bottom right) was blotted in quadruplicate onto a nitrocellulose membrane and probed using the methods described above. The resulting signal produces a monotonically increasing signal that begins to saturate at the higher end of the curve (B). The first six points of this curve are in the linear range and are used to construct the

standard curve. Because the epitope probed in both constructs is identical it is not surprising that both the control and sample protein produced a standard curve with the same slope. The range of protein that can be accurately quantified using this standard is 0 to 900 ng per 2 μL spot.

The analysis of $(TCPBP)_{10}$ binding to BTCP is shown in figure 4.7. The standard curve permits direct quantification of bound protein and the construction of a binding curve (B). This analysis produces an estimate for the binding constant k_D of 2.3 uM. The binding curve also exhibits avidity with a Hill coefficient of 2.3. This is consistent with multimeric protein interactions. Brunauer, Emmet, Teller (BET) analysis of BTCP scaffolds using a 5 point pressure analysis reveals an N_2-accessible surface area of 0.8 m^2/g. This permits the estimation of minimum surface number density as shown in (C). The surface area accessible to EGF-$(TCPB)_{10}$ may be less than the full N_2 accessible surface area if the pore size distribution occludes EGF-$(TCPB)_{10}$ from accessing certain regions of the scaffold. For the purposes of this analysis the discrepancy arising from this effect is assumed to be negligible.

The data in figure 4.7, taken together with characteristic EGFR expression levels indicate that the surface density of tethered EGF-$(TCPB)_{10}$ is more than adequate to stimulate MSCs at a maximal level. For example, at a tethering solution concentration of 1 μM the tethered surface number density is 200 EGF$(TCPBP)_{10}$ per μm^2. A spread cell will have ~ 500 $microns^2$ of surface area in contact with its substrate which would expose it to ~100,000 EGF molecules. By comparison, the typical MSC expresses 10,000 EGFRs. A significant fraction of these would encounter a tethered EGF over the course of several minutes. In this system the EGFs are constrained at the substrate surface and

not as free to diffuse as with soluble EGF and so the kinetics of receptor ligand interaction are not immediately analogous to the soluble case.

With a preliminary characterization of EGF(TCPBP)$_{10}$ surface binding it is possible to begin a preliminary analysis of cellular effects on a cell type that is clinically relevant. The culture of a low passage (P3) primary human mesenchymal stem cells on BTCP scaffolds treated with EGF(TCPBP)$_{10}$ is examined in the next section.

4.9 Cell Culture

Passage two primary human mesenchymal stem cells (from the Texas A&M Health Science Center College of Medicine's Institute for Regenerative Medicine) were culture expanded to provide sufficient numbers of passage three MSCs prior to all cell culture experiments. Expansion medium consisted of αMEM with 2 mM L-glutamine, 16.5% fetal bovine serum, and penicillin/streptomycin (final concentration 100 units/ml and 100 μg/ml streptomycin). Osteogenic medium consisted of 192 ml expansion medium, 10 nM Dexamethasone (20 μl of a 1:10 dilution of a 1 mM stock in MQ water), 20 mM β-glycerolphosphate (8 ml of 0.5 M stock in expansion medium), and 50 μM L-Ascorbic acid 2-phosphate (200 μl of 50 mM stock solution in MQ water

Sterile BTCP scaffolds were blocked with salmon serum buffer treated with EGF(TCPBP)$_{10}$ or left untreated and individually placed into the wells of a 96 well plate. 1,000 to 50,000 cells (as described) were seeded in 200 μL of serum-containing medium (hTMSC) or expansion medium (primary MSC) per well directly onto the scaffolds. Seeded cells were allowed to incubate for 24 hours then were moved into adjacent wells with fresh medium to eliminate the effect of cells which did not seed onto the scaffolds.

Seeding effciciency with this method was consistently 40% as determined by counting cells both on the scaffold and in the remnant well (described in the next section).

4.10 Proliferation Assays

Cellular proliferation was determined using the Alamar Blue assay (Biosource Europe, Nivelle Belgium) at various time points post seeding. At each time point Alamar Blue dye reagent was mixed with either osteogenic or expansion media according to the manufacturer's instructions. Six biological replicates were seeded for each measurement. The tethered BTCP scaffolds were then moved into a UV sterilized Falcon 96 well plate (Becton Dickinson and Co., NJ USA) attached to a MDV series filter plate adapter (Millipore, Bedford, MA). Alamar Blue dye reagent was then added to each well containing a tethered BTCP scaffold and then incubated at 37°C, 5% CO_2 for four hours with gentle mixing by hand every 20 minutes. The filter plate unit was then centrifuged at 1000 RPM for two minutes. This method allowed for complete recovery of dye-media mixture. 100 uL of the resulting dye-media mixture was transferred from the collector plate unit to a new flat-bottom 96-well plate to be read by a SpectraMax M2e multi-well fluorescent plate reader (Molecular Devices Corp.CA, USA) at a 570 nm excitation wavelength and 585 nm emission wavelength. A standard curve was obtained by performing the same assay on known numbers of cells plated in a 12 well plate and cultured for 1, 4, or 7 days to correspond to the respective time point. Because the Alamar blue assay is non-destructive it was possible to directly count the cells with a ViCell hemacytometer (Coulter) in order to calibrate the Alamar Blue signal response to actual cell number.

Hence, a standard curve for each culture condition (expansion medium 'EX' and osteogenic medium 'OS') and each day time point up to 7 days was constructed to assess the magnitude of variation. Metabolic rates under various conditions can vary. As shown in figure 4.8 the slope of each standard curve is an indication of the metabolic activity of the cells in that condition. Variations in the slope of the EX series at different days indicates that cells undergo a shift in metabolism following seeding that can last several days. Under OS medium the slope does not change significantly compared to the day 1 EX (seeding condition). The respective slope for each culture condition and time point was used to convert Alamar Blue data from the corresponding 3D scaffold conditions into cell number. Day 14 and 21 cultures used the respective day 7 slopes. Standard curves for days 14 and 21 were not reliable due to high confluence and cell death at those time points.

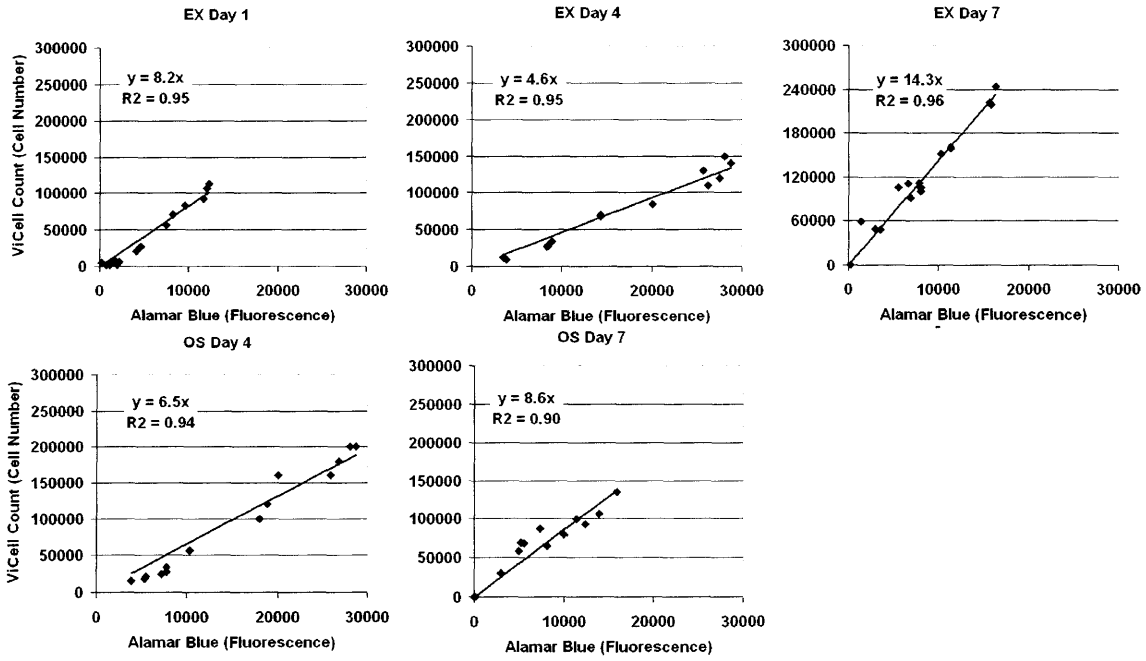

Figure 4.8 – Standard curves for the Alamar Blue based cell proliferation assay
Correlations between cell number and Alamar Blue fluorescence under each culture condition were used to calibrate results for 3D cultures at each day time point up to 7 days. Cell cultured in osteogenic medium exhibited smaller changes in slope over time.

4.11 Influence of cell seeding density and tEGF dose on MSC proliferation

The survival and proliferation of most mammalian cells exhibit a strong dependence on local cell density. Cells secrete various autocrine factors that enhance survival and proliferation at low cell densities and inhibit proliferation at high cell densities. When the concentration of autocrine factors builds up at high cell densities we expect that tEGF may enhance cell proliferation, but whether it can protect cells at very low plating density, or overcome inhibition at high densities is unclear. We therefore assess the proliferation response of MSCs to tEGF using a range of cell seeding densities and surface tethering densities of tEGF.

By screening the effect of seeding density on proliferation profiles over a typical time course it is possible to select a suitable density to use for future experiments. In addition we expect that the surface density of EGF on BTCP can affect the proliferation response of cells. EGF has been observed to exert a biphasic effect on cell proliferation in 2D with concentrations near the EC50 (1 nM). In this system the EGF is tethered on the surface and the equivalent EC50 can only be determined empirically. For the purposes of this experiment cell proliferation is used as a proxy for dose response as shown in figure 4.9.

Cell seeding densitities of 1,000; 25,000, and 50,000 cells per 200 ul (volume used to seed each scaffold) were evaluated in expansion medium. The effect of seeding density on proliferation is clearly evident at the 50,000 cell level in figure 4.9 (rightmost plot). A significant drop in cell number is seen at day 4 with recovery by day 7. This effect is much less pronounced at the 25,000 cell seeding level (center plot) and not evident at the 1,000 cell seeding level. Based on these results a seeding density of 30,000

cells per scaffold was selected. This level of seeding is a good compromise between unwanted biphasic effects in proliferation and the amount of time required to obtain sufficient cell material for other analyses (such as RNA for qRTPCR or protein for alkaline phosphatase activity).

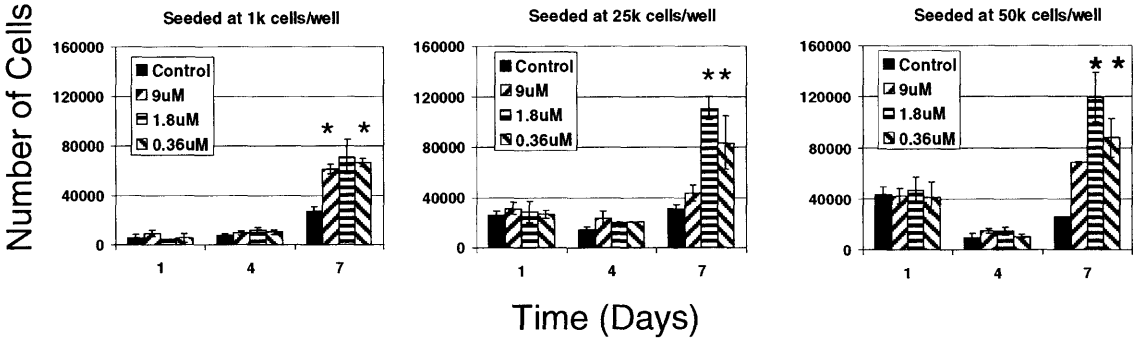

Figure 4.9 – Proliferation of MSCs in expansion medium in 3D TCP scaffolds at various cell seeding densities and EGF(TCPBP)$_{10}$ tethering concentrations
All scaffolds incubated in EX medium and assayed at terminal endpoints using the Alamar Blue based cell proliferation assay. Cell proliferation at high seeding densities (50K) exhibited a sharp minimum at day 4. This effect is attenuated as seeding density is reduced. Cell proliferation exhibited a biphasic relationship with respect to surface EGF(TCPBP)$_{10}$ tethering density at all seeding densities. The tethering concentrations studied correspond to surface densities of 2,000; 400; and 60 EGF molecules / μm^2;
* p=0.05 vs same day control, n=6, +/- s.d.

By day 7 cell proliferation exhibited a biphasic relationship with respect to surface EGF(TCPBP)$_{10}$ tethering density at all cell seeding densities, with an apparent maximum at the 1.8 μM tethering concentration. This corresponds to 400 EGF molecules / μm^2. Based on these results a concentration of 1 μM EGF(TCPBP)$_{10}$ for tethering was selected. A detailed examination of the effects of tethered EGF on proliferation and osteogenic differentiation was carried out and is described in the following section.

4.12 Effect of tEGF on primary MSC proliferation in 3D BTCP scaffolds

The results of a detailed study of the effect of tEGF on MSC proliferation in both EX and OS media are shown in figure 4.10. A cell seeding density of 30,000 per scaffold and tethering concentration of 1 μM $EGF(TCPBP)_{10}$ were used. In EX medium MSCs exhibited approximately 50% increased proliferation vs the control at day 7. By day 14 this effect was no longer evident, with no significant difference between tEGF and control. The parity at 14 days may be imposed by the carrying capacity of the scaffold at high cell densities. With over 400,000 cells per scaffold there may be diffusive transport limitations which impose constraints on EGF stiumulated proliferation. In OS medium the effect of tEGF is more pronounced. At day 7 and 14 tEGF resulted in increases of 62% and 25% over controls, respectively. The increase in available MSCs in 3D scaffolds is of particular interest in a clinical setting where scarcity of MSCs limits the scope of procedures where autologous MSCs would be used.

An increase of 20-60% in the number MSCs at a wound site would significantly improve outcomes and increase the size of defects which could be treated by taking advantage of sparser seeding densities to achieve the same number as with current methods. Whether these increases are significant from a clinical perspective requires careful examination of the effects of tEGF on the early osteogenic differentiation of MSCs in the same context. If the increase in proliferation is accompanied by a decrease in osteogenic potential then the results will be less interesting. However, if early differenation potential can be preserved or even improved then increases in proliferation will have a meaningful effect on tissue formation at wound sites.

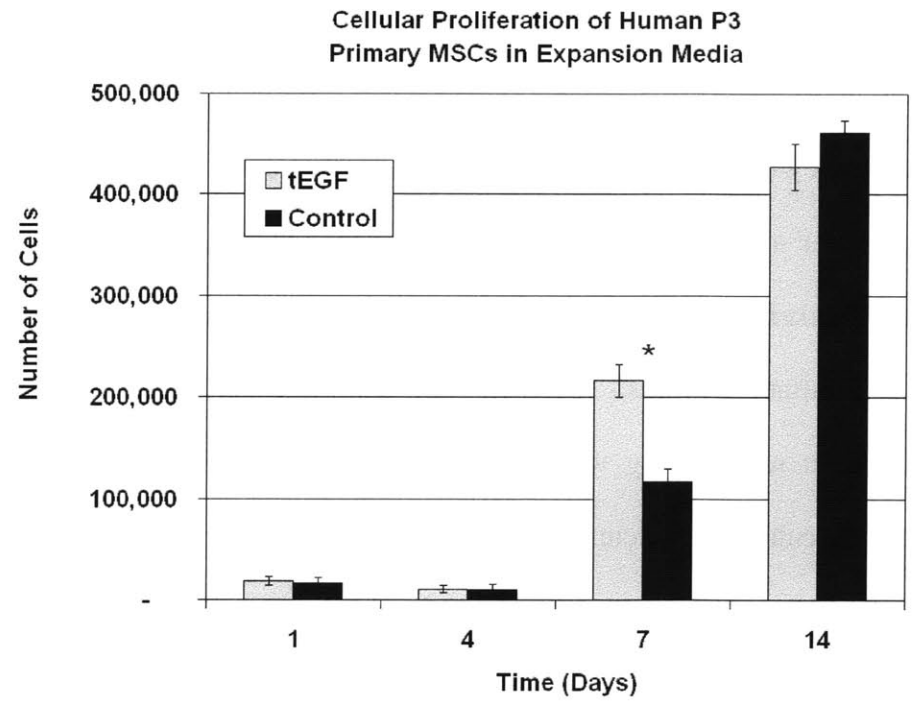

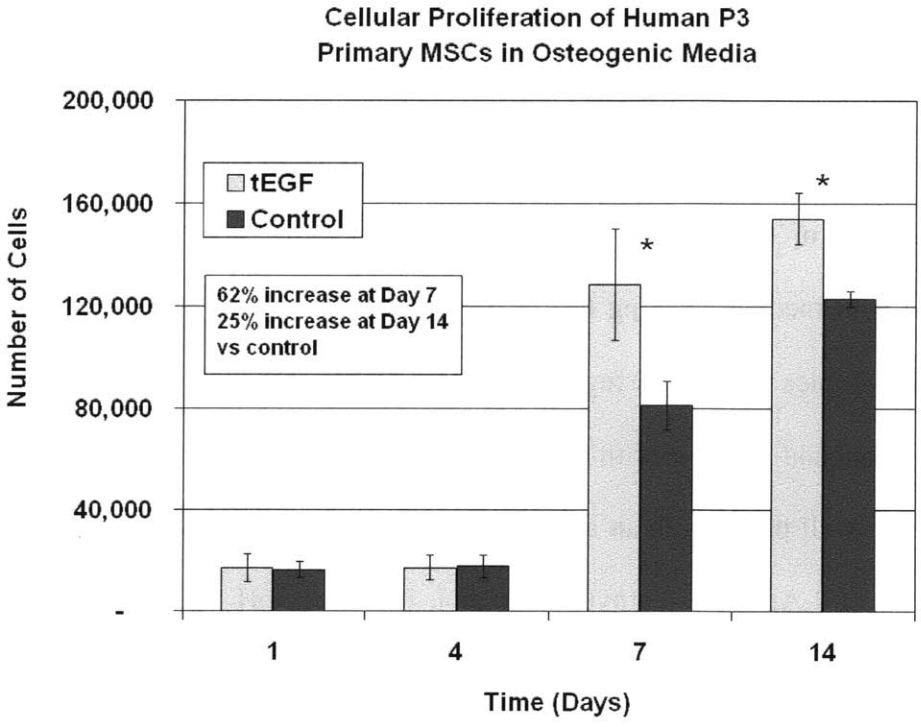

Figure 4.10 – Proliferation of MSCs on 3D TCP scaffolds
tEGF promotes MSC proliferation in both EX and OS medium. Under OS conditions increases of 62% and 25% at days 7 and 14, respectively, are observed for MSCs cultured on scaffolds treated with tEGF. n=6, +/- s.d. *p=0.05 vs respective control.

4.13 Differentiation Assays

The ability of MSCs to underdo osteogenic differentiation is a useful metric to assess the potency of these cells. Early osteogenic differentiation is typically measured by comparing the alkaline phosphatase activity of induced cells with that of uninduced cells. Later markers include panels of osteogenic transcripts as measured by qRTPCR which give quantitative results. Even later (21 days) one can use mineralization assays such as Alizarin red staining which stain deposited calcium. Given the limitation imposed by 3D culture on calcium containing scaffolds this work will focus on alkaline phosphatase assays and qRTPCR to assess osteogenic induction.

Alkaline phosphatase activity was measured using a p-nitrophenol colorimetric assay. Scaffolds were rinsed with PBS twice followed by two freeze-thaw cycles (20 min at -70°C followed by 10 min at 25°C). Two scaffolds from the same condition were added to an epindorf tube, and then manually crushed with a pipet tip. Cells were lysed by adding 200 µl of 0.2% NP-40 in 1 mmol/L $MgCl_2$ to each tube. The tubes were incubated with medium shaking for 15 minutes at 4°C. After 5 min of sonication in a water bath samples were centerfuged at 13,000 RPM for 5 minutes. The supernatant was diluted 10-fold and 100-fold with lysis buffer. Diluted sample lysate and lysis buffer were placed in 96-well plates with an all lysis buffer sample used as a background control. A 1:1 solution of 2-Amino-2-methyl-1-propanol, 1.5 mol/L, pH 10.3 at 258C (Sigma, Q17) and stock substrate solution of p-nitrophenyl phosphate disodium (Sigma) was added to the samples and incubated for 30 min at 37°C; sodium hydroxide was added to stop the reaction. Absorbance at 405 nm was read using SpectraMax M2e multi-well fluorescent plate reader (Molecular Devices Corp.CA, USA).

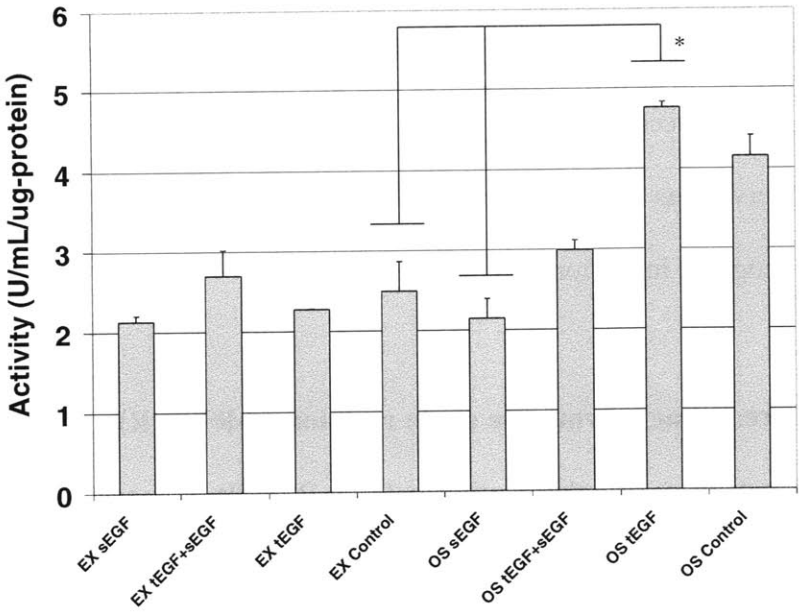

Figure 4.11- Alkaline phosphatase activity assay (Day 7)
Alkaline phosphatase activity of primary human MSCs cultured on 3D TCP scaffolds under the indicated conditions. Cells cultured in the tEGF OS condition exhibit ALP activity that is comparable to that of OS alone. Significantly, sEGF compromises this effect by lowering ALP activity. OS tEGF is significantly different that EX control or OS+sEGF at p=0.05. n=3, +/- s.d. (sEGF is soluble EGF at 1 ng/mL, tEGF is TCP treated with TCPBP as described previously.)

Background signal from the blank control was subtracted from all readings. A serial dilution of p-nitrophenol in sodium hydroxide was used to generate a standard curve in U/mL: a unit is defined as the amount of enzyme which catalyses the liberation of 1 mmol p-nitrophenol per minute at 37°C. The results are normalized by total protein using the BCA assay (Pierce).

The day 7 alkaline phosphatase activity (ALP) of MSCs grown in EX and OS medium with and without soluble EGF and / or tethered EGF were compared as shown in figure 4.11. OS (positive control) and OS+tEGF produced comparable levels as expected which were the highest among the various conditions. Addition of soluble EGF at 1

ng/mL abrogated the effect of osteogenic medium and resulted in activity which was comparable to EX (negative control). Interestingly the addition of soluble EGF to the Os+tEGF condition reduced overall ALP activity by almost 40%. This result appears to confirm prior observations that surface tethered EGF may provide advantages over sEGF by preserving osteogenic induction potential.

4.14 Qantitative real time polymerase chain reaction (q-RTPCR)

A set of osteogenic markers suitable for q-RTPCR was selected based on the published literature in the field of osteogenesis and on previous work in this lab.[30, 38-41] Four markers of particular relevance in osteogenesis are discussed below.

RUNX2 is a transcription factor that is up-regulated in mechanically stressed pre-osteoblasts and is a reliable indicator of bone forming activity. In osteoblasts there is both a stretch dependent and stretch independent activation of RUNX2 which results in activation of the mitogen activated protein kinase (MAPK) cascade. Interactions between RUNX2 and pERK2 result in potentiation of RUNX2 activity. [38] The stimulation of pERK1/2 via HER1 by tEGF may result in amplification of RUNX2 activity through a stretch-independent mechanism simply by virtue of pERK2 up-regulation. Thus observation of up-regulation in RUNX2 activity in MSCs cultured on tEGF treated scaffolds would have at least one mechanistic explanation given the common ERK signaling node.

Osteocalcin (bone gamma-carboxyglutamic acid protein) is a small protein associated with mineralized bone matrix. Hoang found that osteocalcin contains a negatively charged surface that coordinates five calcium ions in an orientation that

complements calcium ions in the hydroxyapatite crystal lattice of natural bone.[42] Osteocalcin is downstream of RUNX2 and has been shown to become up-regulated following up-regulation of RUNX2.[43]

Osterix (SP7) is a zinc finger transcription factor and a regulator of bone cell differentiation that is reported to operate downstream of RUNX2.[40, 44] Possible evidence of this may be seen in figure 4.12 (bottom plots). Here the re-expression of osterix at day 14 following early RUNX2 upregulation under the tEGF condition at day 4 may be a manifestation of this effect.

Osteonectin is a matrix protein that inhibits cell cycle progression and elicits changes in cell morphology. It also exerts influence over the synthesis of extracellular matrix in an osteogenic setting.[41] It also binds to hydroxyapatite and collagen fibers at distal sites accounting for the ability of bone collagen to undergo calcification.[39]

3D BTCP scaffolds were treated with 1 μM $EGF(TCPBP)_{10}$ as described above and seeded at 30,000 cells per scaffold. At the indicated time points RNA was harvested from nine biological replicates per condition using a Qiagen RNEasy Plus II kit (scaffolds were pooled into three biological replicates). The resulting RNA was quantified, normalized to equal concentration then subjected to a two step q-RTPCR reaction using a Qiagen Sybrgreen Quick kit and run on a Chromopho4 thermal cycler with an optical sensor top. Each biological replicate was split into three technical replicates. Melting curves were analyzed at the end of each run to confirm the absence of contamination products. Primers for each gene were obtained from the Qiagen Quantitect primer bank.

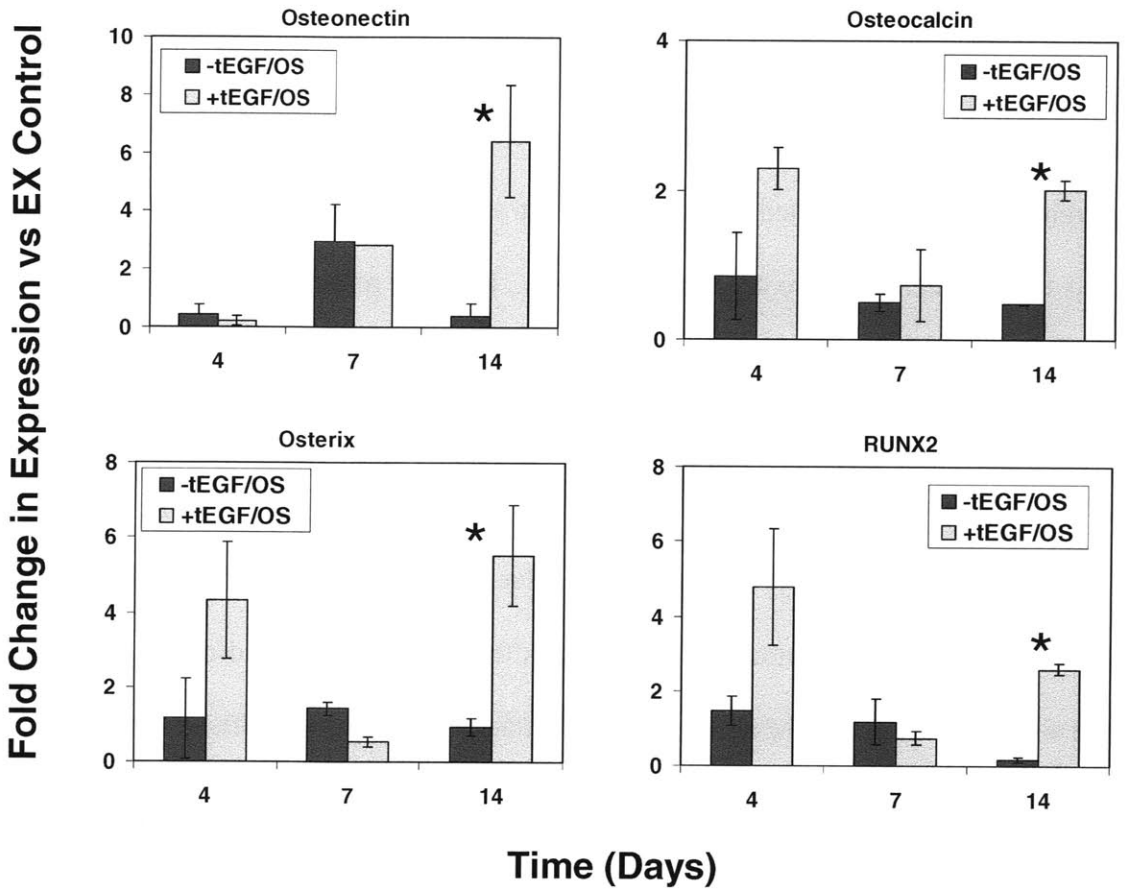

Figure 4.12 – Timecourse of qRT-PCR of osteogenic markers
qRT-PCR data on a set of four osteogenic markers: osteonectin, osteocalcin, osterix, and RUNX2 at days 4, 7, and 14 illustrates the effect of tethered EGF on expression levels of early osteogenic differentiation markers. All four markers exhibit statistically significant upregulation at day 14 ($p<0.05$) vs EX control. n=3 biological and m=3 technical replicates, +/- s.d.

As shown in figure 4.12 all four gene products showed statistically significant up-regulation at day 14 in the tEGF condition. Early up-regulation of RUNX2 of 5-fold may have served as an early up-regulator of downstream factors such as osteocalcin and osterix. A six-fold upregulation of osteonectin at day 14 is indicative of increased matrix deposition as would be expected at later time points. The biphasic expression of

osteocalcin, osterix, and RUNX2 with a minimum at day 7 may be indicative of changes in cell cycle progression toward proliferation as seen in the proliferation data (figure 4.10). The effect of tEGF on the expression of key osteogenic factors during 3D cell culture is a promising result, particularly when taking into consideration effects on proliferation. Taken together these results give a strong indication that tEGF can significantly increase proliferation of MSCs without compromising early osteogenic differentitation. This finding is a positive result in meeting the important objective outlined at the beginning of this chapter.

4.15 Long term survival assay using htMSCs

The impact of tEGF on the survival on MSCs has already been described here and in the literature. Confirming these results in 3D tissue culture would permit extension of these results into clinically relevant settings. The following section describes a long term hTMSC survival assay designed to evaluate the effect of tEGF.

Human telomerase reverse transcriptase immortalized human mesenchymal stem cells (htMSCs) were routinely cultured in Dulbecco's Modified Eagle Medium supplemented with 10% fetal bovine serum for the htertMSCs and 16.5% for the primary human MSCs, 2 mM L-glutamate, Na-pyruvate, non-essential amino acid supplement, and penicillin/streptomycin (final concentration 100 units/ml and 100 μg/ml streptomycin). In certain experiments where indicated, serum was omitted from this medium. Both nuclear staining and histological analysis of the tEGF treated scaffolds shows marked differences in the amount of cellular invasion into the 3D BTCP scaffold and of the relative survival effect at 23 days.

The striking differences observed in figure 4.13 may have added relevance in surgical settings where extensive wound sizes can present very harsh conditions for cell survival. The rescue of already sparse MSCs in a harsh wound environment would be of great clinical benefit.

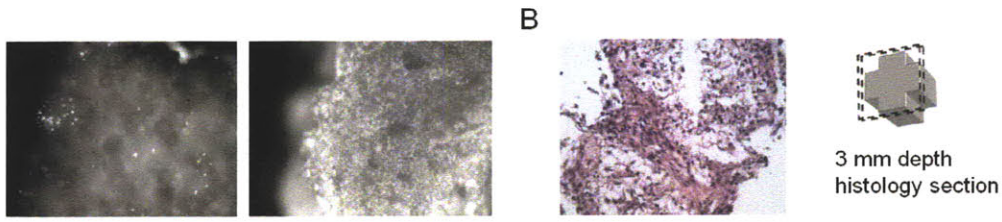

Figure 4.13 –Long term survival of htMSCs under serum starvation and tEGF
(A) Surface treatment of BTCP with (TCPBP)5-EGF promotes the survival of htMSC cells cultured in serum free medium for 23 days as seen with Cytox-16 nuclear DNA stain. Untreated scaffolds exhibit evidence of cell debris and do not exhibit viable cell nuclei. (B) Hoechst and eosin stain of paraffin embedded histology sections of scaffolds treated with (TCPBP)5-EGF show deep penetration of cells into pore structure and morphology consistent with viable htMSCs. Histological analysis of untreated scaffolds did not reveal any cell in-growth.

4.16 Conclusions

This work has demonstrated that MSCs cultured on BTCP scaffolds tethered with EGF proliferate at a greater rate than those cultured on untreated scaffolds and that this increase in proliferation does not compromise the early differentiation potential of MSCs. Significantly, it has been shown that soluble EGF does not confer the same advantage thus implicating a modulation of EGF bioactivity when presented as a matrix bound

ligand. It is also clear that tethered EGF confers a strong survival advantage to htMSC when cultured under extreme conditions such as serum starvation.

The ability to stably tether bioactive components to the surface of BTCP scaffolds using the simple methods described in this study will permit a wide range of basic studies in tissue regeneration and may lead to clinically useful approaches. One particularly promising area is that of spatially guided tissue regeneration such as the vascularization of regenerated bone and the regeneration of osteochondral interfaces.

4.17 References

1. Pinkas-Kramarski, R. et al. Diversification of Neu differentiation factor and epidermal growth factor signaling by combinatorial receptor interactions. *EMBO J* **15**, 2452-2467 (1996).
2. Tzahar, E. et al. A hierarchical network of interreceptor interactions determines signal transduction by Neu differentiation factor/neuregulin and epidermal growth factor. *Molecular and Cellular Biology* **16**, 5276-5287 (1996).
3. Tamama, K., Fan, V.H., Griffith, L.G., Blair, H.C. & Wells, A. Epidermal Growth Factor as a Candidate for Ex Vivo Expansion of Bone Marrow-Derived Mesenchymal Stem Cells. *Stem Cells* **24**, 686 (2006).
4. Griffith, L.G. Emerging Design Principles in Biomaterials and Scaffolds for Tissue Engineering. *Annals of the New York Academy of Sciences* **961**, 83-95 (2002).

5. Muschler, G.F., Nakamoto, C. & Griffith, L.G. Engineering Principles of Clinical Cell-Based Tissue Engineering. *The Journal of Bone and Joint Surgery* **86**, 1541-1558 (2004).

6. Bublil, E.M. & Yarden, Y. The EGF receptor family: spearheading a merger of signaling and therapeutics. *Current Opinion in Cell Biology* **19**, 124-134 (2007).

7. Citri, A. & Yarden, Y. EGF-ERBB signalling: towards the systems level. *Nat Rev Mol Cell Biol* **7**, 505-516 (2006).

8. Miettinen, P.J. et al. Epidermal growth factor receptor function is necessary for normal craniofacial development and palate closure. *Nature Genetics* **22**, 69-73 (1999).

9. Gibbs, S. et al. Epidermal growth factor and keratinocyte growth factor differentially regulate epidermal migration, growth, and differentiation. *Wound Repair and Regeneration* **8**, 192-203 (2000).

10. Tokumaru, S. et al. Ectodomain Shedding of Epidermal Growth Factor Receptor Ligands Is Required for Keratinocyte Migration in Cutaneous Wound Healing. *The Journal of Cell Biology* **151**, 209-220 (2000).

11. Maheshwari, G., Wells, A., Griffith, L.G. & Lauffenburger, D.A. Biophysical Integration of Effects of Epidermal Growth Factor and Fibronectin on Fibroblast Migration. *Biophysical Journal* **76**, 2814-2823 (1999).

12. Traverse, S. et al. Research Paper EGF triggers neuronal differentiation of PC12 cells that overexpress the EGF receptor. *Current Biology* **4**, 694-701 (1994).

13. Freeman, M. Reiterative use of the EGF receptor triggers differentiation of all cell types in the Drosophila eye. *Cell* **87**, 651-660 (1996).

14. Miettinen, P.J. Epidermal growth factor receptor function is necessary for normal craniofacial development and palate closure, *Nature Genetics*, Vol. 127 (1999)

15. Kratchmarova, I., Blagoev, B., Haack-Sorensen, M., Kassem, M. & Mann, M., Vol. 308 1472-1477 (American Association for the Advancement of Science, 2005).

16. Fan, V.H. et al. Tethered Epidermal Growth Factor Provides a Survival Advantage to Mesenchymal Stem Cells. *Stem Cells* **25**, 1241 (2007).

17. Wang, K., Yamamoto, H., Chin, J.R., Werb, Z. & Vu, T.H. Epidermal Growth Factor Receptor-deficient Mice Have Delayed Primary Endochondral Ossification Because of Defective Osteoclast Recruitment. *Journal of Biological Chemistry* **279**, 53848 (2004).

18. Sibilia, M. et al. Mice humanised for the EGF receptor display hypomorphic phenotypes in skin, bone and heart. *Development* **130**, 4515-4525 (2003).

19. Qin, L. et al. Amphiregulin Is a Novel Growth Factor Involved in Normal Bone Development and in the Cellular Response to Parathyroid Hormone Stimulation. *Journal of Biological Chemistry* **280**, 3974 (2005).

20. Chan, S.Y. & Wong, R.W.C. Expression of Epidermal Growth Factor in Transgenic Mice Causes Growth Retardation. *Journal of Biological Chemistry* **275**, 38693-38698 (2000).

21. Kuznetsov, S.A., Friedenstein, A.J. & Gehron Robey, P. Factors required for bone marrow stromal fibroblast colony formation in vitro. *British Journal of Haematology* **97**, 561-570 (1997).

22. Kimura, A., Katoh, O. & Kuramoto, A. Effects of platelet derived growth factor, epidermal growth factor and transforming growth factor-ß on the growth of human marrow fibroblasts. *British Journal of Haematology* **69**, 9-12 (1988).

23. Gronthos, S. & Simmons, P.J. The growth factor requirements of STRO-1-positive human bone marrow stromal precursors under serum-deprived conditions in vitro. *Blood* **85**, 929-940 (1995).

24. Owen, M.E., Clonal analysis in vitro of osteogenic differentiation of marrow CFU-F, Vol. 87 731-738 (1987).

25. Satomura, K. et al. Receptor tyrosine kinase expression in human bone marrow stromal cells. *Journal of Cellular Physiology* **177**, 426-438 (1998).

26. Erbe, E.M., Marx, J.G., Clineff, T.D. & Bellincampi, L.D. Potential of an ultraporous beta-tricalcium phosphate synthetic cancellous bone void filler and bone marrow aspirate composite graft. *Eur Spine J* **10**, S141-146 (2001).

27. Fleming Jr, J.E., George, F., Muschler, C.B. & Isador, H. Intraoperative Harvest and Concentration of Human Bone Marrow Osteoprogenitors for Enhancement of Spinal Fusion. *Orthopedic Tissue Engineering: Basic Science and Practice* (2004).

28. Friedlaender, G.E. et al., Vol. 83 151-158 (JBJS, 2001).

29. Marcantonio, N.A., Cynthia A. Boehm, Richard Rozic, Ada Au,a Alan Wells, & George F. Muschler, L.G.G. Tethered epidermal growth factor increases connective tissue progenitor colony formation. *Stem Cells* **in press** (2008).

30. Platt, M.O. et al. Sustained epidermal growth factor receptor levels and activation by tethered ligand binding enhances osteogenic differentiation of multi-potent marrow stromal cells. *J Cell Physiol* (2009).

31. Bateman, J. et al. Platelet-derived growth factor enhancement of two alloplastic bone matrices. *Journal of periodontology* **76**, 1833-1841 (2005).

32. Whaley, S.R., English, D.S., Hu, E.L., Barbara, P.F. & Belcher, A.M. Selection of peptides with semiconductor binding specificity for directed nanocrystal assembly. *Nature* **405**, 665-668 (2000).

33. Sanghvi, A.B., Kiley, P., Miller, H., Belcher, A.M. & Schmidt, C.E. Biomaterials functionalization using a novel peptide that selectively binds to a conducting polymer. *Nature Materials* **4**, 496-502 (2005).

34. Kenan, D.J. et al. Peptide-PEG amphiphiles as cytophobic coatings for mammalian and bacterial cells. *Chemistry & Biology* **13**, 695-700 (2006).

35. Zeltinger, J., Sherwood, J.K., Graham, D.A., Mueller, R. & Griffith, L.G. Effect of pore size and void fraction on cellular adhesion, proliferation, and matrix deposition. *Tissue engineering* **7**, 557-572 (2001).

36. Schuler, G.D., Altschul, S.F. & Lipman, D.J. A workbench for multiple alignment construction and analysis. *Proteins: Structure, Function, and Genetics* **9** (1991).

37. Clamp, M., Cuff, J., Searle, S.M. & Barton, G.J., Vol. 20 426-427 (Oxford Univ Press, 2004).

38. Ziros, P.G. et al. The bone-specific transcriptional regulator Cbfa1 is a target of mechanical signals in osteoblastic cells. *Journal of Biological Chemistry* **277**, 23934-23941 (2002).

39. Termine, J.D. et al. Osteonectin, a bone-specific protein linking mineral to collagen. *Cell* **26**, 99-105 (1981).

40. Gao, Y., Jheon, A., Nourkeyhani, H., Kobayashi, H. & Ganss, B. Molecular cloning, structure, expression, and chromosomal localization of the human Osterix (SP7) gene. *Gene* **341**, 101-110 (2004).

41. Bradshaw, A.D., Graves, D.C., Motamed, K. & Sage, E.H. SPARC-null mice exhibit increased adiposity without significant differences in overall body weight. *Proceedings of the National Academy of Sciences* **100**, 6045-6050 (2003).

42. Hoang, Q.Q., Sicheri, F., Howard, A.J. & Yang, D.S.C. Bone recognition mechanism of porcine osteocalcin from crystal structure. *Nature* **425**, 977-980 (2003).

43. Mikami, Y., Omoteyama, K., Kato, S. & Takagi, M. Inductive effects of dexamethasone on the mineralization and the osteoblastic gene expressions in mature osteoblast-like ROS17/2.8 cells. *Biochemical and Biophysical Research Communications* **362**, 368-373 (2007).

44. Matsubara, T. et al. BMP2 regulates osterix through Msx2 and Runx2 during osteoblast differentiation. *Journal of Biological Chemistry* **283**, 29119 (2008).

5 Summary and Outlook

This thesis describes the foundational work carried out to make a system of bivalent ligands targeting the HER family of receptors; a system which is capable of profoundly altering cell phenotype. It also describes the discovery and application of an engineered protein to functionalize an important clinical biomaterial in a way that significantly increases the proliferation of low-passage primary human MSCs without compromising osteogenic potential. Taken together these two efforts have established the basic framework needed to apply the work to areas of clinical and biological significance. It is hoped that future work in these areas can benefit from the ideas presented in this thesis.

The bivalent ligand system described here offers a way to bias HER receptors dimerization in a purely exogenous manner. This has immediate applications in the study of the HER receptor system and potential applications in more applied areas such as cancer research and tissue engineering. The nature of HER receptor dimerization and its significance in a variety of biological contexts is currently the subject of intensive study. Having an approach to directly control how HER receptors dimerize is valuable and the system described here may serve as a tool to achieve these effects and answer important questions in HER-related biology.

From the perspective of cancer biology it is well known that HER receptors play an important role in defining many of the features of cancer cells.[1] The ability to control even minor aspects of HER mediated signaling in cancer cells is of immediate interest. The signal silencing effect exerted by bivalent NRG in hTMSCs and in MCF7s (breast

cancer) is consistent with the proposed mechanism of action and is highly suggestive of one approach to modulate signaling in cancer cells.

5.1 Future Work

5.1.1 Biophysical evidence of bivalent ligand effects

Future work with bivalent ligands may benefit from the collection of biophysical evidence to validate the overall design. Several types of experiments could be performed to determine if the bivalent ligand system controls dimerization as expected. These include:

1. FRET measurements using HER1-CFP: HER3-YFP fusions
2. Receptor crosslinking and immunoblotting following ligand dosing
3. Immuno precipitation and immunoblotting following ligand dosing
4. Reporter complementation assay (luciferase or dihydrofolate reductase)

As an example, the development of a FRET sensor would permit direct biophysical measurement of receptor association brought on by bivalent ligands. A simple starting point to achieve this would be to carry out the subcloning CFY and YFP as C-terminal fusions to HER1 and HER-3, respectively. These two receptors are chosen because the proposed ligand system can putatively stimulate HER1-3 heterodimers and because detection of heterodimers is more straightforward than homodimers when using a FRET system. The construction of the FRET reporter is accomplished through PCR

mutagenesis of plasmids containing HER1 and HER3 to introduce the C-terminal fluorescent protein fusions CFP and YFP, respectively. The cloning will also introduce flanking restriction sites to permit subcloning into an expression plasmid. The definitive demonstration of bivalent ligand control over HER dimerization would come from a statistically significant increase in YFP signal when dosing bivalent EGF-NRG ligand (with appropriate controls). Other cell types which have low or null HER1 (CHO cells),[2, 3] or HER3 backgrounds may be required to reduce the amount of endogenous untagged receptor which could deplete signal generating receptor dimer pairs.

Biophysical evidence from radio-labeled binding experiments might also confirm the observation of configurational avidity observed in signaling dose response experiments.[4] Figure 5.1 shows typical dose responses observed with monovalent and bivalent ligands.

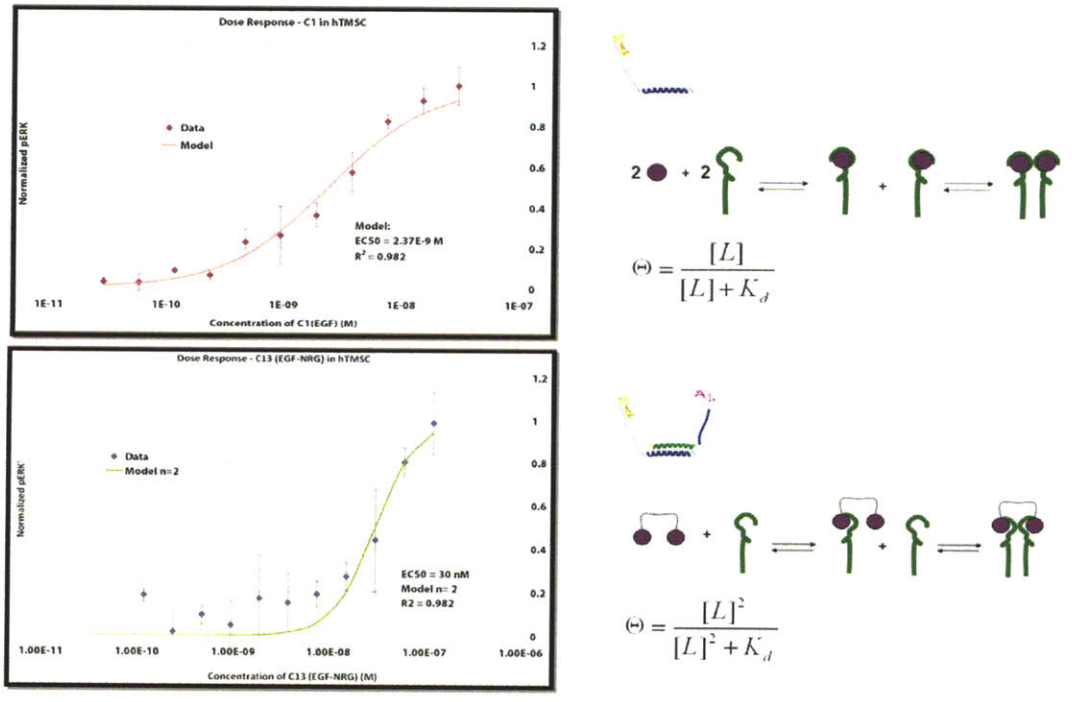

Figure 5.1- Dose responses of htMSCs with monovalent (E) and bivalent ligand (EN) Bivalent ligands consistently give dose responses which are steeper and exhibit Hill coefficients ~2 when fit with a two parameter model.

The bivalent ligand dose response (EE or EN) consistently exhibits a steep response region. A two parameter binding model fits the data well with a kd~30 nM and a Hill coefficient of ~2. A Hill coefficient > 1 is indicative of avidity and is supported by the proposed binding of a bivalent ligand to a receptor dimer pair. Confirming this result by measuring a direct binding isotherm with radiolabled bivalent ligand would be a valuable finding suggestive of the proposed binding mechanism. Additional studies along these lines are discussed in Appendix A.

5.1.2 Animal models of ectopic bone formation

A natural extension of the TCPBP work described in Chapter 4 is to examine the effects of tEGF on ectopic bone formation in an animal model. Confirming the effects observed thus far by using a simple but relevant animal model would support continued work in this area and would justify studies of bone formation in larger animal models. The ultimate goal of this work is to identify methods that can be used to treat large segmental defects in humans, particularly where current methods fall short of regenerating sufficient tissue to regain function. Although the regulatory hurdles associated with implementing a TCPBP-EGF based approach are very high, the demonstration of added benefit from spatially controlled delivery of biologically active proteins to sites of injury would be immensely valuable and would prompt additional efforts in this area.

5.2 References

1. Witton, C.J., Reeves, J.R., Going, J.J., Cooke, T.G. & Bartlett, J.M.S. Expression of the HER 1-4 family of receptor tyrosine kinases in breast cancer. *The Journal of Pathology* **200**, 290-297 (2003).
2. Olsson, P. et al. Uptake of a boronated epidermal growth factor–dextran conjugate in CHO xenografts with and without human EGF-receptor expression. *Anti-Cancer Drug Design* **13**, 279-289 (1998).
3. Krug, A.W. et al. Human Epidermal Growth Factor Receptor-1 Expression Renders Chinese Hamster Ovary Cells Sensitive to Alternative Aldosterone Signaling. *Journal of Biological Chemistry* **277**, 45892-45897 (2002).
4. Whitty, A. Cooperativity and biological complexity. *Nature Chemical Biology* **4**, 435-439 (2008).

Appendix A – Stochastic 2D cell migration simulator

This appendix describes the details of a stochastic simulation of 2D cell migration on a porous membrane. This simulation seeks to describe the impact of cell directional persistence on transwell migration that may provide insights into the apparent correlation between the transwell migration and reduced persistence in 2D cell migration described in Chapter 3. The simulation is implemented in Matlab (Mathworks, Natick, MA). The ability of the simulator to replicate real cell migration is illustrated in figure A1. Parameters used to generate the ensemble of cell trajectories is shown under '**Inputs**'.

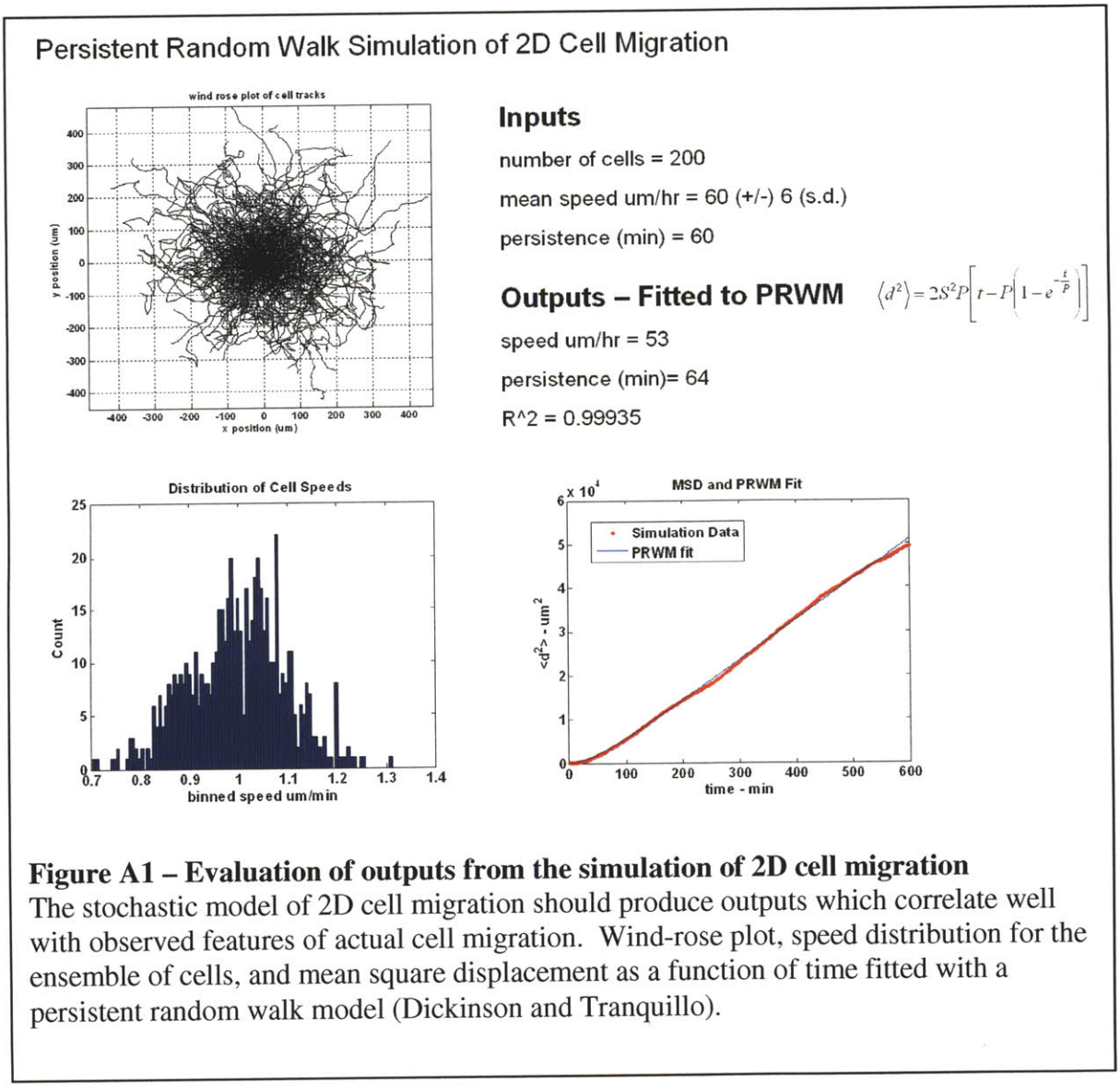

Figure A1 – Evaluation of outputs from the simulation of 2D cell migration
The stochastic model of 2D cell migration should produce outputs which correlate well with observed features of actual cell migration. Wind-rose plot, speed distribution for the ensemble of cells, and mean square displacement as a function of time fitted with a persistent random walk model (Dickinson and Tranquillo).

A representative wind-rose plot for an ensemble of 200 cells is shown (top left). Each cell is assigned a speed at each time step randomly selected from a normally distributed cell speed distribution with a specified mean and standard deviation. An example of the distribution of cell speeds resulting from a simulation is plotted in Figure A1 (bottom left), where a normal distribution is clearly evident. Fitting of the ensemble of MSDs with a persistent random walk model is shown in figure A1 ('**Outputs**' and bottom right). Close agreement between the input parameters and the fitted outputs is a good indication of the suitability of the stochastic simulator in capturing aspects of real cell migration described by the PRWM. The persistence for each cell at each time step is randomly sampled from a direction vector. In this case the direction vector is linearly arrayed with no weighting distribution thus random re-sampling at each time step produces a Poisson distributed set of persistences as shown in Figure A2 (rightmost histogram).

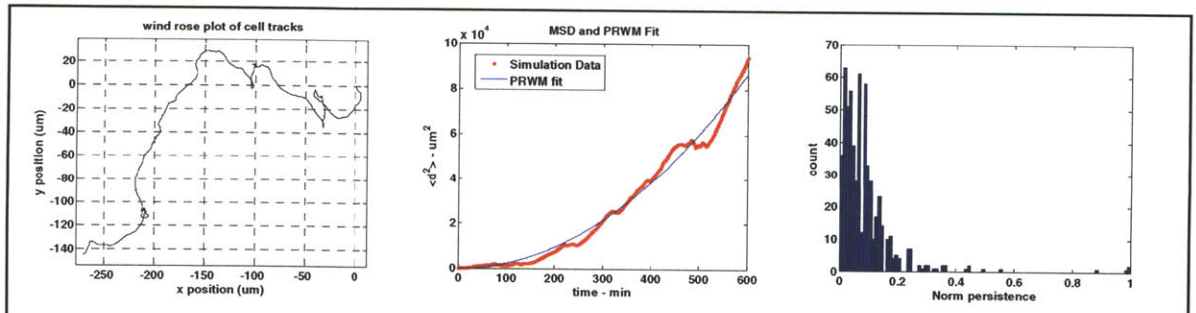

Figure A2 – Evaluation of outputs from the simulation of 2D cell migration for a single cell
Inputs: mean speed = 1 um/min, s.d. of speed = 0.1 um/min, persistence = 40 minutes

With the aid of this simulator it is possible to investigate simple questions about cell migration. For example, for cells migrating on a 2D porous surface (such as a transwell membrane) is the frequency of pore encounters correlated with directional

persistence? This question may only likely be valid in conditions where cells are sparsely seeded and migrating under conditions which probe chemokinesis as opposed to chemotactic directional migration. In order to implement an instance of this question in the simulator a few modifications are required. One is to introduce a pore field which is representative of the distribution of pores in a transwell membrane and which have a diameter characteristic of actual pores (8 um, in this case). Another is to randomize the starting positions of cells on the 2D surface.

Figure A3 illustrates the results of three simulations of cell migration under different persistence conditions. Qualitatively, one can observe that the frequency of pore encounters is lower under conditions of low cell directional persistence by comparing the number of pores (red dots) that do not meet a cell trajectory in the case of P=10 (leftmost) with P=160 (rightmost).

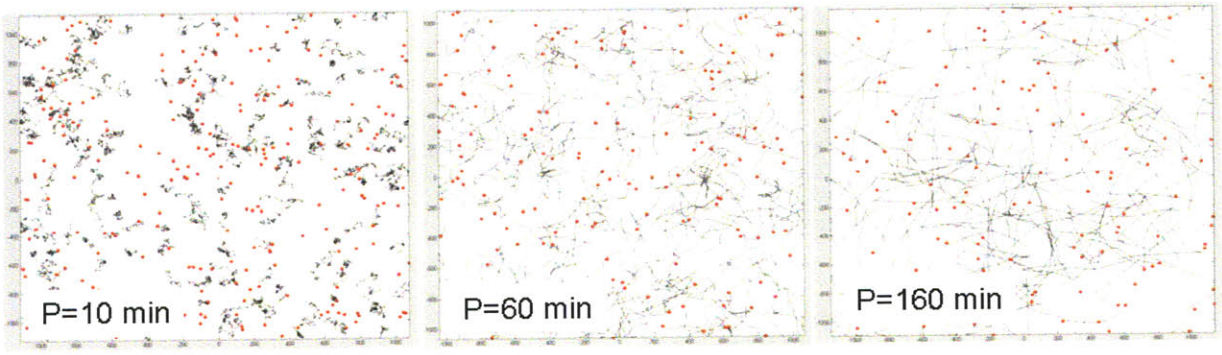

Figure A3 –Simulation of 2D cell migration on a porous membrane at various levels of directional persistence
Number of cells = 200, simulation time = 600 minutes, speed = 1 um/hr, persistence (as indicated on each plot). Length is 2000 microns on a side. Red dots are 8 μm diameter pores.

MATLAB Code Follows

```
%Persistent Random Walk Model Simulation of 2D Cell Migration on a Porous Membrane
%Luis Alvarez - April 2009

function migration
clear all
close all
n=600;                                  %number of time steps to examine
t=1;                                    %minutes per step
timevector=linspace(0,n*t,n)';
T=t*n;                                  %total simulation time (minutes)
numcell=100;                            %number of cells

%% Generate a Gaussian speed distribution matrix
mean_speed=1;                                           %microns/minute
stdev_speed=0.1;
s = (normrnd(mean_speed,stdev_speed,10000,1));
s(find(s<0))=0;                                         % cells do not have %negative speed
in this %model
shist=0;

%% Define persistence in terms of a unit directional vector
persistence=60;
number_of_directions=100;
p=2*number_of_directions*persistence;
dirvect=linspace(-1,1,p);
spread=2*p/persistence;

%% size of plot field
size=15*mean_speed*n*t/sqrt(mean_speed*n*t);      % keeps plot window to %appropriate size
based on how far cells move

%% Generate cell trajectories based on inputs
for j=1:numcell

    a0=round(p*rand());
    b0=round(p*rand());

    x=zeros;
    y=zeros;

   %uncomment to give each cell a %random starting point
    %x(1)=round(3*size*rand().*(-1)^round(3*rand()));
    %y(1)=round(3*size*rand().*(-1)^round(3*rand()));

    speed=s(ceil(length(s)*rand()));%use this line if you want to give %each cell a
       different but %constant speed throughout the simulation.  To do this change s(i)
       in the 'for loop' below to %'speed'.  Assumes a different speed (selected randomly
       from Gaussian speed distribution).  %The %current default is to randomly resample
       the cell speed matrix at %each time step.

    for i = 1:n-1

            %a0=ceil(p*rand());
            %b0=ceil(p*rand());

        a0=(a0+spread*(-1)^ceil(rand()*2));
        if a0>p a0=round(p*rand());%mod(a0,p);
        end
        if a0<1 a0=round(p*rand());%mod(abs(a0),p);
        end
        if a0==0 a0=round(p*rand());
        end

        b0=(b0+spread*(-1)^ceil(rand()*2));
        if b0>p b0=round(p*rand());%mod(b0,p);
        end
        if b0<1 b0=round(p*rand());%mod(abs(b0),p);
        end
        if b0==0 b0=round(p*rand());
        end
```

```
        dirx=dirvect(a0); %pick initial x direction index for dirvect
        diry=dirvect(b0); %pick initial y direction index for dirvect

        x(i+1)=x(i)+s(i)*(dirx)./sqrt((dirx).^2+(diry).^2); %sqrt corrects speed
%(pythagoras)
        y(i+1)=y(i)+s(i)*(diry)./sqrt((dirx).^2+(diry).^2);

        shist(i)=s(i);
    end

    %% cummulative (pathlength) and net (origin to end) distances
    distance_from_origin=(x(end).^2+y(end).^2).^0.5;
    cum_distance=(x.^2+y.^2).^0.5';
    cum_distance=flipud(cum_distance);


    %find the individual pathlengths of each step by calculating the %difference between
%step n and n-1
    for h=1:length(cum_distance)-1;
        suma(h)=cum_distance(h)-cum_distance(h+1)';
    end

    total_distance=sum(abs(suma)'); %sum all the pathlengths to get the full %patlength
    distance_from_origin/total_distance*100;
    std(abs(suma')); % a metric for persistence

    persist=distance_from_origin/(speed*T);

    %% Matrix of Cell Ensemble Data - this mod stores data from each cell
    a=[x' y'];
    EX(:,j)=a(:,1); % stores historical x positions for each cell
    EY(:,j)=a(:,2); % stores historical y positions for each cell
    EDAT(:,j)=[j; total_distance; distance_from_origin;
distance_from_origin/total_distance; persist];

end
        %% Pore field
        %find max min for X and Y to define extent of pore field (~ [max min] %+/- 10 um)
        maxX=max(max(EX));
        minX=min(min(EX));
        maxY=max(max(EY));
        minY=min(min(EY));

        npores=500/2;%nubmer of pores- will need 100 centers (a,b): (x-%a)^2+(y-b)^2=R^2:
        R=4; % pore radius in microns

        maxa=maxX;   %keep pores inside cell field by subtracting R or adding R
        mina=minX;
        maxb=maxY;
        minb=minY;

        %Create pore field
        porecentersapos=2*maxa*rand(npores,1);%generate 'npores' number of %centers
        porecentersbpos=2*maxb*rand(npores,1);
        porecentersaneg=2*mina*rand(npores,1);%generate 'npores' number of %centers
        porecentersbneg=2*minb*rand(npores,1);

        cor1=ones(length(porecentersapos))*(-maxX);
        cor1=cor1(:,1);

        aa=[porecentersapos+cor1; porecentersaneg];
        bb=[porecentersbpos+cor1; porecentersbneg];
        XXX=0;
        YYY=0;
        botYYY=0;

        for hh=1:npores
            a=aa(hh);
            b=bb(hh);
            x=linspace(a-R, a+R);
```

```
            y=(R^2-(x-a).^2).^0.5+b;
            ybot=-(R^2-(x-a).^2).^0.5+b;
            XXX=[XXX x];
            YYY=[YYY y];
            botYYY=[botYYY,ybot];
        end

%% PLOT results
    figure(1)
    %set(0,'DefaultAxesColorOrder',[1 0 0;0 1 0;0 0 1])
    plot(EX,EY,'k-',XXX,YYY,'r.',XXX,botYYY,'r.') %,poresx,poresy,'bo'
    %plot(EX,EY,'k-') %,poresx,poresy,'bo'
    grid on
    xlabel('x position (um)','fontsize',14,'fontweight','bold')
    ylabel('y position (um)','fontsize',14,'fontweight','bold')
    title('wind rose plot of cell tracks','fontsize',14,'fontweight','bold')
    axis([-8*size 8*size -8*size 8*size])
    set(gca,'fontsize',14,'fontweight','bold')
msd=mean(((EX.^2+EY.^2).^0.5).^2,2); % msd between steps: correct according to
Lauffenburger paper


beta=[mean_speed t]; %initial guess for <s^2> and P
beta = nlinfit(timevector,msd,@mymodel,beta);

msd_model=(2*beta(1)*beta(2).*timevector.*(1-beta(2)./timevector.*(1-exp(-
timevector./beta(2)))));

EDAT=EDAT';
sqdisp=EDAT(:,2).*EDAT(:,2);

'speed um/hr'
(beta(1).^0.5)*60

'persistence (min)'
round(beta(2))

msd_model(1)=0; %first value is NaN, need to set to zero.
RSQ=corrcoef(msd,msd_model);
['R^2 = ', num2str(RSQ(2))]
'msd(end)^.5/(n*t) - um/hr'
(msd(end)).^0.5./(n*t)*60


%% this function is the persistent random walk model from Dickinson and Tranquillo:
% <d^2> = nd*<s^2>*P*t*[1-P/t*(1-exp(-t/P))]
function yhat = mymodel(beta, timevector)
 yhat = (2*beta(1).*beta(2).*timevector.*(1-beta(2)./timevector.*(1-exp(-
timevector./beta(2)))));
```